Crowdsensing and Resource Allocation in Shared Spectrum

Xuhang Ying

A dissertation
submitted in partial fulfillment of the
requirements for the degree of

Doctor of Philosophy

University of Washington

2018

Reading Committee:

Sumit Roy, Chair

Radha Poovendran, Chair

Sreeram Kannan

Milind M. Buddhikot

Program Authorized to Offer Degree:
Electrical Engineering

University of Washington

Abstract

Crowdsensing and Resource Allocation in Shared Spectrum

Xuhang Ying

Co-Chairs of the Supervisory Committee:
Professor Sumit Roy
Electrical Engineering

Professor Radha Poovendran
Electrical Engineering

The exponential growth of mobile data services has translated into a proportionate surge in demand for greater wireless broadband capacity. Within today's fixed spectrum allocation regime, exclusive spectrum access rights are granted to federal and commericial users, but a significant portion of the licensed spectrum has been underutilized by primary users (PUs). To alleviate artificial spectrum scarcity, *spectrum sharing* has been proposed to allow secondary users (SUs) to opportunistically access the locally unoccupied spectrum, called White Spaces (WS), so long as they do not cause harmful interference to PUs. To this end, the FCC is actively pursuing policy innovations to create shared spectrum, including WS in TV bands (TVWS) and the 3.5 GHz Citizens Broadcast Radio Service (CBRS) band, which often relies on a spectrum manager that manages the shared spectrum access, such as the database administrator (DBA) in TVWS and the Spectrum Access System (SAS) in CBRS.

Our work begins by showing that the empirical DBA models for TV coverage estimation are locally inaccurate, since they do not explicitly account for local obstructions. Therefore, we propose augmenting the DBA approach with *spatial-statistics-based radio mapping* using Kriging and show that it achieves more accurate coverage boundary estimation, which leads to fewer missing WS opportunities (type-I errors) while keeping misclassifications (type-II

errors) under a certain limit.

Scaling spatial-statistics-based radio mapping to larger areas inevitably meets cost limitations. An economically viable alternative is *crowdsensing*, that is, outsourcing sensing tasks to spatially distributed users with mobile devices that are outfitted with spectrum sensors. In order to attract user participation for crowdsensing, we propose an *auction-based incentive mechanism*, in which each user submits a bid (the minimum acceptable payment) for providing spectrum data and receives a payment when selected. We show that the proposed scheme is truthful, computationally efficient, individually rational, and budget feasible.

We also consider the design of a *pricing-based incentive mechanism*, in which the platform who constructs radio maps makes one-time offers (the incentive for participation) to selected users (either sequentially or in batches) and collects data from those who accept the offers. We formulate pricing mechanism design as expected utility maximization, where the expected utility captures the tradeoff between radio mapping performance (location and data quality), crowdsensing cost, and uncertainty in offer outcomes (possible expiration and rejection). We show that the proposed user selection algorithm provides a provable performance guarantee and the proposed mechanism outperforms the baseline mechanisms.

After WS opportunities are identified, it is crucial to efficiently allocate resources (e.g., available channels) to SUs. To this end, we study SAS-assisted dynamic channel assignment in the CBRS. We propose a novel graph representation to capture spatially varying channel availability, channel contiguity, and coexistence opportunities, which allows us to employ or develop efficient algorithms with provable performance guarantees.

As the last piece of this thesis, we study the problem of monitoring whether Wi-Fi and duty cycled LTE Unlicensed (LTE-U) are sharing channel access time in a fair manner. We propose a scheme that allows the spectrum manager to estimate the duty cycle of a target LTE-U system and detect duty cycling misbehaviors with a high probability of detection, while keeping the false alarm probability under a certain limit.

TABLE OF CONTENTS

LIST OF FIGURES

GLOSSARY

ACK: Acknowledgment

ADC: Analog to Digital Conversion

CA: Channel Assignment

CBRS: Citizens Broadcast Radio Service

CBSD: Citizens Broadcast Radio Service Device

CCA: Clear Channel Assessment

CR: Cognitive Radio

CS: Carrier Sensing

CSAT: Carrier Sensing Adaptive Transmission

CSMA/CA: Carrier-Sense Multiple Access with Collision Avoidance

CV: Cross Validation

DBA: Database Administrator

DCF: Distributed Coordination Function

DFS: Dynamic Frequency Selection

DIFS: DCF Interframe Spacing

DPA: Dynamic Protection Area

DSA: Dynamic Spectrum Access

ED: Energy Detection

ESC: Environment Sensing Capability

EU: Expected Utility

FCC: Federal Communication Commission

FFT: Fast Fourier transform

FSS: Fixed Satellite Services

GAA: Generalized Authorized Access

GP: Gaussian Process

K-NN: k-Nearest Neighbor

LBT: Listen Before Talk

LR: Longley-Rice

LTE-LAA: LTE Licensed Assisted Access

LTE-U: LTE Unlicensed

MAC: Medium Access Control

MC: Monte Carlo

MI: Mutual Information

MSE: Mean Squared Error

M(W)IS: Maximum (Weighted) Independent Set

OK: Ordinary Kriging

PA: Priority Access

PAL: Priority Access License

PHY: Physical Layer

PPA: PAL Protection Area

PSD: Power Spectral Density

PU: Primary User

IA: Incumbent Access

RSSI: Received Signal Strength Indicator

SAS: Spectrum Access System

SNR: Signal to Noise Radio

SIFS: Short Interframe Spacing

SU: Secondary User

REM: Radio Environment Map

USM: Unconstrained Submodular Maximization

USRP: Universal Software Radio Peripheral

WS: White Space

ACKNOWLEDGMENTS

This dissertation would have not been possible without the help and support of my colleagues, friends, and family.

I thank my advisors, Sumit Roy and Radha Poovendran, for their invaluable guidance and mentoring over the years at University of Washington. Their commitment to both research and excellence has inspired me throughout my PhD.

I thank my committee, Milind Buddhikot (Nokia Bell Labs), Sreeram Kannan, and Arvind Krishnamurthy, for their time, service, and helpful comments. I also thank Andrew Clark (Worcester Polytechnic Institute) and Linda Bushnell, whom I consider as mentors, for their helpful dicussion and invaluable advice as I was approaching the end of my PhD.

I would like to extend my deep thanks to the current and former graudate students and post-docs of the Fundamentals of Networking Lab (FuNLab) and the Network Security Lab (NSL). The current generation of NSL, consisting of Zhipeng (Leo) Liu, Hossein Hosseini, Baicen Xiao, Sang Sagong, Joanna Mazer, Dinuka Sahabandu, and Yize Chen, have created a warm and collaborative work environment. I also thank former NSL students, including Phillip Lee, Chou-Chang (Jack) Yang, Elisabeth Senmarti Robla, Truc Pham, Laila Abudahi, Kalikinkar Mandal, and Qiong Lin, as well as (former) FuNLab students, including Hossein Savafi, Yue Yang, Farzad Hessar, Shwan Ashrafi, Colby Boyer, Abdulmohsen Mutairi, Benjemin Morgan, Chang Wook Kim, Anish Ashok, Rohan Patidar, Abhinav Jadon, and Morteza Mehrnoush, for their help and advice througout my PhD.

Finally, I extend my deepest gratitude to my mother, father, and my grandparents for their priceless love and selfless support.

To the love of my life, Shuo Zhang.

DEDICATION

To my parents and grandparents

To coffee, basketball, and Seattle

Chapter 1

INTRODUCTION

The increasing penetration of mobile devices (e.g., smartphones, tablets) and the proliferation of multimedia applications have translated into a rapidly growing demand for greater wireless broadband capacity. According to Ericsson forecasts [2], mobile broadband subscriptions will reach 8.5 billion, and the total mobile data traffic will reach around 110 ExaBytes (10^{18} Bytes) per month by 2023, with a compound annual growth rate of 42%. Such a trend will continue to accelerate in the next few years, which is also anticipated by parties including Cisco, Qualcomm, and the UTMS forum [3–5]. Therefore, it is a great challenge for network operators to expand wireless network capacity and keep up with the sky-rocketing demand.

Several main solutions have been proposed to meet the capacity challenge [4,6,7], including i) higher spectral efficiency by improving radio link (PHY/MAC) performance (increase in bps/Hz), ii) network densification by deploying more small cells (increase in bps/Hz/m^2), and iii) more spectrum for broadband access (increase in Hz). As the current PHY/MAC performance is approaching the Shannon theoretical limits [8] and network densification faces various technical challenges [9], it is most straightforward to provide more spectrum, as the Shannon capacity increases linearly with the bandwidth. In practice, however, spectrum is a very scarce, expensive resource and currently the availability of new spectrum cannot keep up with the demand.

Despite of spectrum scarcity, it has been acknowledged in the 2012 PCAST report [10] that today's apparent shortage of spectrum is in fact an illusion arising from the way spectrum is managed. Historically, spectrum was managed by granting exclusive rights of using a specific frequency at a specific location to federal and commercial users. Long term

commercial licenses have been generally assigned through competitive bidding, and winners receive exclusive spectrum access to frequencies of their choice (i.e., licenses) with regulatory protection that prevents other services infringe on those frequencies (i.e., no interference). Nevertheless, numerous studies [10–18] have shown that a significant portion of the licensed spectrum is in fact underutilized by licensed or primary users (PUs), which, if shared, has the full potential in expanding network capacity and spurring economic growth. Therefore, regulatory bodies like the Federal Communication Commission (FCC) are pursing policy innovations to change spectrum usage from exclusivity to sharing, in order to move spectrum availability from scarcity to abundance.

Under the paradigm of shared spectrum, secondary users (SUs) are allowed to opportunistically access the locally unoccupied spectrum, which is called White Space (WS), subject to the no-harmful-interference-to-PUs condition. In 2008, the FCC passed a historic ruling that allows unlicensed devices to operate in TVWS [19]. In the 2012 PCAST report [10], the U.S. government pushed it further by announcing its intentions to share 1000 MHz of federal government spectrum with commercial systems. Towards this goal, the FCC targeted release of the 3550-3700 MHz band, termed Citizens Broadband Radio Service (CBRS), which is primarily used by high-powered Department of Defense radar systems and non-federal Fixed Satellite Services (FSS) earth stations, to enable deployment of relatively low-powered network technologies such as small cells. In addition to the current spectrum sharing initiatives by the FCC (Figure 1.1) [20], a total of 1160 MHz federal spectrum is under study or will be investigated in the future [21].

In order to coordinate dynamic access to shared spectrum, several sharing mechanisms have been adopted: i) manual coordination between PUs and SUs as in the Advanced Wireless Services (AWS-3) [22], ii) Listen Before Talk (LBT) as in the Medical Device Radiocommunications Service (MedRadio) [23], iii) Dynamic Frequency Selection (DFS) as in the U-NII bands [24], and iv) deployment of spectrum managers, such as the database administrators (DBA) in TVWS [19] and the conceptually similar database called Spectrum Access Server (SAS) in the CBRS [25]. In this thesis, we focus on addressing the following challenges

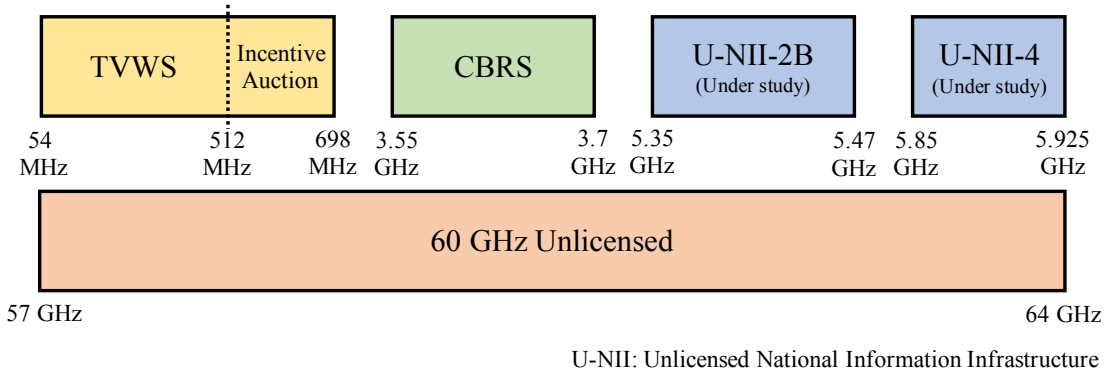

Figure 1.1: Selected spectrum sharing initiatives by the FCC.

arising from deploying spectrum managers with applications in TVWS and CBRS:

- **Coverage/protection area estimation**: In TVWS, PUs (including both transmitter and receivers) within the TV coverage region are protected from SUs, and the coverage contours are determined by comparing the Received Signal Strength Indicator (RSSI) against a preset threshold (e.g., -84 dBm/6 MHz for digital TV services [19]). SUs are not allowed to transmit within a minimum separation distance from the border of the protected contour [17, 18]. A similar notion called protection areas is also defined for incumbents (including authorized federal and FSS users) and licensed SUs[1] in the CBRS. For instance, each licensed SU has a default protection contour based on the -96 dBm/10 MHz signal strength, within which the aggregate interference from other SUs cannot exceed -80 dBm/10 MHz.

  In order to estimate coverage/protection contours, empirical radio propagation models including the FCC curves [19] and the Longley-Rice model [26] are widely adopted by DBAs. However, there exist concerns about the local accuracy of modeled-based RSSI estimation, including the fact that these models do not properly account for built

[1]Unlike the TVWS, the CBRS adopts a three-tiered spectrum access framework that includes incumbents, licensed SUs, and unlicensed SUs. More details will be provided in Chapter 5.

environments (e.g., buildings) in outdoor dense urban areas and indoors [18, 27, 28]. Therefore, one of the questions we try to answer is *how to augment the DBA approach with measurements via radio mapping in order to achieve more accurate estimation of coverage/protection boundaries.*

- **Crowdsensed radio mapping:** While measurement-driven radio mapping has the potential for accurate RSSI and coverage/protection boundary estimation, it usually requires a reasonable amount of local measurements from (static or dynamic) sensors or measurement campaigns, which inevitably meets cost limitations when scaled to a wide area. An economically viable alternative is via crowdsensing [29, 30], that is, outsourcing spectrum sensing tasks to spatially distributed users with mobile devices that are outfitted by spectrum sensors. Nevertheless, users would consume resources such as computing power, storage, and battery for sensing, and would be less likely to participate if appropriate compensations or rewards are not provided. Therefore, we try to answer the next question – *how to design incentive mechanisms for crowdsensed radio mapping.*

- **Dynamic resource allocation**: After WS opportunities are identified, it is crucial for spectrum managers to efficiently allocate available channels to SUs in order to optimize the overall network performance while meeting FCC regulations. There are several challenges to be addressed. First, the set of available channels is spatially varying in both TVWS and CBRS, which mainly arises from the fact that PUs and licensed SUs are spatially distributed. Second, it is necessary to aggregate contiguous channels of smaller bandwidths in shared spectrum (e.g., 6 MHz channels in TVWS and 10 MHz channels in CBRS) to support operations of various radio access technologies (e.g., Wi-Fi requires 20 MHz channels [31]) and meet multi-channel demands. In the CRBS, it is further required by the FCC that the same (contiguous) channel(s) be assigned to geographically contiguous license areas of the same licensee [25]. Third, Wi-Fi like MAC protocols such as CSMA/CA [31] and LBT in LTE-LAA [32] are

becoming increasingly popular, which enable co-channel coexistence for SUs in close proximity. Therefore, the problem we try to address is *how to dynamically assign channels and leverage coexistence opportunities while meeting the channel availability and contiguity constraints.*

- **Fairness monitoring**: When SUs are assigned the same channels, it is important to achieve fair coexistence and enforce equal spectrum access rights. It is widely believed that Wi-Fi and LTE are among the most dominant technologies that will be deployed in unlicensed/shared bands [33–36]. In this thesis, we are interested in fair sharing of channel access time between Wi-Fi and duty cycled LTE Unlicensed (LTE-U) [37, 38]. While Wi-Fi/LTE-U coexistence has drawn a lot of attention [33, 39–42], a concerning fact has often be neglected: Wi-Fi networks, as benign users, can only access the channel during LTE-U OFF time, while ON/OFF time is under unilateral control of LTE-U networks. As a result, LTE-U, as self-interested users, may have incentives to misbehave by transmitting with a larger duty cycle that exceeds the assigned limit (e.g., 50% when one LTE-U network coexists with one Wi-Fi network), so as to gain a greater share in channel access time and throughput. Therefore, the problem we try to address is *how to design a duty cycle estimation and misbehavior detection scheme that monitors channel access time fairness for Wi-Fi/LTE-U coexistence.*

1.1 Contributions of this Thesis

As illustrated in Figure 1.2, this thesis covers three topics in shared spectrum: i) incentivized crowdsensing for spatial-statistics-based radio mapping, ii) dynamic resource allocation, and iii) fairness monitoring. The specific contributions are described as follows.

1.1.1 Spatial-Statistics-Based Radio Mapping for TV Coverage Estimation

Our first work is motivated by concerns about local accuracy of RSSI and coverage/protection boundary estimation based on empirical radio propagation models employed by DBAs, in-

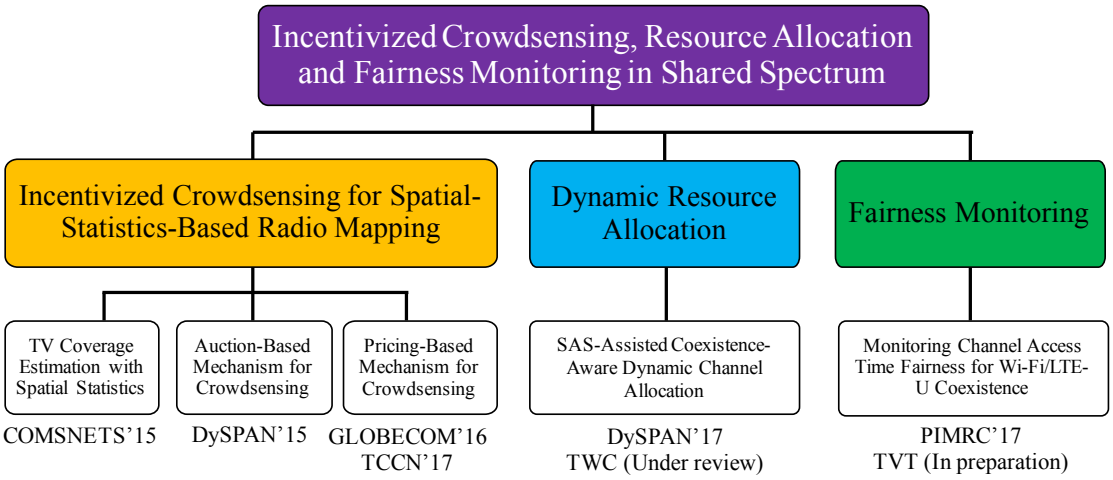

Figure 1.2: Organization of this thesis.

cluding the fact that they do not properly account for built environments (e.g., buildings, trees). In this work, we conducted a measurement campaign (i.e., war-driving) over a 4.6 km-by-5 km suburban region in Seattle, WA, and collected I/Q samples of 31 permissible TV channels at 240 locations. We use the collected data to quantify the RSSI prediction errors of DBA models – the FCC Curves and the Longley-Rice model, and we show that the DBA models tend to over-estimate RSSI by omitting man-made or natural local obstructions.

We apply a well-known statistical interpolation technique called Kriging to radio mapping by estimating the RSSI value at an unmeasured location from nearby available measurements. We show that measurement-driven Kriging achieves consistently good performance. We then quantify the boundary estimation performance in terms of type-I/II errors for three approaches: i) Kriging on measurement data followed by estimation, ii) estimation on measurement data using k-Nearest Neighbor (k-NN) classifier, and iii) estimation on predicted field strengths using DBA models. We show that Kriging reduces type-I errors by 46.1% compared to DBA models while keeping type-II error rate under 5%, which is also an improvement over the k-NN approach. More importantly, both measurement-driven approaches perform significantly better than the DBA models that suffer from high type-I error rates.

1.1.2 Auction-Based Crowdsensing for Spatial-Statistics-Based Radio Mapping

In order to attract user participation for crowdsensed radio mapping, we investigate and develop reverse auction-based incentive mechanisms, in which each user submits a bid (the minimum acceptable payment) for providing spectrum data and receives a payment when selected. We first develop a budget-free mechanism with a cardinality constraint (an upper limit on the number of selected users) and show that it is truthful, computationally efficient, and individually rational. We then develop a budget-feasible mechanism by translating the budget constraint into the best cardinality constraint using the bisection method. We conduct extensive simulations to evaluate the performance of the proposed mechanism and compare it against the state-of-the-art budget-feasible mechanism. Our results reveal that the proposed mechanism makes full use of the budget and performs significantly better compared to the baseline with improvements of 18%-22% in terms of maximizing the average prediction error variance (Kriging variance) reduction.

1.1.3 Pricing-Based Crowdsensing for Spatial-Statistics-Based Radio Mapping

We also consider the design of a pricing-based incentive mechanism, in which the platform who constructs radio maps makes one-time offers (the incentive for participation) to selected users (either sequentially or in batches) and collects data from those who accept offers. We develop pricing mechanisms based on expected utility (EU) maximization, where EU captures the tradeoff between radio mapping performance (location and data quality), crowdsensing cost, and uncertainty in offer outcomes (possible expiration and rejection).

Specifically, we consider both sequential offering, where one best price offer is sent to the best user in each round, and batched offering, where a batch of offers is made in each round. For the later, we show that EU is submodular in the discrete domain, and propose a mechanism that first fixes the pricing rule, and selects users based on unconstrained submodular maximization (USM); it then compares different pricing rules to find the best batch of offers in each round. We show that USM-based user selection has a provable performance guaran-

tee. We evaluate and compare the proposed mechanisms against the utility-maximization-based baseline mechanisms. Our results show that our single-batch mechanism is better than the single-batch baseline mechanism with an improvement ranging from 8.5% to 40.5%. If more batches are allowed, our multi-batch mechanism achieves close performance with the multi-batch baseline mechanism, but requires much fewer batches (2.5 versus 7.7 batches on average) and thus a much smaller delay.

1.1.4 SAS-Assisted Coexistence-Aware Dynamic Channel Assignment

Different from TVWS, the CBRS adopts a three-tiered spectrum access framework that consists of i) Incumbent Access, ii) Priority Access (PA), and iii) Generalized Authorized Access (GAA). In this work, we study SAS-assisted dynamic channel assignment (CA) for PA and GAA tiers in the CBRS. We introduce the node-channel-pair conflict graph to capture pairwise interference, channel and geographic contiguity constraints, spatially varying channel availability, and coexistence awareness. The proposed graph presentation allows us to formulate PA CA and GAA CA with binary conflicts as max-cardinality CA and max-reward CA, respectively. Approximate solutions can be found by a heuristic-based algorithm that aims to solve the maximum weighted independent set problem.

We further formulate GAA CA with non-binary conflicts as max-utility CA. We show that the utility function is submodular and the problem is an instance of matroid-constrained submodular maximization. We propose a polynomial-time algorithm based on local search that provides a provable performance guarantee. Extensive simulations using a real-world Wi-Fi hotspot location dataset are conducted to evaluate the proposed algorithms. Our results have demonstrated the advantages of the proposed graph representation and improved performance of the proposed algorithms over the baseline algorithms.

1.1.5 Monitoring Channel Access Time Fairness for Wi-Fi/LTE-U Coexistence

As the last piece of this thesis, we study the problem of monitoring channel access time fairness for Wi-Fi/LTE-U coexistence. we propose a scheme that allows the spectrum manager

managing the shared bands to estimate the duty cycle of a target LTE-U network based on PHY layer observations from a nearby Wi-Fi AP, without interrupting normal Wi-Fi operations. We further propose a thresholding scheme to detect duty cycling misbehavior (i.e., determining if the duty cycle exceeds the assigned limit) and analyze its performance in terms of detection and false alarm probabilities. The proposed schemes are implemented in ns3 and evaluated with extensive simulations. Our results show that the proposed scheme provides an estimate within $\pm 1\%$ of the true duty cycle and detects misbehavior with a duty cycle 2.8% higher than the limit with a detection probability of at least 95%, while keeping the false alarm probability less than or equal to 1%.

1.2 Organization of this Thesis

This dissertation is organized as follows. Chapter 2 discusses the application of a spatial-statistics-based technique called Kriging to radio mapping for TV coverage estimation. Chapters 3 and 4 present an auction-based incentive mechanism and a pricing-based incentive mechanism for crowdsensed radio mapping, respectively. Chapter 5 discusses SAS-assisted coexistence-aware dynamic channel assignment in the CBRS. Chapter 6 presents a fairness monitoring scheme that estimates duty cycle and detects possible duty cycling misbehavior of the LTE-U network when coexisting with a Wi-Fi network in the shared spectrum.

Chapter 2

SPATIAL-STATISTICS-BASED RADIO MAPPING FOR TV COVERAGE ESTIMATION

The exponential growth of wireless mobile services has translated into a proportionate surge in demand for additional network capacity. While spectrum is a scarce and expensive resource, a significant portion of licensed spectrum has been grossly underutilized by PUs. To address the artificial scarcity of spectrum, spectrum sharing has been proposed to allow SUs to opportunistically access locally unoccupied spectrum or WS, subject to a no-harmful-interference-to-PUs constraint.

The first potential application of spectrum sharing was intended for the VHF/UHF TV bands, concurrent with the transition from analog-to-digital over the broadcast in the United States. In 2008, the FCC opened up (portions of) unused TV band spectrum [19]. As per the FCC ruling [43,44], SUs must obtain information regarding locally available spectrum by contacting a geo-location DBA to retrieve a list of available channels. A core output of DBA querying is the estimated coverage contours of primary sources (TV transmitters) based on suitable propagation models (notably, the FCC Curves [19] prescribed by the FCC for all current DBAs). In any case, the contour is determined by comparing the estimated RSSI at a location to a preset threshold (e.g., 41 dBμV/m or -84 dBm for digital TV services[1]). SU devices are not allowed to operate within this region plus the vicinity, which is the so-called "no-talk" zone.

Concerns about local accuracy of RSSI estimation based on propagation models include the fact that these do not account properly for built environments (e.g. buildings) in dense

[1]This threshold is subject to calculation for DTV stations using the Longley-Rice methodology based on the receive system model in [19, 26]. The FCC ignores actual waveform information (e.g., ATSC 1.0), which should be considered as a weakness.

urban outdoors as well as indoors [28]. As a result, DBAs may not estimate coverage regions accurately, causing possible interference to PUs or missing WS opportunities. On the other hand, local spectrum sensing is generally more accurate, but is expensive and labor-intensive, making sampling at all locations over a large geographical region practically infeasible. This leads to a natural proposition given the respective advantages of both approaches – can these be effectively combined, namely, by conducting a small amount of local measurements over fringe areas of protected regions predicted by DBAs, using statistical interpolation techniques to estimate RSSIs at unmeasured points, and finally refining protected contours based on interpolation results?

In [45, 46], authors applied well-established geo-statistical interpolation technique called *Kriging* to coverage prediction and showed that it is able to achieve competitive or better performance as compared to propagation models. While this prior work serves as the immediate inspiration, they limited themselves to signal interpolation and did not actually explore the problem of TV coverage estimation, which is the main interest in protecting PUs.

In this work, we conducted a vehicle-based measurement campaign over a 4.6 km-by-5 km suburban region in Seattle, WA, to collect I/Q samples of 31 permissible UHF channels at 240 locations. We then evaluate and compare the measurement-based Kriging approach followed by classification for coverage region estimation against the DBA model-based approach. Our specific contributions are as follows.

- As a baseline, we quantify the RSSI prediction errors of DBA models, i.e., the FCC Curves and Longley-Rice (LR) model. Our results show that they tend to over-estimate RSSI values by omitting man-made or local obstructions (e.g., buildings, trees).

- We compare the boundary estimation performance of three approaches in terms of type-I/II errors: i) Kriging-based estimation, ii) k-Nearest Neighbor (k-NN) based estimation, and iii) DBA model based estimation. Our result show that for a given TV service threshold (-84 dBm), the Kriging-based approach reduces type-I errors by 46.1% as compared to DBA models while keeping type-II error rate under 5%, which

also outperforms the k-NN approach. Both measurement-driven approaches perform much better than the DBA models that suffer from high type-I error rates.

The remainder of this chapter is organized as follows. Section 2.1 reviews recent Kriging applications in radio mapping, and Section 2.2 provides brief background on Kriging. Our measurement campaign is described in Section 2.3. We compare Kriging-based RSSI and boundary estimation against the DBA models in Sections 2.4 and 2.5, respectively. This chapter is concluded in Section 2.6.

2.1 Related Work

Radio mapping approaches rest on two broad thematic pillars – use of analytical propagation models for *a priori* prediction of RSSI complemented by measurement-driven *a posteriori* techniques. The performance of propagation models has been investigated earlier in [47, 48]. Recently in [28], authors systematically analyzed the accuracy of various propagation models using a large dataset. Data-driven spatial interpolation with statistical methods rests on the work of Daniel Krige originally developed for mining applications, which is later applied to other fields such as soil science, hydrosciences, and radio mapping [49–53].

The comparative use of predictive path loss models (such as the FCC Curves and the LR model) and Kriging based approaches for RSSI estimation has only a sparse recent history. In [45], authors compared the RSSI estimation performance of the LR model against Kriging for a single TV source and showed that Kriging achieves better performance than propagation models with a small amount of measurements. The authors further analyzed the multi-transmitter scenario and empirically demonstrated the advantages of Kriging in [46]. Unlike [52], we do not track (slow channel fading) variations and defer investigation of temporal interpolation to future work. In this work, we attempt a structurally similar exercise specifically for the mapping of TV channels. We compare the prediction accuracy of the FCC curves and the LR point-to-point model in predicting available channels. We also conducted a measurement campaign in TV bands for a typical sub-urban region in Seattle,

WA of approx. 23 sq. km and extended Kriging techniques for boundary estimation – for comparison against model based predictive techniques.

2.2 Spatial Interpolation – Kriging

The RSSI (in dBm) at a point in a region of interest $D \in \mathbb{R}^2$ is modeled as a random field $Z(\mathbf{x})$, and any set of measured RSSI values $\{Z(\mathbf{x}_i) : i = 1, 2, ..., n\}$ is considered a realization of the underlying random process. One of the most widely used Kriging techniques, called Ordinary Kriging (OK), models $Z(\mathbf{x})$ with a mean field μ and a residual $\delta(\mathbf{x})$, that is,

$$Z(\mathbf{x}) = \mu + \delta(\mathbf{x}), \mathbf{x} \in D, \tag{2.1}$$

where μ is an unknown constant. In radio mapping, one may interpret μ as being determined by the path loss and large-scale fading effects and $\delta(\cdot)$ as possible sampling errors. In OK, $Z(\mathbf{x})$ is assumed to be *intrinsically stationary*, i.e.,

$$\mathbb{E}[Z(\mathbf{x})] - \mathbb{E}[Z(\mathbf{x} + \mathbf{h})] = 0, \tag{2.2}$$

$$\mathbb{E}[(Z(\mathbf{x}) - Z(\mathbf{x} + \mathbf{h}))^2] = 2\gamma(\mathbf{h}), \tag{2.3}$$

where $\gamma(\mathbf{h})$ is the *semivariogram* and $\mathbf{h}$ is the *distance lag* between two locations[2]. Generalized Kriging techniques drop this constant-mean assumption by applying a varying-mean model (e.g., Universal Kriging). In this work, we report results using OK (and defer investigation of other Kriging methods to future work).

2.2.1 Semivariogram $\gamma(h)$

The semivariogram $\gamma(h)$ captures the spatial continuity or correlation of the signal field, i.e., two points closer in space tend to have more correlated RSSI values than those farther apart.

[2] $\mathbf{h}$ is a vector with an amplitude and direction. A semivariogram that considers directions is called an anisotropic semivariogram, otherwise, isotropic. In this work, we consider isotropic semivarograms and leave anisotropy for our future work.

Constructing empirical semivariogram $\hat{\gamma}(h)$ from measured data

In this study, we adopt the Cressie-Hawkin robust estimator [54] given as below:

$$\hat{\gamma}(h) = \frac{1}{2} \cdot \frac{\left\{ \frac{1}{N(h)} \sum_{N(h)} (Z(\mathbf{x}_i) - Z(\mathbf{x}_j))^{1/2} \right\}^4}{(0.457 + 0.494/N(h))}, \tag{2.4}$$

where $\mathbf{x}_i$ and $\mathbf{x}_j$ are locations that are separated by approximately h and $N(h)$ is the total number of such pairs. Compared to the classical estimator used in [50], the Cressie-Hawkin estimator is more robust to atypical observations and outliers [54].

Fitting $\hat{\gamma}(h)$ with parametric models

The next step is to fit $\hat{\gamma}(h)$ with parametric models, such as exponential, Gaussian, spherical, and cubic models. For example, the exponential model is defined as:

$$\gamma(h) = a + (s - a) \left(1 - e^{-3h/r}\right), h \geq 0, \tag{2.5}$$

where the nugget a represents the discontinuity around the origin caused by sampling errors and small-scale variability, the range r is the distance where the model first flattens out, and the sill s is the limit of $\gamma(h)$ when h goes to infinity, which measures the maximum variance between two points that are far apart. The Weighted Least Squares is performed to determine the best parameters for each model, using the available package in `geoR` [55].

Choosing the best fitted model

To find the best among competing fitted models, we cross-validate each fitted model with the same training dataset used for semivariogram estimation. A popular cross-validation (CV) technique called the leave-one-out CV works as follows: each and every data point is excluded from the training dataset, whose value is then predicted by OK with the proposed model using the remaining data and compared with its true value. The one with the smallest mean squared error (MSE) is selected as the best model.

2.2.2 Interpolation

In OK, the predicted value $\hat{Z}(\mathbf{x}_0)$ at an unmeasured location $\mathbf{x}_0$ is a linear combination of the measured values at nearby locations $\{Z(\mathbf{x}_i) : i = 1, 2, ..., n\}$, that is,

$$\hat{Z}(\mathbf{x}_0) = \sum_{i=1}^{n} \omega_i Z(\mathbf{x}_i), \tag{2.6}$$

where the weights $\{\omega_i\}$ are normalized (i.e., $\sum_{i=1}^{n} \omega_i = 1$) so that the estimator is unbiased. The prediction error is quantified by the MSE:

$$\sigma_E^2(\mathbf{x}_0) = E[(\hat{Z}(\mathbf{x}_0) - Z(\mathbf{x}_0))^2] \tag{2.7}$$

$$= -\gamma(0) + 2\sum_{i=1}^{n} \gamma(\mathbf{x}_i - \mathbf{x}_0) - \sum_{i=1}^{n}\sum_{j=1}^{n} \omega_i \omega_j \gamma(\mathbf{x}_i - \mathbf{x}_j), \tag{2.8}$$

The minimization of MSE $\sigma_E^2(\mathbf{x}_0)$ with respect to $\{\omega_i\}$ under the normalization constraint leads to a set of linear equations, solving which results in the optimal values of $\{\omega_i^*\}$:

$$\begin{pmatrix} \omega_1 \\ \omega_2 \\ ... \\ \omega_n \\ \lambda \end{pmatrix} = \begin{pmatrix} \gamma(d_{11}) & ... & \gamma(d_{1n}) & 1 \\ \gamma(d_{21}) & ... & \gamma(d_{2n}) & 1 \\ ... & ... & ... & ... \\ \gamma(d_{n1}) & ... & \gamma(d_{nn}) & 1 \\ 1 & ... & 1 & 0 \end{pmatrix}^{-1} \cdot \begin{pmatrix} \gamma(d_{01}) \\ \gamma(d_{02}) \\ ... \\ \gamma(d_{0n}) \\ 1 \end{pmatrix}, \tag{2.9}$$

where $d_{ij} \equiv |\mathbf{x}_i - \mathbf{x}_j|$ is the Euclidean distance between locations i and j and λ is the Lagrange parameter used to enforce the normalization constraint. The minimized MSE is called the *Kriging variance*, which represents the prediction uncertainty at location $\mathbf{x}_0$.

2.3 Measurement Campaign

A vehicle-based measurement campaign was conducted over a 4.6 km-by-5 km sub-urban area (Figure 2.1) with a typical geographical layout (e.g., streets, trees, buildings) in Seattle lasting two and a half days. Our goal is to evaluate the efficacy of Kriging in estimating RSSI and coverage boundaries for TV transmitters. A total of 31 permissible 6-MHz UHF channels (CH 21-51) from 512 to 698 MHz were sampled at a total of 240 different locations.

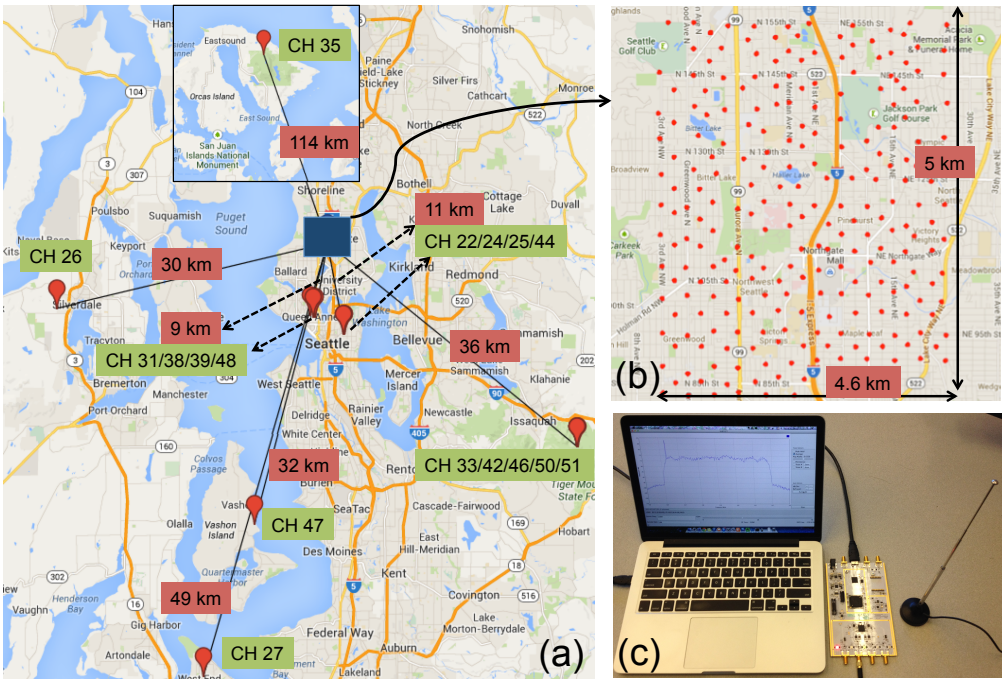

Figure 2.1: (a) Locations of TV transmitters whose TV service regions cover the sampled region according to the FCC curves. (b) 240 sample locations (in red dots). (c) Spectrum analyzer that consists of a laptop, a USRP B210 [1], and a 3 dBi omni-directional antenna.

2.3.1 Equipment and Setup

During the measurement campaign, the antenna of the spectrum analyzer (Figure 2.1) was securely mounted on the top of a van. The resulting antenna height was around 2.2 meters above ground. In order to calibrate the spectrum analyzer, we fed tones with known signal power at a known frequency using a signal generator into the spectrum analyzer. We then recorded I/Q samples, estimated uncalibrated signal power at the corresponding bin, and computed the average offset based on 900 measurements. In order to determine the noise level, we fed nothing to USRP and estimated the calibrated signal strength over a 6-MHz channel. The maximum signal strength (with noise only) out of 500 measurements was taken as the noise level.

2.3.2 Sampling Design

We adopted a grid sampling design and determined measurement locations as follows. First, we defined the region of interest and generated a "uniform" (equilateral triangular) sample grid similar to [50]. To balance opportunity costs (e.g., labor, time etc.) and interpolation resolution, a grid spacing of approximate 350 meters was chosen, resulting in a total of 240 sample locations. However, due to various physical constraints (e.g., roads, buildings, trees etc.), we were not able to comply with the original sampling plan strictly, and thus the eventual sampling layout appeared a little irregular at many places. That being said, our measurement campaign reflected the complexity of practical sampling over a large geographical region and the irregularity in obtained data. In practice, we did not follow any particular sampling order and sampled in a way that was smooth and efficient.

2.3.3 Measurement Methodology

Our measurement consisted of two phases: i) I/Q sample collection, and ii) energy-detection-based post-processing. In the first phase, we prepared a Python script which tuned USRP to the center frequency of a 6 MHz channel and sampled the signal at a rate of 8 MHz for 0.5 seconds. The main reason of over-sampling a channel was to minimize FFT edge effects by dropping the first and last 12.5% bins of obtained periodograms (up to a total of 25% bins – 2 MHz) later at the post-processing stage.

Raw I/Q samples for a single channel were then stored in shorts (i.e., two bytes for an I or Q sample), generating a data file of size 16 MB. After sampling a channel, the script waited for 0.5 seconds before switching to the next one to ensure successful tuning. Hence, it took approximately 30 seconds to perform a complete scan for 31 channels.

The script varied a key parameter called the USRP gain (ranging from 0 to 72) to adjust SNR when sampling signals, especially weak ones. If the targeted signal at the sampled location is strong, a high gain would cause Analog-Digital-Conversion (ADC) saturation, distorting power spectral density (PSD) and RSSI data. In order to do avoid possible ADC

saturation for any channel at any location, we set the gain to a conservative value of 26. On the other hand, for a particular channel (CH 35) that exhibits weak signals, we chose a higher gain of 36 to obtain more accurate RSSI readings. Given the above USRP settings, the measured noise levels were -82.29 dBm and -92.92 dBm for gains of 26 and 36 respectively.

In the post-processing phase, we used MATLAB to perform energy detection based on I/Q samples. In addition to over-sampling, we also applied Blackman-Harris windowing before performing FFT to further minimize the effect of spectral leakage. The number of FFT bins was 2048 for a 8-MHz band (before truncation), and the frequency resolution of was 3.9 KHz per bin. After dropping 25% of bins, a total of 1536 bins were obtained for a 6 MHz channel. Then we computed PSD by averaging 100 periodograms, and the equivalent sensing duration was 25.6 ms[3]. Eventually, we could get a 240-by-3 matrix of output data for each channel containing $(X, Y, RSSI)$ at 240 locations[4].

2.4 RSSI Estimation

RSSI estimation is the building block for predicting coverage regions of primary sources. In this section, we demonstrate the application of OK to RSSI prediction and quantify its performance improvements over the DBA models (i.e., FCC Curves and Longley-Rice).

2.4.1 An OK Example

Figure 2.2 illustrates the general procedure of Kriging. After sampling and post-processing, the (truncated) empirical semivariogram $\hat{\gamma}(\mathbf{h})$ (Figure 2.3(b)) was estimated from measured data using the robust estimator in Eq. (2.4). The lag spacing was 0.35 km, which was same as the sample spacing, and 1/3 of the maximum pairwise distance was chosen as the maximum lag distance (2.3 km). Next, four popular models, i.e., exponential, Gaussian, spherical and cubic models were fitted to $\hat{\gamma}(\mathbf{h})$, and the exponential one was selected based on CV results.

[3]Different from real-time spectrum sensing, sensing duration was not critical for Kriging applications. Hence, we chose a relatively long sensing duration to achieve good performance of energy detection.

[4]Locations were converted from geo-coordinates with respect to a reference point.

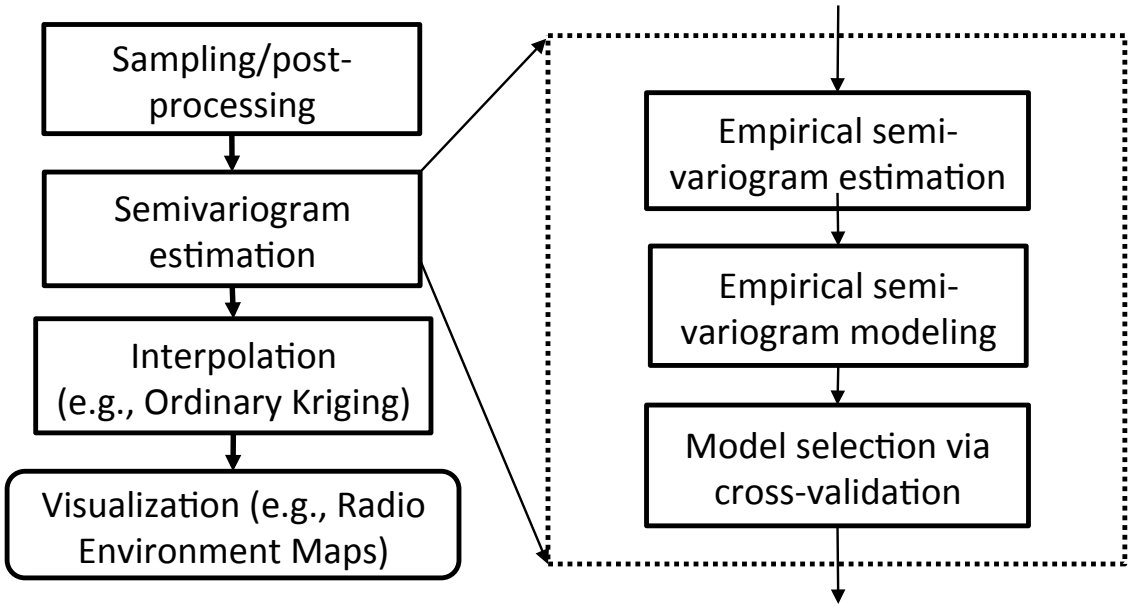

Figure 2.2: General procedure of radio mapping using Kriging. First of all, spatial sampling will be conducted over the geographical region of interest to collect spectrum measurements, followed by necessary post-processing. Then empirical semivariogram can be estimated from measurements and fitted by parametric semivariogram models. Once a reasonable semivariogram is in place, it can be used to interpolate the RSSI value at an unmeasured location from available measurements and eventually generate a radio map for visualization.

In order to visualize a radio environment map, the geographical region is discretized into a mesh of grid points at a chosen resolution. For example, with a resolution of 0.03 km, there are a total of over 28,400 points for the target region. We then interpolated the RSSI value for each grid point and obtained its corresponding Kriging variance. Finally, we plotted both Kriging predictions and variances on maps as shown in Figures 2.3(c) and 2.3(d).

2.4.2 Kriging Versus DBA Models

In order to compare the performance between OK, LR and the FCC Curves, we investigated four channels (CH 25, 31, 33, 50) with diverse channel characteristics (Table 2.1), whose average SNR exceeded 15 dB so that noise power could be omitted. Representing the simplest

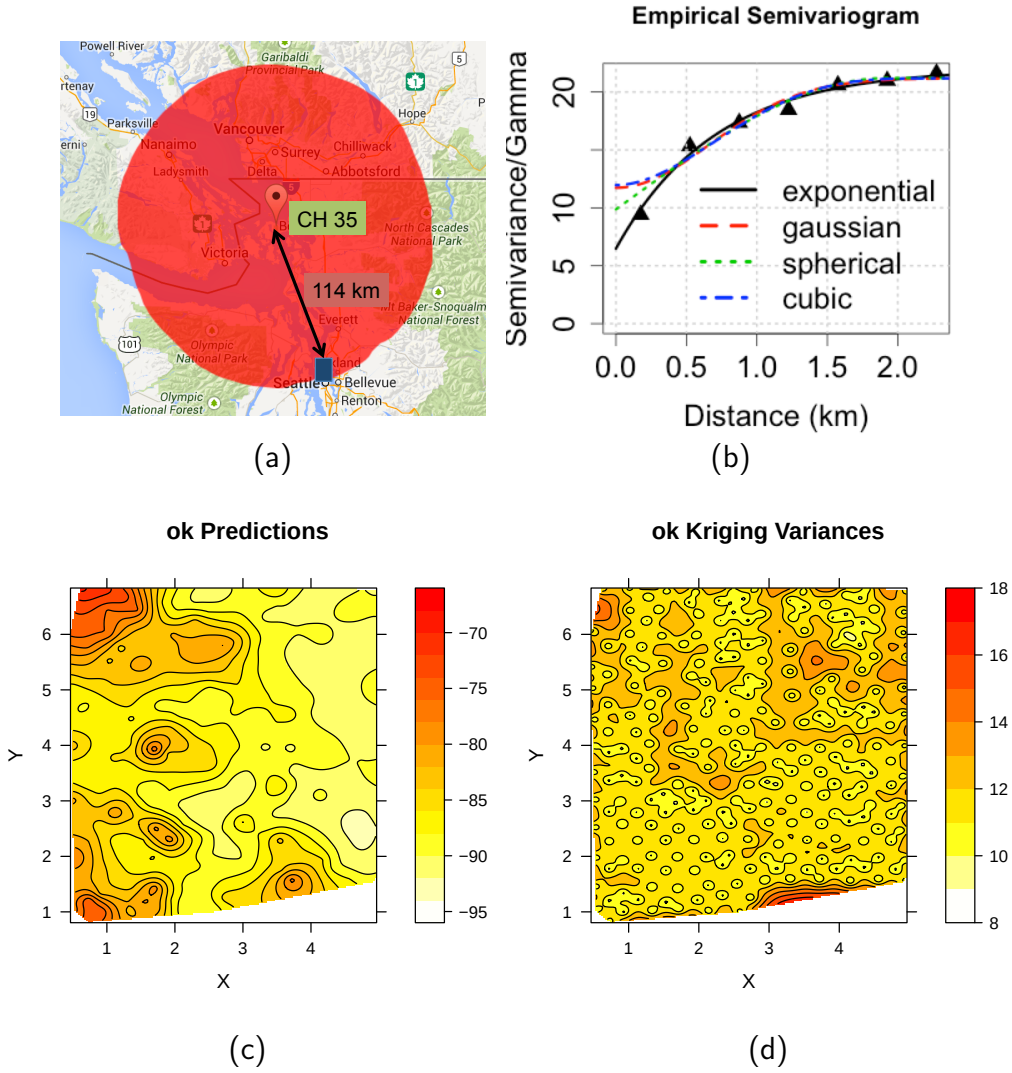

Figure 2.3: (a) TV transmitter of CH 35 and its DBA coverage region (in red). (b) Empirical semivariogram and four fitted parametric models (exponential, Gaussian, spherical, and cubic). Based on CV results, the exponential model was chosen with a nugget of 6.48, a range of 2.11, and a sill of 22.02. (c) RSSI map. (d) Kriging variance map. Red indicates large values, while white implies small values. Lines in (c)/(d) are contours representing different RSSI/Kriging variance values (not shown due to limit of space).

CH	ERP	HAAT	Dist.	μ	σ	ME (dB)			RMSE (dB)			OK Gain
	(dBW)	(m)	(km)	(dBm)	(dB)	OK	LR	FC	OK	LR	FC	Over FC
25	60.00	290	11.32	-50.34	7.11	0.02	31.59	27.27	5.15	32.45	28.10	22.95
31	58.45	218	9.48	-53.46	8.34	0.00	30.65	26.57	5.79	31.51	27.92	22.13
33	56.02	716	35.95	-68.86	6.59	-0.07	27.86	21.60	5.21	29.06	22.63	17.42
50	53.08	719	35.98	-52.06	8.87	0.00	14.99	8.95	5.72	19.78	12.75	7.03

Table 2.1: Performance comparison between OK, LR and FCC Curves (FC) in terms of mean error (ME) and root mean squared error (RMSE). The OK gain is defined as the amount of RMSE reduced by OK compred to FC. The term ERP stands for effective radiate power, and HAAT stands for height above average terrain. Note that Kriging performs significantly better than DBA models.

method, OK's performance may serve as the lower-bound of the Kriging family. To ensure fair comparison, the following equation was used to convert fields strength predictions (dBμV/m) of DBA models to signal strengths (dBm):

$$P_{dBm} = E_{dB\mu V/m} - 20logf_{MHz} + G_{dBi} - 77.2 \tag{2.10}$$

where f_{MHz} is the center frequency of a channel and $G_{dBi} = 3\ dBi$ is the antenna gain.

The leave-one-out CV technique was applied and two metrics were adopted to quantify the prediction performance: i) the bias or mean error (ME) – the average difference between predicted and measured RSSI (ground truth), and ii) the root mean squared error (RMSE) between the prediction and ground truth.

We have two observations from results in Table 2.1. First, OK achieves a ME value very close to 0, since it is an unbiased estimator. While FC causes a smaller ME than LR, both over-estimate the RSSI and lead to a ME as high as 31.59 and 27.27 dB, respectively. Second, OK consistently produces a RMSE of 5-6 dB, which is significantly better than DBA models, primarily because DBA models do not explicitly account for environmental obstructions. In addition, we observe that the performance of DBA models differs from channel to channel,

thus making OK gain channel-dependent.

2.5 Boundary Estimation

In this section, we introduce two metrics to measure the boundary estimation performance and compare Kriging against the DBA models and the popular k-Nearest Neighbor (k-NN) classifier, applied to our problem.

2.5.1 Performance Metrics

TV coverage regions are essentially decision regions (Figure 2.3(a)) defined by their boundaries, based on which we may predict at a given location whether a channel is either available for unlicensed access (labeled with 1, TV service unavailable) or occupied (labeled with 0, TV service available). In DBAs, the channel availability label is determined via simple thresholding as follows:

$$\hat{L}_{DBA}(\mathbf{x}) = \begin{cases} 1, & \text{if } \hat{Z}_{DBA}(\mathbf{x}) < \Gamma \\ 0, & \text{otherwise} \end{cases} \tag{2.11}$$

where $\hat{Z}_{DBA}(\mathbf{x})$ is the predicted field strength (dBμV/m), $\hat{L}_{DBA}(\mathbf{x})$ the predicted label, and Γ a preset full-power DTV service threshold (i.e., 41 dBμV/m).

Hence, it is essentially a classification problem to determine channel availability at a given location. Given N measurements, we evaluate the performance of a classification scheme or boundaries via leave-one-out CV as follows. First, one data point is excluded from the entire dataset, whose label is predicted based on estimated boundaries derived from the remaining data. The measured RSSI value at that location is treated as ground truth, and its true label is obtained through thresholding. Comparing the predicted label against the true label, we get two types of errors:

- *Type I*: a channel is predicted to be occupied (0), when it is actually available (1).
- *Type II*: a channel is predicted to be available (1), when it is actually occupied (0).

We repeat the above procedure for each data point and count type-I/II errors for a particular boundary estimation scheme and arrive at:

- *Type I error rate* ϵ_1:
$$\epsilon_1 = \frac{\text{\# of Type-I Errors}}{\text{\# of True 1 Labels}}, \tag{2.12}$$
- *Type II error rate* ϵ_2 :
$$\epsilon_2 = \frac{\text{\# of Type-II Errors}}{\text{\# of True 0 Labels}}. \tag{2.13}$$

Notably, the cost of the two types of errors is *asymmetric* per the FCC ruling, and we seek to reduce ϵ_1 (i.e., missing spectrum opportunities), while keeping ϵ_2 (i.e., possible interference) below an acceptable limit.

2.5.2 Methods

Method I – DBA Boundary

To first predict the field strength at a given location from a TV transmitter, a DBA model takes engineering parameters such as the distance between transmitter and receiver, channel, effective radiate power, antenna height and patterns, as well as terrain data as inputs (for Longley-Rice), and outputs the field strength (dBμV/m) without any local measurements.

In order to further determine boundaries of a transmitter, a DBA finds the farthest point for each azimuth value (0-360 degrees centered at TV transmitter location), whose predicted field strength is above the TV service threshold (41 dBμV/m). By connecting those points with a continuous line, a DBA is able to obtain boundaries that define a TV coverage region.

Method II – k-NN Boundary

k-NN normally takes labels of measured (training) data with respect to a threshold Γ as true inputs and predicts the label of an unmeasured (testing) location as follows. First, it searches for the k nearest neighbors for the given location based on Euclidean distance and

uses the majority label among k neighboring labels as the predicted label (any tie is broken randomly).

Since k is user-defined, the optimal value k^* can be determined from the training dataset through CV as follows. First, the entire training set is randomly divided into M (e.g., 10) subsets. For a given k, each and every subset are excluded, whose labels are predicted based on true labels of other four subsets. Then we could count type-I/II errors and compute ϵ_1/ϵ_2 accordingly. Different values of k from 1 to k_{max} (some large value) are examined, and the one with minimum ϵ_2 (with higher priority) is chosen as k^*.

Obviously, k-NN boundary estimation performance evaluated with the testing dataset in terms of ϵ_1 and ϵ_2 largely depends on Γ. Hence, one way to control k-NN boundaries is to use an adjusted threshold $\Gamma' = (1+\alpha)\Gamma$ to label training data instead of Γ, where $\alpha \geq 0$. For example, if $\Gamma = -84$ dBm and we want to make k-NN more conservative in predicting available channels, we may choose a lower $\Gamma' = -85$ dBm ($\alpha = 1.2\%$).

Method III – Kriging Boundary

We use Eq. (2.11) to produce a labeling rule for Kriging by recognizing the prediction uncertainty at a given location as follows:

$$\hat{L}_{Kri}(\mathbf{x}) = \begin{cases} 1, & \text{if } \hat{Z}_{Kri}(\mathbf{x}) < \Gamma - \lambda \cdot \sigma(\mathbf{x}) \\ 0, & \text{otherwise} \end{cases}, \tag{2.14}$$

where $\sigma(\mathbf{x})$ is the Kriging standard deviation and $\lambda \geq 0$ is a control parameter. Given $Z(\mathbf{x}) > \Gamma$ (occupied) and $\hat{Z}_{Kri}(\mathbf{x}) < \Gamma$ (predicted to be available), $\lambda_{min} = (\Gamma - \hat{Z}_{Kri}(\mathbf{x}))/\sigma(\mathbf{x})$ is the minimum value to change the predicted label from 1 to 0 (no type II errors).

Note that the objectives of α in k-NN and λ in Kriging are consistent: the predicted RSSI at a given location has to be low enough to be labeled as 1 (available); otherwise, we would rather label it as 0 to avoid possible type II errors (even at the cost of increased type I errors). Their effects will be explored in the next section.

2.5.3 Controlling k-NN and Kriging Boundaries

In order to understand the impact of control parameters α and λ on k-NN and Kriging boundaries, we investigated CH 35 whose predicted boundary region via the FCC Curves falls within the measurement region. The TV service threshold Γ was set to be -84 dBm [19]. Note that the dataset for CH 35 collected with a USRP gain of 36 was used, as they better captured signal power at different locations. We varied α and λ and computed corresponding ϵ_1 and ϵ_2 with the approach described in Section 2.5.1.

	$\alpha(\%)$	**0**	**2.0**	**4.0**	**6.0**	**7.0**
	ϵ_1 (%)	12.8	16.7	27.2	47.8	59.4
***k*-NN**	$\epsilon_2(\%)$	43.3	38.3	18.3	8.3	5.0
	sum (%)	56.1	55.0	45.5	46.1	64.4
	λ	**0**	**0.40**	**0.80**	**1.03**	**1.34**
	ϵ_1 (%)	10.0	16.7	30.0	41.7	53.9
Kriging	ϵ_2 (%)	46.7	31.7	18.3	10.0	5.0
	sum (%)	56.7	48.4	48.3	51.7	58.9

Table 2.2: Impact of control parameters α and λ on type-I/II error rates ϵ_1/ϵ_2. $\Gamma = -84$ dBm. When α and λ increase, ϵ_2 is reduced and ϵ_1 is increased for both k-NN and Kriging.

We observe from Table 2.2 that by increasing α and λ, ϵ_2 may be effectively reduced. For instance, when $\alpha = 7.0\%$ and $\lambda = 1.34$, we become more conservative in predicting available channels, and ϵ_2 of both k-NN and Kriging boundaries is reduced to 5%. Second, there exists a trade-off between ϵ_1 and ϵ_2 when λ changes, as illustrated in Figure 2.4. For example, with $\lambda = 0.4$, a total of 9 type-II errors are reduced but 12 type-I errors are introduced.

Complete elimination of type-II errors for Kriging boundaries requires $\lambda = 2.00$, which would introduce a large amount of type-I errors. It implies that the predicted RSSI values at a few locations are much lower than the threshold and their true (measured) values, and it is Kriging's under-estimation at those locations that causes type-II errors. In order to determine

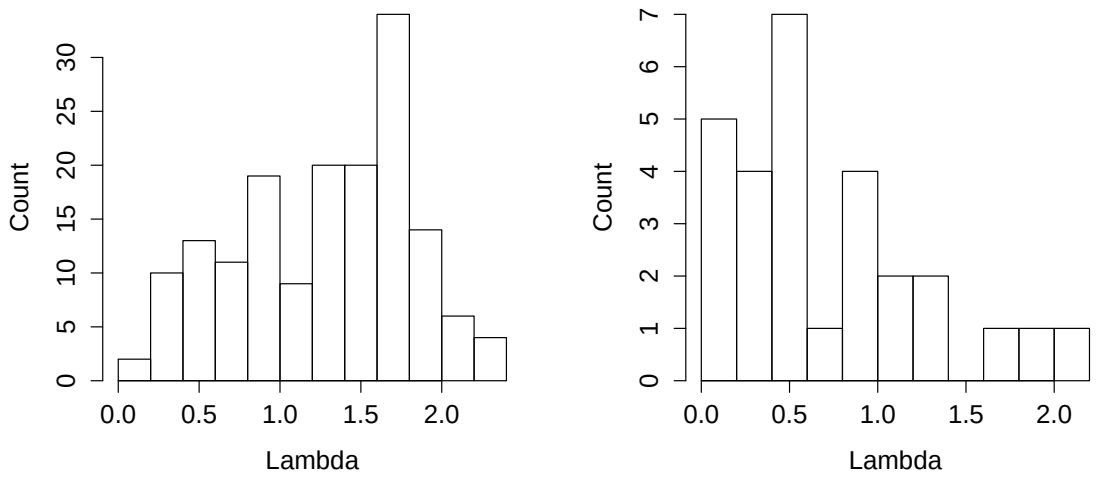

(a) Introduced type I errors

(b) Reduced type II errors

Figure 2.4: Histogram of λ_{min} that changes a predicted label from 1 (available) to 0 (occupied) for $\Gamma = -84$ dBm. In (a), both predicted and true labels are 1, and changes in predicted labels from 1 to 0 introduce type I errors. In (b), predicted labels are 0 while the true labels are 1 (type-II errors). Hence, changes in predicted labels from 1 to 0 eliminate type-II errors.

whether they are outliers (possibly due to sampling errors), additional measurements may be conducted at the same and nearby locations to improve the RSSI estimation and subsequent boundary estimation.

2.5.4 Performance Comparison

In this experiment, we compared the performance of Kriging, k-NN and DBA boundaries for CH 35. Based on both FCC Curves and Longley-Rice boundaries, the channel is occupied at all locations within the sampled region (i.e. predicted labels are always 0), leading to $\epsilon_2 = 0$ while $\epsilon_1 = 100\%$. To ensure fair comparison, we adjusted Kriging and k-NN boundary

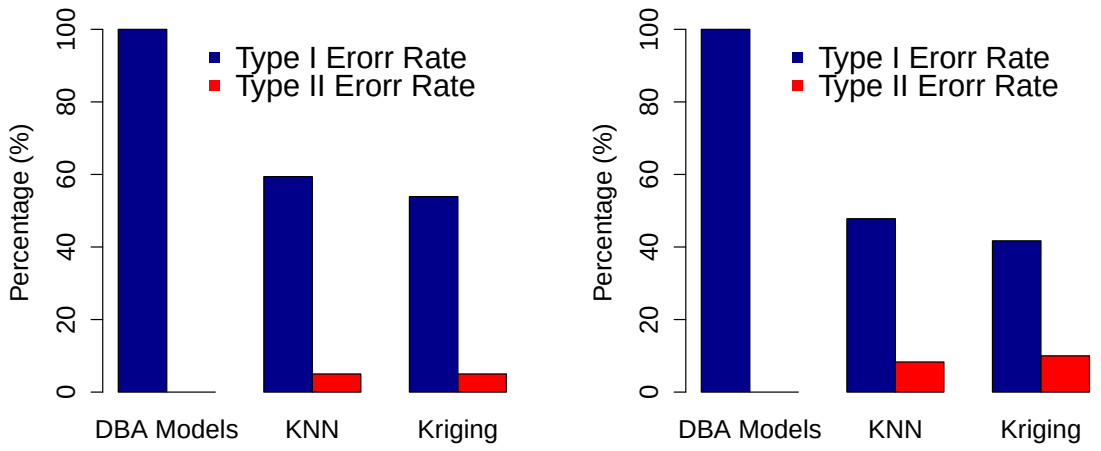

(a) $\epsilon_2 \leq 5\%$ (b) $\epsilon_2 \leq 10\%$

Figure 2.5: Comparison between DBA models, k-NN and Kriging boundaries for Γ = -84 dBm. (a) $\alpha = 7.0\%$, $\lambda = 1.34$. (b) $\alpha = 6.0\%$, $\lambda = 1.03$.

estimation in such a way that ϵ_2 was no larger than 5% or 10%, and compared corresponding ϵ_1 when $\Gamma = -84$ dBm.

As shown in Figure 2.5, Kriging achieves significant performance improvement over the DBA boundary prediction with gains of 46.1% and 58.3% in ϵ_1 for $\epsilon_2 \leq 5\%$ (i.e., fewer than 3 type II errors) and 10% (i.e., fewer than 6 type II errors) respectively. Although k-NN boundaries cause 6% higher ϵ_1 than Kriging, they also perform very well compared to DBA prediction. The primary reasons that Kriging and k-NN have very close performance are that i) both fundamentally use spatial (neighbor-based) information, and ii) are measurement-driven, which better captures the local environment. Nevertheless, Kriging uses more soft information (i.e. RSSI values) than binary labels (as in k-NN) and from more than k neighbors.

Figure 2.6 illustrates k-NN and Kriging boundaries using all data points for $\Gamma = -84$

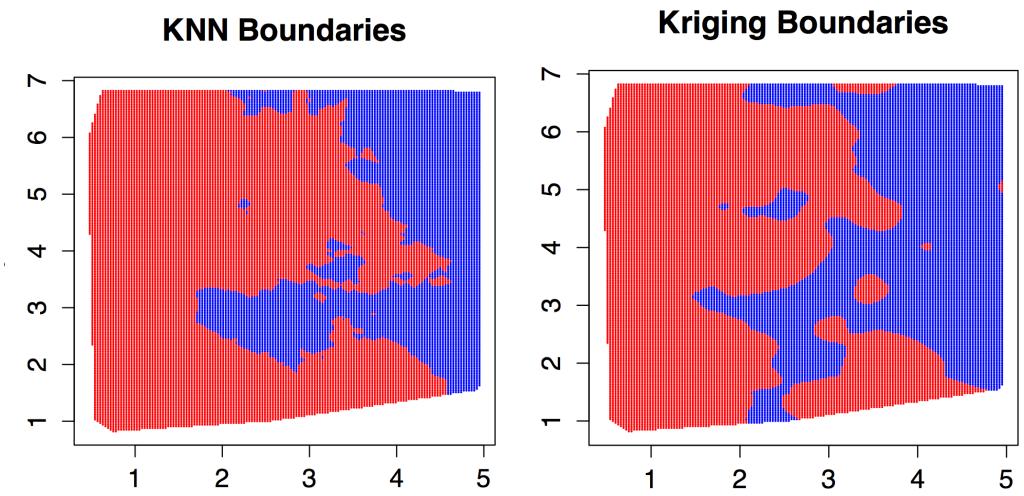

(a) $\epsilon_2 \leq 5\%$ (b) $\epsilon_2 \leq 5\%$

Figure 2.6: Coverage regions (in red) defined by (a) k-NN ($\alpha = 7.0\%$) and (b) Kriging boundaries ($\lambda = 1.34$) for $\Gamma = -84$ dBm. The non-coverage region is in blue.

dBm. While the coverage region predicted are very similar, Kriging appears to produce more smooth boundaries as compared to k-NN. This is mainly because k-NN considers the nearest k neighbors, and thus two nearby locations could end up with different labels, if the majority of their respective neighborhoods have different labels. Furthermore, both tend to create red/blue "holes" due to data points with large/low RSSI values that are very different from their neighbors.

2.5.5 Impact of TV Service Threshold

While the TV service threshold is chosen to be -84 dBm by the FCC, it would be interesting to compare k-NN and Kriging boundaries for different Γ values. The results are shown in Table 2.3. We can see that despite of fairly close performance, Kriging performs generally better than k-NN in estimating boundaries with a gain as high as 16.5%. More importantly, both achieve significant and consistent performance improvement over DBA models.

	Γ **(dBm)**	-83	-84	-85	-86
	k**-NN**	53.9	59.4	58.3	74.8
$\epsilon_2 \leq 5\%$	**Kriging**	56.0	53.9	52.6	58.3
	Gain	-2.1	5.5	5.7	16.5
	k**-NN**	47.1	47.8	46.3	49.7
$\epsilon_2 \leq 10\%$	**Kriging**	39.3	41.7	39.4	49.1
	Gain	7.8	6.1	6.9	0.6

Table 2.3: ϵ_1 (%) of k-NN and Kriging boundaries for different TV service thresholds for a bounded ϵ_2. The gain is the reduced amount in ϵ_1 of Kriging compared to k-NN.

2.6 Conclusion and Future Work

In this study, we quantified RSSI prediction performance for both DBA models and Kriging. We compared the performance of Kriging boundaries against DBA and k-NN boundaries with data collected at 240 locations over a 4.6 km-by-5 km sub-urban area. Our results show that since empirical DBA models do not take into account local obstructions, they tend to over-estimate RSSI, while measurement-based Kriging achieves consistently good performance. Furthermore, Kriging boundaries achieves a type-I error rate of 46.1%, which is 6.5% lower than DBA and k-NN boundaries respectively while keeping type-II error rate under a low limit (5%) for a given service threshold (-84 dBm), and such improvement also exists for different thresholds.

There are several interesting future directions. First, OK assumes a constant mean and isotropic semivariogram, while more advanced Kriging techniques can relax these assumptions and potentially improve prediction accuracy. For instance, the Universal Kriging [56] assumes a general polynomial trend model by expressing the mean as a linear combination of polynomials. Suitable path loss models such as Longley-Rice can also be used for the mean field component, which mitigates adverse effects of non-stationarity in measurement data.

Second, current radio mapping focuses on spatial interpolation, while wireless radio sig-

nals exhibit temporal variations due to shadowing and changes on the transmitter side (e.g., power) etc. Hence, it would be interesting to interpolate RSSI in both space and time based on real-time measurements collected from a network of low-cost spectrum sensors.

Third, as measurements are collected over a wider geographical area, significant disparities in the observed RSSI begin to appear. For example, some isolated locations report very weak RSSI (which are likely to be dominated by noise) that is not well-represented by path loss models. This implies the heuristic – apply Kriging post classification to the inside/outside-coverage regions separately to obtain more reliable Kriging results [57] and continue performing joint classification and interpolation iteratively until convergence.

Chapter 3

AUCTION-BASED CROWDSENSING FOR SPATIAL-STATISTICS-BASED RADIO MAPPING

In this previous chapter, we considered the problem of applying Kriging, a measurement-driven spatial-statistic-based technique, to estimating RSSI and coverage boundaries in order to construct accurate radio maps for white space networking. We showed that the Kriging-based approach outperforms the DBA models in coverage estimation by significantly reducing the type-I error rate, while keeping the type-II error rate under a certain limit.

Moving forward, Kriging can potentially facilitate white space networking by enhancing real-time radio mapping and improving spatial-temporal white space identification. It can also provide accurate estimation of protection areas for incumbents and licensed SUs in other shared bands including the 3.5 GHz CBRS band. However, Kriging requires a reasonable amount of local spectrum sensing data in the geographical region of interest, scaling such data collection via (either static or dynamic) sensors or measurement campaigns to wide-aware spectrum sensing inevitably meets cost limitations. One approach of low-cost wide-area spectrum sensing is to leverage *crowdsensing*, that is, outsourcing sensing tasks to spatially distributed users in the targeted region with mobile devices that are outfitted with spectrum sensors. Prior works such as [58–60] on crowdsensing implicitly assumes voluntary user participation, which may not be true in practice, because users would have to contribute their own resources (e.g., computing power, storage, and battery) for sensing and thus expect some form of compensation in return.

In this chapter, we study the problem of incentiving users to participate in crowdsensing for spatial-statistics-based radio mapping under the *reverse-auction* framework [61–64]. In this framework, participating users want to sell their location-specific spectrum data to the

platform (a centralized server that collects spectrum data and performs radio mapping), each of which has a privately known sensing *cost* and receives a *payment* when selected. We consider *self-interested* users who tend to declare higher prices (*bids*) than their true costs in order to maximize their own *utility* (i.e., payment minus true cost). We develop a *computationally efficient*, *individually rational*, *budget feasible*, and *truthful* incentive mechanism for crowdsensed radio mapping. We make the following specific contributions:

- We propose a crowdsensing system that periodically acquires spectrum data from users to construct radio maps via spatial statistics under a budget constraint.

- We develop an auction-based budget-free mechanism with a cardinality constraint and show that it is truthful, computationally efficient, and individually rational. We further develop a budget-feasible mechanism by translating the budget constraint into the best cardinality constraint using the bisection method.

- We conduct extensive simulations to evaluate the performance of the proposed mechanism and compare it against the state-of-art budget-feasible mechanism in [64]. Our results reveal that the proposed mechanism makes full use of the budget and performs significantly better compared to the baseline with improvements of 18%-22% in terms of maximizing the average prediction error variance (Kriging variance) reduction.

The remainder of this chapter is organized as follows. Section 3.1 reviews related work and Section 3.2 introduce preliminaries for this work. Our system model and mechanism are presented in Sections 3.3 and 3.4, respectively. Simulation results are provided in Section 3.5. This chapter is concluded in Section 3.6.

3.1 Related Work

In crowdsensing, users are usually assumed to be self-interested and tend to take strategic actions. Hence, it is desirable to design a truthful mechanism that motivates users to reveal their true costs. In [62], authors proposed an auction-based truthful mechanism for a scenario

where sensing tasks have predetermined location tags and values, and users are only allowed to compete for tasks within their own coverage regions. However, the implicit assumption was that collected data was not location-specific and the budget constraint was not considered. In [65] and [66], similar geometric coverage models for tasks and users were considered, but they do not fit our radio mapping scenario. Instead, we consider a general task without location tags and all users are allowed to compete for it. Based on user locations, the spatial sampling approach is taken to select users.

In [63,64], authors proposed truthful and budget-feasible incentive mechanisms for general submodular monotone functions. Their mechanisms adopt the proportional share allocation rule, and winner selection stops when the bid of next user exceeds a proportional share of its contribution. Although this rule provides an upper bound on the actual payment, which ensures budget-feasibility, the bound may be loose and thus the mechanism creates budget surplus. In our mechanism, we adopt the bisection method to make full use of the budget.

3.2 Preliminaries

In this section, we briefly review Kriging approach for spatial interpolation and describe the spatial sampling design problem for Kriging. We then introduce the Myerson's characterization theorem that specifies the sufficient and necessary conditions for truthfulness.

3.2.1 Statistical Interpolation - Kriging

As described in the previous chapter (Section 2.2), Kriging employs a Gaussian random field model for RSSI at a point x, which is given by $Z(x) = \mu(x) + \delta(x)$, where $\mu(x)$ and $\delta(x)$ are the mean and the residual at location x, respectively. The former term captures path loss and shadowing at different locations, and the later represents possible sampling errors.

At the core of this engine is the semivariogram $\gamma(\cdot)$ that captures the variance between two points as a function of their distance. In practice, $\gamma(\cdot)$ is estimated from measurements and then fitted with parametric models such as spherical and exponential models. In OK, $Z(x)$ is assumed to be intrinsically stationary, i.e., $\mathbb{E}[Z(x)] = \mu(x) = \mu$ and $\mathbb{E}[(Z(x_1) -$

$Z(x_2))^2] = 2\gamma(h)$, where μ is an unknown constant and $h = ||x_1 - x_2||$ (assuming isotropic semivariograms). The relationship between $\gamma(h)$ and the covariance function $C(h)$ is $C(h) = C(0) - \gamma(h)$. In this work, we focus on OK due to its popularity.

Given a set of measurements $\mathcal{A}$ at locations $x_1, x_2, ..., x_n$, the predicted value at an unmeasured point x_0 is given by $\hat{Z}(x_0) = \sum_{i=1}^{n} \omega_i Z(x_i)$. Minimization of the MSE $\mathbb{E}[(\hat{Z}(x_0) - Z(x_0))^2]$ with respect to $\{\omega_i\}$ leads to a set of linear equations. The optimal coefficients are given by $\omega^* = (\omega_i^*)_{i\in\mathcal{A}} = \Sigma_{\mathcal{A}\mathcal{A}}^{-1}\Sigma_{\mathcal{A}\mathbf{x}_0}$, where $\Sigma_{\mathcal{A}\mathcal{A}}$ is the covariance matrix and $\Sigma_{\mathcal{A}\mathbf{x}_0}$ is the vector of cross-covariances between $\{Z(x_i)\}$ and $Z(x_0)$. The minimized MSE, also called the Kriging variance (K-var), is given by

$$\sigma^2_{\mathbf{x}_0|\mathcal{A}} = \sigma^2_{\mathbf{x}_0} - \Sigma^T_{\mathcal{A}\mathbf{x}_0}(\Sigma^{-1}_{\mathcal{A}\mathcal{A}})^T\Sigma_{\mathcal{A}\mathbf{x}_0}, \tag{3.1}$$

where $\sigma^2_{\mathbf{x}_0}$ is the K-var when $\mathcal{A} = \emptyset$[1]. Since K-var measures the prediction uncertainty at an unmeasured location, it is often used as a estimator design metric, that is, a smaller K-Var value implies a better estimator.

3.2.2 Spatial Sampling Design

A classic spatial sampling design problem discussed in [67] is the following. Consider a set of candidate sample locations $\mathcal{C}$ and a set of unmeasured locations $\mathcal{D}$, which are often a grid discretization of a continuous region. The task is to choose a subset $\mathcal{A} \subseteq \mathcal{C}$ up to k elements that minimizes the average K-var over $\mathcal{D}$, or equivalently, maximizes the average K-var reduction[2] $\phi(\mathcal{A})$, which is given by

$$\phi(\mathcal{A}) = \frac{1}{|\mathcal{D}|}\sum_{x_0\in\mathcal{D}}\left(\sigma^2_{x_0} - \sigma^2_{x_0|\mathcal{A}}\right) \tag{3.2}$$

[1]Strictly speaking, $\sigma^2_{\mathbf{x}_0}$ is undefined according to Eq. (3.1) when $|\mathcal{A}| = 0$; when $|\mathcal{A}| = 1$, it depends on both $C(0)$ and μ, which is unknown. Due to this reason, `GeoR` [55], the widely-used geo-statistics library in R, requires at least two data points for Kriging. In our implementation, when $\mathcal{A} = \emptyset$ (no data points in the region of interest), we bypass the issue by introducing two data points that are very far away from the target region; for $|\mathcal{A}| = 1$, we simply add a second data point very close to the existing one.

[2]An alternative metric is the mutual information [68]. Since the two criteria share very similar properties such as submodularity and monotonicity, we focus on the average K-var reduction in this work. However, our discussion also extends to the mutual information criterion. In Chapter 4, we will consider the use of mutual information for spatial sampling design.

Since the problem $\max_{\mathcal{A}\subseteq\mathcal{C},|\mathcal{A}|\leq k}\phi(\mathcal{A})$ is NP-hard in general [69], it is difficult to compute the optimal solution. Nevertheless, the existence of structural properties in $\phi(\mathcal{A})$ including *submodularity* and *monotonicity* [69, 70] with respect to the cardinality of $\mathcal{A}$ allows us to obtain an approximate solution via heuristic-based (greedy) algorithms.

Formally, a set function $f : 2^{\mathcal{C}} \rightarrow \mathcal{R}$ is called submodular, if $f(\mathcal{A}\cup\{x\}) - f(\mathcal{A}) \geq f(\mathcal{B}\cup\{x\}) - f(\mathcal{B})$ for any $\mathcal{A}\subseteq\mathcal{B}\subseteq\mathcal{C}$ and any $x \in \mathcal{C}\setminus\mathcal{B}$. The notion of submodularity describes the diminishing returns behavior: adding a new element increases f more, if there are fewer elements so far, and less, if there are more elements. A set function $f : 2^{\mathcal{C}} \rightarrow \mathcal{R}$ is said to be monotone, if $f(\mathcal{A}) \leq f(\mathcal{B})$ for any $\mathcal{A}\subseteq\mathcal{B}\subseteq\mathcal{C}$. In fact, $\phi(\mathcal{A})$ is also non-negative. It was shown in [71] that for a submodular, monotone, and non-negative function, a greedy algorithm finds an approximate solution guaranteed to be within $1 - 1/e$ of the optimal solution, and no polynomial-time algorithm can achieve a better guarantee unless P = NP.

3.2.3 Myerson's Characterization Theorem

In mechanism design, truthfulness refers to a dominant strategy that incentives users to report true costs regardless of other users' bids [61]. Let the cost, bid and payment of user i be c_i, b_i and p_i, respectively. A mechanism $\mathcal{M}$ consists of a *selection* rule $\chi : (\mathbf{b}, \mathbf{x}) \rightarrow 2^{[n]}$, and a *payment* rule $\psi : (\mathbf{b}, \mathbf{x}) \rightarrow \mathcal{R}_+^n$, where $\mathbf{b}$ and $\mathbf{x}$ are the bid and location vectors respectively. Since the cost is the only private parameter, the sufficient and necessary conditions for truthfulness have been specified in the Myerson's characterization theorem [63, 72].

Theorem 3.1 (Myerson's Characterization)**.** *In single parameter domains, a mechanism $\mathcal{M} = (\chi, \psi)$ is truthful if and only if:*

1. *χ is monotone: $\forall i \in \Omega$, if $b_i' \leq b_i$ then $i \in \chi(b_i, b_{-i}, \mathbf{x})$ implies $i \in \chi(b_i', b_{-i}, \mathbf{x})$ for any given b_{-i}, that is, a winner keeps winning if it unilaterally decreases his bid, and*

2. *ψ pays winners the threshold amounts: $p_i = \sup\{b_i : i \in \chi(b_i, b_{-i}, \mathbf{x})\}$ for any given b_{-i}, that is, the payment is the maximum bid that still wins,*

where $b_{-i} = (b_j)_{j \neq i,\ j \in \Omega}$ *denote the bids of users except user* i*.*

A simple example is the single-good second-price (reverse) auction with private costs [61], where the user with the lowest bid is the only winner (selection rule), who is paid the second lowest bid (payment rule). We may verify its truthfulness with Myerson's characterization. First, the selection rule is monotone, that is, the winner still wins if it submits an even lower bid. Second, the winner is paid the threshold amount: if it submits a bid higher than the second lowest bid, it is no longer the winner. Hence, the second-price auction is truthful.

3.3 System Model

Figure 3.1 illustrates the proposed system for crowdsensed radio mapping. It consists of a centralized server called *platform*, and *users* equipped with mobile devices that are capable of spectrum sensing. Users are spatially distributed and connected to the platform. We assume that each user knows its current geo-location with high accuracy and is able to collect high-quality[3] spectrum data.

The platform seeks to acquire sensing data from users periodically for the spectrum band of interest. At the beginning of a period, the platform announces a sensing request *without* specific location tags, which contains detailed sensing instructions (such as center frequency, sampling rate etc.). Each user i in the desired region D can compete for the task, who will incur a privately known cost $c_i > 0$ for sensing. We assume no entry or any other overhead costs, that is, a user does not incur a fee to bid nor does it pay to communicate with the platform. Each user i who is interested in participation submits its current location x_i and a bid $b_i \geq c_i$, the minimum payment it is willing to accept. Denote the set of bidders as $\Omega = \{1, 2, ..., n\}$ at locations $\{x_1, x_2, ..., x_n\}$, where $n \geq 2$ and $x_i \in D$. Upon receiving a bid-

[3]Data quality depends on various factors in practice such as noise power and local environment (e.g., indoor/outdoor). In this paper, we assume that sensing-capable devices (or antennas) are located outdoors, whose noise power are low enough to reliably sense the presence of primary signals in bands of interest. For instance, if a user wants to compete for sensing tasks in TV bands, its device should be able to sense as low as the service threshold of -84 dBm over a 6 MHz channel for full-power digital TV [19]. To enforce this assumption, the platform may ask users to report their noise levels and local environments, and only allow qualified users to compete for a particular task.

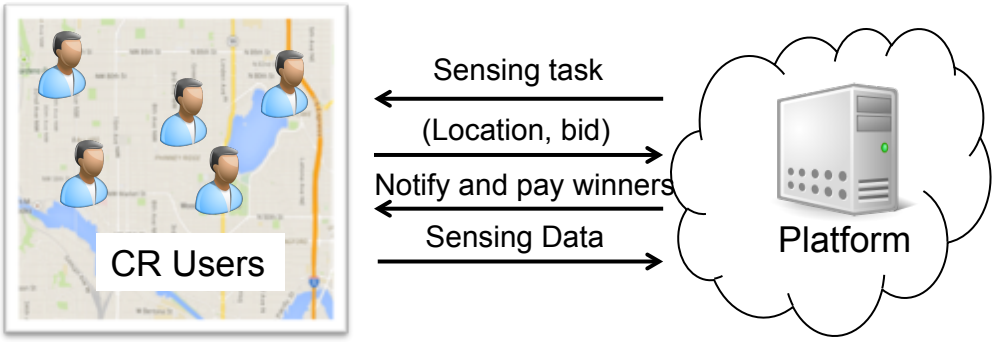

Figure 3.1: Proposed crowdsensing system for radio mapping that implements an auction-based incentive mechanism. In each period, the platform announces a sensing task without specific location requirements, and interested users can sign up by submitting their current locations and bids of their choice. After collecting bids from all users, the platform selects a set of winners and determines corresponding payments. Payments are then made to winners in exchange for sensing data.

location profile $(\mathbf{b}, \mathbf{x})$ where $\mathbf{b} = (b_1, b_2, ..., b_n)$ and $\mathbf{x} = (x_1, x_2, ..., x_n)$, the platform selects a winner subset $\mathcal{A} \subseteq \Omega$ and determines the payment $p_i > 0$ for each winner $i \in \mathcal{A}$ ($p_i = 0$ for $i \notin \mathcal{A}$). Finally, it pays winners in exchange for the sensing data.

We assume that users are rational and make decisions in their best interest. Each user i has a utility of $p_i - c_i$, if selected, and 0 otherwise. We are interested in the strategic case, in which each user aims to maximize its own utility by taking strategic actions, for example, submitting a bid (possibly) much higher than its true cost. In addition, we assume non-collaborative users who are honest in following the protocol. Considerations of security and privacy enhancement within this framework is left as future work.

The platform aims to maximize $\phi(\mathcal{A})$[4] for a given budget B. We assume that $\gamma(h)$ or

[4]The metric of "average" K-var reduction implicitly assumes equally important subregions with the same accuracy requirement. In practice, accuracy requirement may vary over subregions, and those that require greater interpolation accuracy will need more samples in general. To account for this case, our proposed framework may be generalized in the following two ways. First, the platform may assign larger budgets to more important subregions and smaller budgets to others, given the same budget in total. Alternatively,

$C(h)$ is known to the platform as prior knowledge for the current period. Our objective is to design a *mechanism* $\mathcal{M} = (\chi, \psi)$ with the following properties:

- **Computational efficiency**: Selection and payment rules can be computed in polynomial time[5].
- **Individual rationality**: Each winner has a non-negative utility, i.e., $p_i \geq b_i$ for $i \in \mathcal{A}$.
- **Budget feasibility**: The total amount of payments does not exceed a given budget B, that is, $\sum_{i \in \mathcal{A}} p_i \leq B$.
- **Truthfulness**: It is a dominant strategy for users to report their true costs regardless of other users' bids.

The first three properties are desirable features of a real-world crowdsensing system, and the final property counteracts the possibility of market manipulation and strategizing.

3.4 Incentive Mechanism Design

In this section, we develop an auction-based budget-free mechanism with a cardinality constraint. We then propose a budget-feasible version that enforces the budget constraint by translating it to a carefully chosen cardinality constraint. We show that the proposed mechanism is computationally efficient, individually rational, budget feasible, and truthful, and explain how it works through an illustrative example.

3.4.1 Budget-Free Mechanism with a Cardinality Constraint

In the budget-free case, the platform takes a bid-location profile $(\mathbf{b}, \mathbf{x})$ that consists of n users (denoted as $\Omega = \{1, 2, ..., n\}$) and a cardinality constraint k as input and wants to

the platform may adopt a "weighted" criterion and assign more weights to unmeasured locations from subregions that require greater accuracy. As a result, the platform can select more samples from those subregions by maximizing the "weighted" $\phi(\mathcal{A})$.

[5]The computational complexity is evaluated in terms of the number of calls to $\phi(\mathcal{A})$.

solve the following constrained optimization problem:

$$\max_{\mathcal{A}\subseteq\Omega} \ \phi(\mathcal{A}) \ \text{ s.t. } |\mathcal{A}| \leq k. \tag{3.3}$$

Since both individual rationality and truthfulness will be enforced in payment determination using Theorem 3.1, they are not imposed as explicit constraints. While the problem in Eq. (3.3) is very similar to the classical spatial sampling problem (Section 3.2.2), a greedy algorithm that only considers user locations and iteratively selects users with the maximum marginal contribution cannot yield a truthful mechanism. In other words, a winner can submit an arbitrarily high bid and still win give the above greedy algorithm, since the selection rule is independent of users' bids. Therefore, we need to jointly consider location and bid for winner selection in order to achieve truthfulness. In this work, we adopt the normalized marginal contribution (i.e., the marginal contribution of a user divided by its bid) as the metric [63, 64], which will yield a monotone selection rule, as we will show later.

The budget-free mechanism is provided in Algorithm 1. As we can see, the selection rule (Lines 3-7) is a greedy algorithm that selects winners iteratively according to their normalized marginal contribution, until k winners are selected. Denote the set of winners up to the (j-1)-th iteration as $\mathcal{A}_{j-1}$, where $j \geq 1$ and $\mathcal{A}_0 = \emptyset$. When selecting the j-th winner, the marginal contribution of each user $i \in \Omega \setminus \mathcal{A}_{j-1}$ is $m_{\mathcal{A}_{j-1}}(i) = \phi(\mathcal{A}_{j-1} \cup \{i\}) - \phi(\mathcal{A}_{j-1})$. Define $[j] = \arg\max_{i\in\Omega\setminus\mathcal{A}_{j-1}} \frac{m_{\mathcal{A}_{j-1}}(i)}{b_i}$, which is the index of the j-th winner over Ω. To simplify notation, we write $m_{[j]}$ instead of $m_{\mathcal{A}_{j-1}}([j])$. Note that $\phi(\mathcal{A}_j) = \sum_{i\leq j} m_{[i]}$ for all $j \leq k$. The submodularity of $\phi(\mathcal{A})$ implies that

$$m_{[1]} \geq m_{[2]} \geq ... \geq m_{[k]}, \tag{3.4}$$

and the selection order implies that

$$\frac{m_{[1]}}{b_{[1]}} \geq \frac{m_{[2]}}{b_{[2]}} \geq ... \geq \frac{m_{[k]}}{b_{[k]}}. \tag{3.5}$$

We now show that Eq. (3.5) is true by contradiction. Consider winners $[i]$ and $[j]$, where $i < j$. Suppose that $\frac{m_{[i]}}{b_{[i]}} < \frac{m_{[j]}}{b_{[j]}}$. Denote the marginal contribution of the j-th winner in the

Algorithm 1 `budget_free_mechanism`$(\mathbf{b}, \mathbf{x}, k)$

Input: $(\mathbf{b}, \mathbf{x})$ – bid-location profile, k – cardinality constraint

Output: $\mathcal{A}$ – selected subset, $\mathbf{p}$ – payments

$\Omega \leftarrow \{1, 2, ..., n\}$ // Or $\Omega \leftarrow \{x_1, x_2, ..., x_n\}$
// Selection Rule
$\mathcal{A} \leftarrow \emptyset, \mathcal{U} \leftarrow \Omega$
while $\mathcal{U} \neq \emptyset$ **and** $|\mathcal{A}| < k$ **do**
  $j \leftarrow \arg\max_{i \in \mathcal{U}} \left(\phi(\mathcal{A} \cup \{i\}) - \phi(\mathcal{A})\right) / b_i$
  $\mathcal{A} \leftarrow \mathcal{A} \cup \{j\}, \mathcal{U} \leftarrow \mathcal{U} \setminus \{j\}$
end while
// Payment Rule
for $i \in \Omega$ **do** $p_i \leftarrow 0$ **end for**
for $i \in \mathcal{A}$ **do**
  $\Omega' \leftarrow \Omega \setminus \{i\}$
  $\mathcal{A}' \leftarrow \emptyset, \mathcal{U} \leftarrow \Omega'$
  while $\mathcal{U} \neq \emptyset$ **and** $|\mathcal{A}'| < k$ **do**
    $j \leftarrow \arg\max_{l \in \mathcal{U}} \left(\phi(\mathcal{A}' \cup \{l\}) - \phi(\mathcal{A}')\right) / b_l$
    $m'_j \leftarrow \phi(\mathcal{A}' \cup \{j\}) - \phi(\mathcal{A}')$ $\tilde{m}_i \leftarrow \phi(\mathcal{A}' \cup \{i\}) - \phi(\mathcal{A}')$
    $\tilde{m}_i \leftarrow \phi(\mathcal{A}' \cup \{i\}) - \phi(\mathcal{A}')$
    $p_i \leftarrow \max\{p_i, \frac{\tilde{m}_i}{m'_j} \cdot b_j\}$
    $\mathcal{A}' \leftarrow \mathcal{A}' \cup \{j\}, \mathcal{U} \leftarrow \mathcal{U} \setminus \{j\}$
  end while
end for
return $\mathcal{A}, \mathbf{p}$

i-th iteration as $m'_{[j]}$. In the presence of submodularity, we have $m'_{[j]} = m_{\mathcal{A}_{i-1}}([j]) \geq m_{[j]} = m_{\mathcal{A}_{j-1}}([j])$, since $\mathcal{A}_{i-1} \subseteq \mathcal{A}_{j-1}$. Hence, it holds that $\frac{m_{[i]}}{b_{[i]}} < \frac{m_{[j]}}{b_{[j]}} \leq \frac{m'_{[j]}}{b_{[j]}}$. In other words, the j-th winner would have been selected earlier in the i-th iteration, which is a contradiction with our assumption. Therefore, Eq. (3.5) is true.

Next comes payment determination. The key is to find the maximum bid each winner can submit that allows it to win. The corresponding pseudo-codes are in Lines 10-20. Consider the i-th winner among Ω, denoted as $[i]$. Define a new set $\Omega' = \Omega \setminus \{[i]\}$. Similar to Eq. (3.5), sort users in Ω' according to their normalized marginal contribution. Denote the first $(j-1)$ winners among Ω' as $\mathcal{A}'_{j-1}$, and the index of the j-th winner as $[j]'$. In order for winner $[i]$ to replace winner $[j]'$, its normalized marginal contribution needs to be larger than that of winner $[j]'$, that is,

$$\frac{m_{\mathcal{A}'_{j-1}}([j]')}{b_{[j]'}} < \frac{m_{\mathcal{A}'_{j-1}}([i])}{b_{[i]}}. \tag{3.6}$$

So the maximum bid (i.e., the conditional threshold payment) for winner $[i]$ that allows it to replace winner $[j]'$ is

$$p_{[i],[j]'} = \frac{m_{\mathcal{A}'_{j-1}}([i])}{m_{\mathcal{A}'_{j-1}}([j]')} \cdot b_{[j]'}. \tag{3.7}$$

Note that as long as winner $[i]$ is ahead of any winner $[j]' \in \Omega'$ in terms of ordering, where $j \leq k$, it is guaranteed that the i-th winner still wins. Therefore, the maximum bid (i.e., the threshold payment) for the i-th winner is

$$p_{[i]} = \max_{1 \leq j \leq k} \{p_{[i],[j]'}\}, \ i = 1, 2, ..., k. \tag{3.8}$$

3.4.2 Budget-Feasible Mechanism

We now consider the budget constraint. Denote the problem in Eq. (3.3) and the corresponding winner set as $H(\mathbf{b}, \mathbf{x}, k)$ and $\mathcal{A}_k$ respectively. The total payment is $P_{total}(k) = \sum_{i \in \mathcal{A}_k} p_i$, which is a function of k. Then the budget-feasible version aims to solve the following problem:

$$\max_k H(\mathbf{b}, \mathbf{x}, k) \text{ s.t. } P_{total}(k) \leq B. \tag{3.9}$$

Suppose $k_1 < k_2$ and denote the corresponding winner sets as $\mathcal{A}^{(1)}$ and $\mathcal{A}^{(2)}$. It is easy to see that $\mathcal{A}^{(1)} \subset \mathcal{A}^{(2)}$ because both adopt the same selection rule. Since $\phi(\mathcal{A})$ is monotonically increasing, a larger k value results in a larger $\phi(\mathcal{A})$ value. Hence, Eq. (3.9) is equivalent to maximizing k such that $P_{total}(k) \leq B$. One simple way is to enumerate every k value in order until the total payment exceeds the budget. Alternatively, the bisection method may be used to speed up the search process by leveraging the fact that $P_{total}(k)$ is a monotonically increasing function of k.

Lemma 3.1. *The total payment of the budget-free mechanism is a monotonically increasing function of k.*

Proof. Suppose $k_1 < k_2$. Let the outputs of the budget-free mechanism given k_1 and k_2 be $(\mathcal{A}^{(1)}, \mathbf{p}^{(1)})$ and $(\mathcal{A}^{(2)}, \mathbf{p}^{(2)})$ respectively. As in Eq. (3.5), we sort users according to their normalized marginal contribution, and denote the i-th winner as $[i]$. Then, we have $\mathcal{A}^{(1)} = \{[1], [2], ..., [k_1]\} \subset \mathcal{A}^{(2)} = \{[1], [2], ..., [k_2]\}$. Denote the payments as $\{p_{[i]}^{(1)} : i = 1, 2, ..., k_1\}$ and $\{p_{[i]}^{(2)} : i = 1, 2, ..., k_2\}$. For any $i \leq k_1$, it holds that

$$\begin{aligned} p_{[i]}^{(2)} &= \max\{\max_{1 \leq j \leq k_1} p_{[i],[j]'}, \max_{k_1 < j \leq k_2} p_{[i],[j]'}\} \\ &= \max\{p_{[i]}^{(1)}, \max_{k_1 < j \leq k_2} p_{[i],[j]'}\} \geq p_{[i]}^{(1)}. \end{aligned} \tag{3.10}$$

For any $i \in (k_1, k_2]$, $p_{[i]}^{(2)} > 0$. Hence, we have $\sum_{1 \leq i \leq k_2} p_{[i]}^{(2)} > \sum_{1 \leq i \leq k_1} p_{[i]}^{(1)}$. □

The budget-feasible mechanism is provided in Algorithm 2. The bisection method requires a lower bound l for k such that the budget constraint can be met, and an upper bound u such that the budget constraint cannot be met. A tolerance value ϵ is also needed as the stopping condition. We assume that the budget is neither too small nor too large, so that the winning set contains at least one sample but not all samples are affordable. Hence, we set $l = 1$, $u = n$, and $\epsilon = 1$ as in Line 1. In the while loop (Lines 2-12), the midpoint between u and l is fed to the budget-free mechanism to check the budget constraint: if yes, the midpoint becomes the new lower bound, and the new upper bound otherwise. The number of calls to the budget-free mechanism is $\log_2((u - l)/\epsilon) \approx \log_2(n)$.

Algorithm 2 `budget_feasible_mechanism`$(\mathbf{b}, \mathbf{x}, B)$

Input: $(\mathbf{b}, \mathbf{x})$ – bid-location profile, B – budget

Output: $\mathcal{A}$ – selected subset, $\mathbf{p}$ – payments

$l \leftarrow 1$, $u \leftarrow n$, $\epsilon \leftarrow 1$
while $u - l > \epsilon$ **do**
  $k \leftarrow \lfloor (u-l)/2 \rfloor$
  $(\mathcal{A}', \mathbf{p}') \leftarrow$ `budget_free_mechanism`$(\mathbf{b}, \mathbf{x}, k)$
  $P_{total} \leftarrow \sum_{i \in \mathcal{A}'} p'_i$
  if $P_{total} \leq B$ **then**
    $l \leftarrow k$
    $\mathcal{A} \leftarrow \mathcal{A}'$, $\mathbf{p} \leftarrow \mathbf{p}'$
  else
    $u \leftarrow k$
  end if
end while
return $(\mathcal{A}, \mathbf{p})$

3.4.3 Analysis

Now we prove that the proposed budget-feasible mechanism is also computationally efficient, individual rational, and truthful.

Lemma 3.2. *The proposed budget-feasible mechanism is computationally efficient, that is, the selection and payment rule can be computed in polynomial time.*

Proof. For the budget-free mechanism, the complexity of the greedy selection is $\mathcal{O}(kn)$, since finding the user with maximum normalized marginal contribution takes $\mathcal{O}(n)$ time and we need to find k such users. For payment determination, the greedy process is executed repeatedly to determine each winner's payment. So the complexity is $\mathcal{O}(k^2 n)$ for the budget-free mechanism. Since k is bounded by n, the overall complexity for a general k is bounded

by $\mathcal{O}(n^3)$. Moreover, the budget-feasible mechanism uses the bisection method that requires $\log_2(n)$ calls to the budget-free mechanism in the worst case. Hence, the overall complexity becomes $\mathcal{O}(n^3 \log_2 n)$, which is in polynomial time. □

Lemma 3.3. *The proposed budget-feasible mechanism is individually rational.*

Proof. Since $p_{[i]} \geq p_{[i],[j]'}$ for $i = 1, 2, ..., k$, it suffices to prove that $p_{[i],[j]'} \geq b_{[i]}$ for some j. Observe that the first $(i-1)$ winners over Ω are the same with those over Ω', i.e., $\mathcal{A}'_{i-1} = \mathcal{A}_{i-1}$. Due to the absence of winner $[i]$ in Ω', some other user now becomes winner $[i]'$, who ranks behind winner $[i]$ in the original set when it is present, that is,

$$\begin{aligned} & \frac{m_{\mathcal{A}_{i-1}}([i]')}{b_{[i]'}} \leq \frac{m_{\mathcal{A}_{i-1}}([i])}{b_{[i]}} \\ \Rightarrow & \frac{m_{\mathcal{A}'_{i-1}}([i]')}{b_{[i]'}} \leq \frac{m_{\mathcal{A}'_{i-1}}([i])}{b_{[i]}} && \text{(Since } \mathcal{A}'_{i-1} = \mathcal{A}_{i-1}\text{)} \\ \Rightarrow & p_{[i],[i]'} = \frac{m_{\mathcal{A}'_{i-1}}([i])}{m_{\mathcal{A}'_{i-1}}([i]')} \cdot b_{[i]'} \geq b_{[i]} && (3.11) \end{aligned}$$

Hence, it holds that $p_{[i]} \geq p_{[i],[i]'} \geq b_{[i]}$ for $i = 1, 2, ..., k$. □

Lemma 3.4. *The proposed budget-feasible mechanism is truthful.*

Proof. We first prove that the selection rule is monotone. Consider the i-th winner, denoted as $[i]$. If winner $[i]$ announces a bid $b'_{[i]} < b_{[i]}$, it is true that $\frac{m_{[i]}}{b'_{[i]}} > \frac{m_{[i]}}{b_{[i]}} \geq \frac{m_{[k]}}{b_{[k]}}$ and thus winner $[i]$ still wins. In other words, bidding a smaller value cannot push winner $[i]$ backwards in the sorting. Hence, the selection rule is monotone.

We then prove that the payments are threshold amounts. Assume that winner $[i]$ announces a bid $b_{[i]} > p_{[i]}$. By definition, we know $b_{[i]} > p_{[i],[j]'}$ for all $1 \leq j \leq k$ and $b_{[i]} > p_{[i],[k]'}$ in particular. It means that when winner $[i]$ bids this amount, it will not be placed ahead of the k-th winner, even if it is included in the sorting again. Hence, winner $[i]$ cannot win by bidding $b_{[i]} > p_{[i]}$ and $p_{[i]}$ the threshold payment to winner $[i]$. By invoking Theorem 3.1, it holds that the proposed budget-feasible mechanism is truthful. □

The above lemmas prove the following theorem.

Theorem 3.2. *The proposed budget-feasible mechanism is computationally efficient, individually rational, and truthful.*

3.4.4 An Illustrative Example

We use the example in Figure 3.2 to illustrate the proposed incentive mechanism. The square is the region of interest for radio mapping, which is discretized into a mesh grid of 9 locations. There are four interested users located at x_1, x_2, x_3, x_4, labeled as 1 through 4. Suppose that they bid 0.1, 0.2, 0.3, and 0.4, respectively and the budget is 0.5. The semivariogram $\gamma(h)$ is a spherical model, given by $\gamma(h) = a + (s-a)\left(\frac{3}{2}(\frac{h}{r}) - \frac{1}{2}(\frac{h}{r})^3\right)$ for $0 \leq h \leq r$, and $\gamma(h) = s$ for $h > r$, where $a = 0, s = 5$ and $r = 3$. Values of $\phi(\mathcal{A})$ are given in Table 3.1.

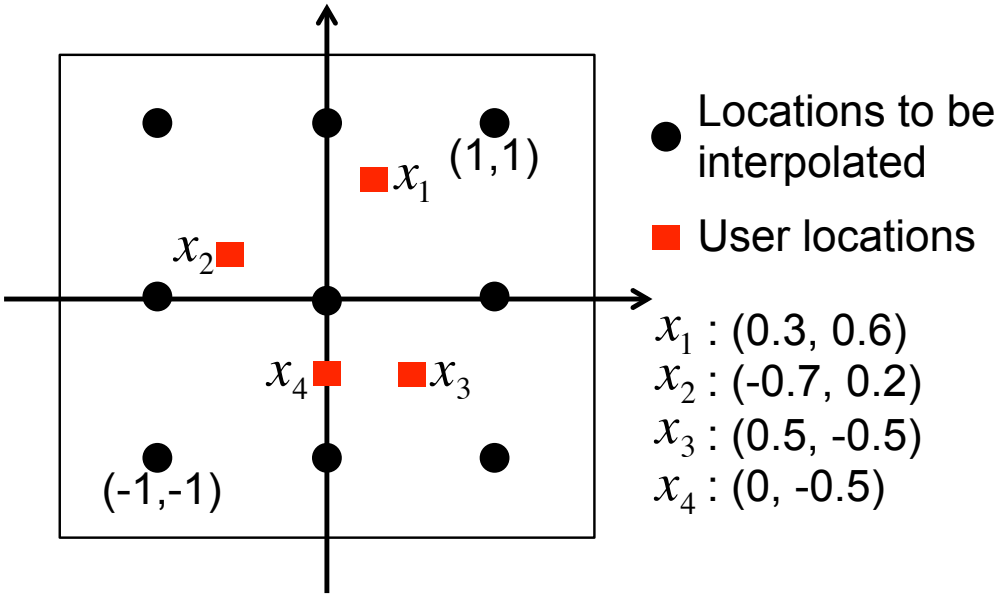

Figure 3.2: Topology of an illustrative example for the proposed incentive mechanism. In this example, there are a total of four users (red squares) who are interested in participating crowdsensing, and the platform wants to recruit a set of users for a given budget and use their sensing data to interpolate the RSSI values at the unmeasured locations (back circles).

$\mathcal{A}$	$\phi(\mathcal{A})$	$\mathcal{A}$	$\phi(\mathcal{A})$
$\emptyset$	0	$\{2,3\}$	6.38
$\{1\}$	4.34	$\{2,4\}$	5.99
$\{2\}$	4.29	$\{3,4\}$	5.23
$\{3\}$	4.29	$\{1,2,3\}$	7.03
$\{4\}$	4.55	$\{1,2,4\}$	6.89
$\{1,2\}$	6.00	$\{1,3,4\}$	6.54
$\{1,3\}$	6.04	$\{2,3,4\}$	6.55
$\{1,4\}$	6.22	$\{1,2,3,4\}$	7.20

Table 3.1: Average K-var reduction $\phi(\mathcal{A})$ for any given subset $\mathcal{A} \subseteq \{1,2,3,4\}$.

We first demonstrate how the budget-free mechanism works. Observe that the greedy selection order by the normalized marginal contribution is given by: $1 \to 2 \to 3 \to 4$. The process of computing threshold payments for a single and two winners (i.e., $k = 1$ and 2) is as follows. For $k = 1$, we have $[1] = 1$ (the only winner is 1):

- In the absence of $[1]$, the only winner is $[1]' = 2$. To compute its payment, we have $\mathcal{A}'_0 = \emptyset$ and $p_{[1],[1]'} = \frac{m_{\mathcal{A}'_0}([1])}{m_{\mathcal{A}'_0}([1]')} \cdot b_{[1]'} = \frac{4.34}{4.29} \cdot 0.2 \approx 0.202$, which means that $p_{[1]} = p_{[1],[1]'} = 0.202$. Hence, the payment to the sole winner is 0.202.

For $k = 2$, we have $[1] = 1$ and $[2] = 2$:

- In the absence of $[1]$, winners are $[1]' = 2$ and $[2]' = 3$.

  1. $\mathcal{A}'_0 = \emptyset$, $p_{[1],[1]'} = \frac{m_{\mathcal{A}'_0}([1])}{m_{\mathcal{A}'_0}([1]')} \cdot b_{[1]'} = \frac{m_\emptyset(1)}{m_\emptyset(2)} \cdot b_2 = \frac{4.34}{4.29} \cdot 0.2 \approx 0.202$;
  2. $\mathcal{A}'_1 = \{[1]'\} = \{2\}$, $p_{[1],[2]'} = \frac{m_{\mathcal{A}'_1}([1])}{m_{\mathcal{A}'_1}([2]')} \cdot b_{[2]'} = \frac{m_{\{2\}}(1)}{m_{\{2\}}(3)} \cdot b_3 = \frac{6.00-4.29}{6.38-4.29} \cdot 0.3 \approx 0.245$;
  3. $p_{[1]} = \max\{p_{[1],[1]'}, p_{[1],[2]'}\} = 0.245$;

- In the absence of [2], winners are $[1]' = 1$ and $[2]' = 3$.

  1. $\mathcal{A}'_0 = \emptyset$, $p_{[2],[1]'} = \frac{m_{\mathcal{A}'_0}([2])}{m_{\mathcal{A}'_0}([1]')} \cdot b_{[1]'} = \frac{m_\emptyset(2)}{m_\emptyset(1)} \cdot b_1 = \frac{4.29}{4.34} \cdot 0.1 \approx 0.099$;
  2. $\mathcal{A}'_1 = \{[1]'\} = \{1\}$, $p_{[2],[2]'} = \frac{m_{\mathcal{A}'_1}([2])}{m_{\mathcal{A}'_1}([2]')} \cdot b_{[2]'} = \frac{m_{\{1\}}(2)}{m_{\{1\}}(3)} \cdot b_3 = \frac{6.00-4.34}{6.04-4.34} \cdot 0.3 \approx 0.293$;
  3. $p_{[2]} = \max\{p_{[2],[1]'}, p_{[2],[2]'}\} = 0.293$;

- Hence, the payments to winners $[1] = 1$ and $[2] = 2$ are 0.245 and 0.293 respectively, and the total is 0.538.

Now we consider the budget-feasible mechanism. The bisection method is first initialized with $l = 1$ and $u = 4$. Then it checks the budget feasibility when $k = \lfloor (4+1)/2 \rfloor = 2$, and realizes that the budget constraint cannot be met (as shown above). So it sets $u = 2$. Now since the gap between the lower and upper bounds is within the tolerance (i.e., $\epsilon = 1$), the mechanism returns the result when $k = l$, which is a budget-feasible solution.

3.5 Performance Evaluation

In this section, we evaluate the performance of proposed mechanisms and compare them against the baseline mechanism in [64]. For convenience, we use the abbreviations *BFreeMech* and *BFeaMech* for the budget-free and budget-feasible mechanisms, respectively.

3.5.1 Baseline Mechanism

In [64], authors proposed a randomized budget-feasible mechanism for general submodular monotone functions, which is computationally efficient, individually rational, and truthful. There are two main differences between their mechanism and ours. First, their mechanism is randomized: with a probability of 0.4, it returns a single user with the maximum (unnormalized) marginal contribution and pays it B; otherwise, it runs a greedy scheme that selects multiple users and determines payments based on Myerson's characterization. The logic behind the randomness is the following. In some extreme cases, there exists some user with a very large marginal contribution and a very high cost (that is less than B). As a result,

it will never be selected by a greedy algorithm, which results in unbounded performance. Hence, the randomized approach is adopted in order to derive a certain performance bound.

Second, in their greedy scheme, the budget constraint is enforced through the proportional share allocation condition. Specifically, the greedy scheme selects the user with the largest normalized marginal contribution in the j-th iteration only if $b_{[j]} \leq \frac{B}{2}\frac{m_{[j]}}{\sum_{i\in\mathcal{A}_{j-1}\cup\{[j]\}} m_i}$, and stops otherwise. This condition ensures that the final payment to winner $[i]$ in the winner set $\mathcal{A}_k$ is bounded above by $\frac{m_{[i]}}{\phi(\mathcal{A}_k)} \cdot B$; then the total payment will be bounded by B since $\frac{\sum_{i\leq k} m_{[i]}}{\phi(\mathcal{A}_k)} \cdot B = B$. Since it is very unlikely for multiple samples to have a $\phi(\mathcal{A})$ value than a single sample's in radio mapping, we consider their greedy scheme as the baseline mechanism.

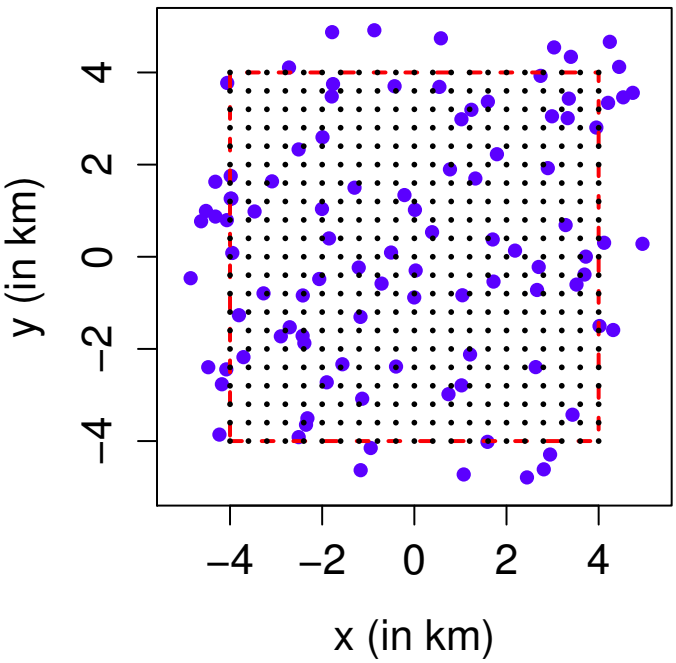

Figure 3.3: Sample topology with 100 randomly distributed users (in blue dots) over a 10km-by-10km region. The region of interest is the inner red square, which is discretized into a total of 121 locations (in black dots).

3.5.2 Simulation Setup

A sample topology with 100 users is provided in Figure 3.3, whose locations are randomly generated from the spatial Poisson random process within a 10km-by-10km region. The region of interest is the 8km-by-8km square, which is discretized into a mesh grid of 121 locations. This is because in practice estimation errors tend to be dominated by the border areas [46] and hence we focus on radio mapping for the inner region. User costs are i.i.d. random variables drawn from the uniform distribution over $[0, \kappa_{max}]$. Since the normalized marginal contribution is used as the metric in our proposed mechanism, the scale of κ_{max} has no impact on winner selection and payments are proportional to κ_{max}. Without loss of generality, we set $\kappa_{max} = 1$. The semivariogram $\gamma(h)$ is an exponential model obtained from a real-world measurement campaign in a suburban area [73], which is given by $\gamma(h) = a + (s - a)\left(1 - e^{-3h/r}\right)$, where $a = 6.48$, $s = 22.02$, and $r = 2.11$.

3.5.3 Evaluation of BFreeMech

As discussed in Section 3.4, the budget constraint of BFeaMech is closely related to the cardinality constraint of BFreeMech. Hence, we are interested in understanding the impact of the cardinality constraint on P_{total} and $\phi(\mathcal{A})$ for BFreeMech. In addition, we define the payment overhead as the difference between the total payment and the total amount of bids.

In this simulation, we first generated 30 sets of random costs and locations for 100 users. In each experiment, a particular number of users were randomly sampled from the 100 users; for the same set of users, BFreeMech was executed with a cardinality constraint varied from 5 to 30. Results were averaged over 30 experiments and are shown in Figure 3.4.

Impact of k on P_{total}

We can observe from Figure 3.4(a) that the average P_{total} is always monotonically increasing and it tends to increase at a faster rate as k increases. This is mainly because with fewer users, the platform needs to pay more to the next winner, which leads to a larger increase

in P_{total} on average. Moreover, for a relatively small k (e.g., less than 15) compared to the number of users n, we do not observe a significant difference in the average total payment. When k becomes larger, the average P_{total} tends to be inversely proportional to the number of participating users. For instance, when $k = 25$, the average total payment is 21.0 with $n = 40$ users, which is almost halved to 9.6 with $n = 80$ users.

Impact of k on $\phi(\mathcal{A})$

As shown in Figure 3.4(b), the average $\phi(\mathcal{A})$ increases as k increases, but the increasing rate keeps decreasing, because of the submodularity property of $\phi(\mathcal{A})$. On the other hand, unlike P_{total}, the number of users has little effect on the average value of $\phi(\mathcal{A})$. It means that the performance of radio mapping mainly depends on the number of selected users, and more participating users can effectively reduce the total payment.

Impact of k on payment overhead

As mentioned earlier, the actual payment made to a winner is always higher than its bid to ensure individual rationality and truthfulness. Hence, for a set $\mathcal{A}$ of k winners, we can define the *payment overhead ratio* α as

$$\alpha = \frac{\sum_{i \in \mathcal{A}} p_i - \sum_{i \in \mathcal{A}} b_i}{\sum_{i \in \mathcal{A}} b_i}. \tag{3.12}$$

As illustrated in Figure 3.5, when k is relatively small compared to n, α varies between 0.9 and 1.2 for different values of n. In other words, the platform needs to pay roughly double the total amount of bids to ensure truthfulness. On the other hands, when k is closer to n (e.g., more than 20 winners out of 40 users), α tends to increase rapidly. It implies that the platform may need to limit the number of winners depending on the number of participants, so as to avoid large payment overheads.

3.5.4 Comparison with Baseline Mechanism

Now we compare the performance of BFeaMech against the baseline mechanism. For fair comparison, the same set of user costs and locations was fed to both mechanisms, and results were averaged over 30 experiments.

Impact of Number of Users

Figure 3.6 illustrates the impact of n with a budget of 5. We can see that the average number of purchased samples (or selected users) tends to increase linearly as a function of n for both mechanisms, but the slope of BFeaMech is greater than that of the baseline mechanism (Figure 3.6(a)). As a result, BFeaMech performs much better than the baseline mechanism in terms of average $\phi(\mathcal{A})$ for the same n, with an improvement of 19.1%-21.2% for different n (Figure 3.6(b)).

Impact of Budget

Figure 3.7 illustrates the impact of the budget B on the average number of purchased samples (or selected users) and average $\phi(\mathcal{A})$ for both mechanisms. We set $n = 100$. As shown in Figure 3.7(a), the average number of purchased samples increases as B increases for both mechanisms, but it grows much faster for BFreaMech as compared to the baseline mechanism. The reason is as follows. Suppose that k winners are selected by the baseline mechanism. It holds that $b_{[k+1]} > \frac{B}{2}\frac{m_{[k+1]}}{\sum_{i\in\mathcal{A}_k\cup\{[k+1]\}} m_i}$, or equivalently, $\frac{m_{[k+1]}}{b_{[k+1]}} < 2\frac{\sum_{i\in\mathcal{A}_k\cup\{[k+1]\}} m_i}{B}$. In order to get the $(k+1)$-th winner, the budget has to increase in a way so that the right-hand side is less or equal to the left-hand side. If we plot the average budget as a function of the number of winners k for the baseline mechanism (Figure 3.8), we can see that it tends to increase exponentially as k increases, and thus the additional budget needed to get one more winner keeps increasing. Also notice that the total payment to k winners made by BFreeMech is much less than the budget required by the baseline mechanism. Since both mechanisms determine payments in a very similar manner, it implies that the baseline mechanism does

not make full use of the budget, and a larger budget will lead to a greater surplus. Therefore, BFreaMech tends to make better use of the additional budget and is able to purchase more samples than the baseline mechanism for radio mapping.

As shown in Figure 3.7(b), the difference in the number of purchased samples directly translates into the difference in $\phi(\mathcal{A})$. The average $\phi(\mathcal{A})$ of both mechanisms is monotonically increasing as B increases and tends to grow at a lower rate. Nevertheless, BFeaMech outperforms the baseline mechanism by 18.5%-22.3% in terms of the average $\phi(\mathcal{A})$.

3.6 Conclusion and Future Work

In this work, we developed an incentivized crowdsensing system that acquires spectrum data periodically from users, which aims to maximize the average prediction error (Kriging variance) variance reduction $\phi(\mathcal{A})$ for a given budget. We first proposed a computationally efficient, individually rational, and truthful incentive mechanism with a cardinality constraint. On top of it, we proposed a budget-feasible mechanism by translating the budget constraint to a suitable cardinality constraint with the bisection method.

We conducted extensive simulations to evaluate the performance of the proposed mechanisms and compare them against a baseline mechanism. Our results show that the baseline mechanism does not make full use of the given budget, and the proposed mechanism achieves significantly better performance over the baseline mechanism, with improvements of 18%-22% in terms of the average $\phi(\mathcal{A})$ for different numbers of users and budgets.

There are several interesting future directions. First, the current objective function assumes homogeneous subregions with the same accuracy requirement. We may extend the current formulation to account for heterogeneous subregions by assigning weights or distributing the given budget to reflect various priorities. Second, we have assumed honest users in this work, but free-riders can provide random data without actual sensing or malicious users can report manipulated data in order to corrupt the radio map. It would be interesting to address the above issues and enhance the proposed system with security measures.

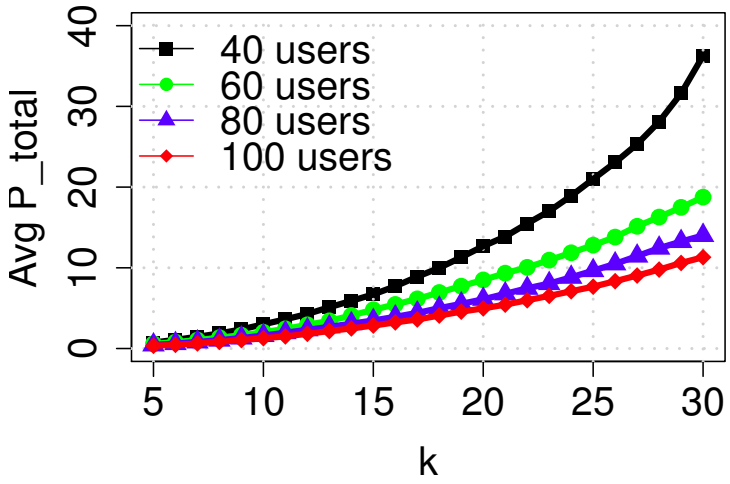

(a)

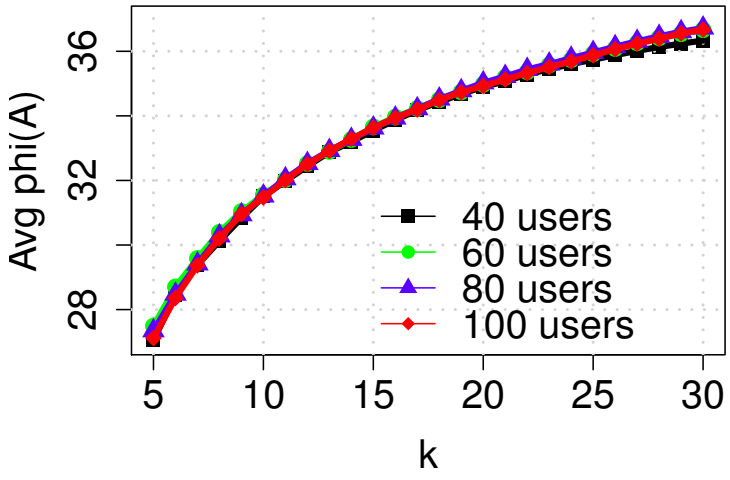

(b)

Figure 3.4: Impact of the cardinality constraint k on P_{total} and $\phi(\mathcal{A})$. (a) Average P_{total} as a function of k for different n (number of users). We observe that P_{total} increases monotonically with k and decreases as n increases. (b) Average $\phi(\mathcal{A})$ as a function of k for different numbers of users. We observe that the average $\phi(\mathcal{A})$ increases with k and it is not affected by n.

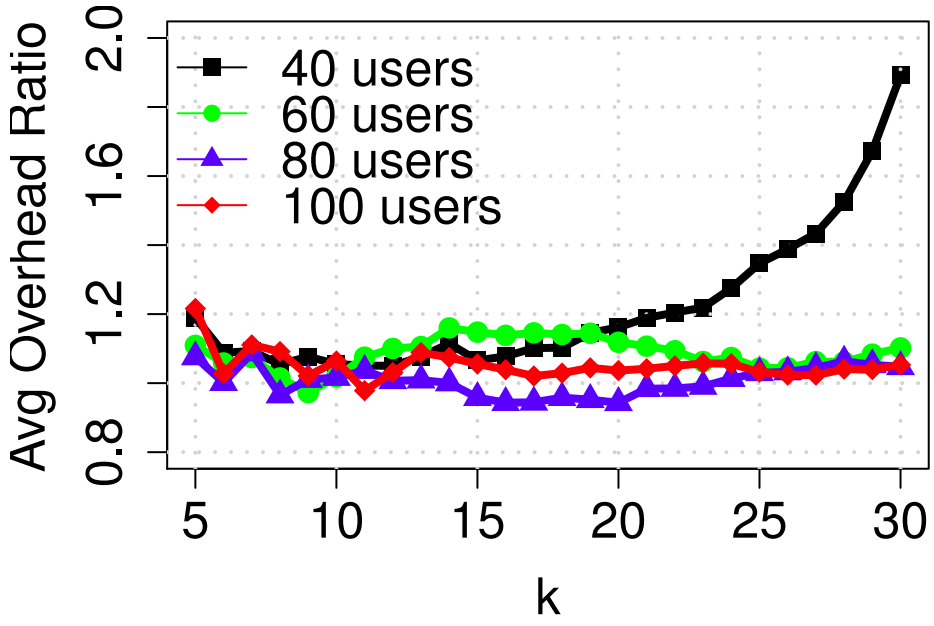

Figure 3.5: Average payment overhead ratio as a function of k for different n (number of users). We observe that when k is relatively small as compared to n, α fluctuates between 0.9 and 1.2, which implies that the platform needs to roughly double the amount of payments to achieve truthfulness. In contrast, with $n = 40$ and when k gets closer to n, we observe a significant increase in payment overhead.

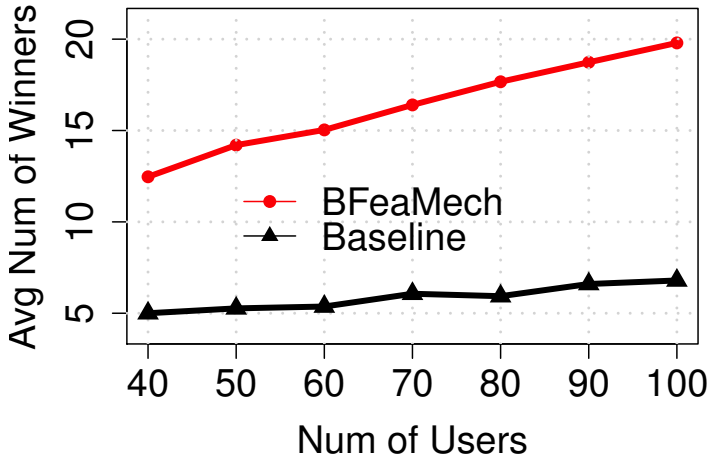

(a)

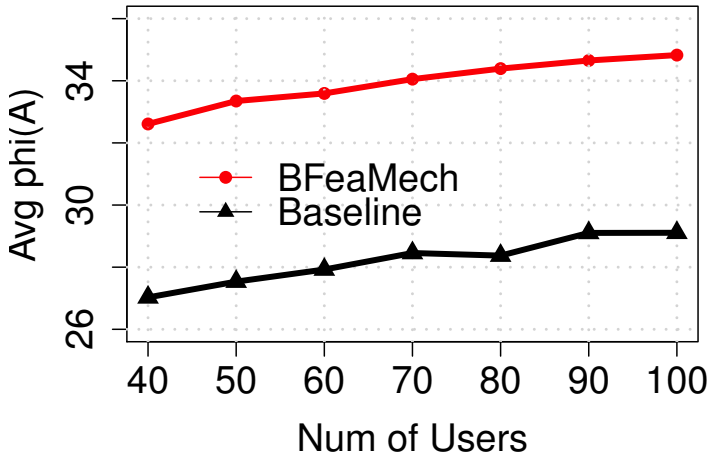

(b)

Figure 3.6: Impact of number of users n on the performance of BFeaMech and the baseline mechanism. (a) Average number of winners or purchased samples as a function of n. (b) Average $\phi(\mathcal{A})$ as a function of n. We observe that BFeaMech consistently achieves an average value of $\phi(\mathcal{A})$ 19.1%-21.2% higher than that of the baseline mechanism for different n.

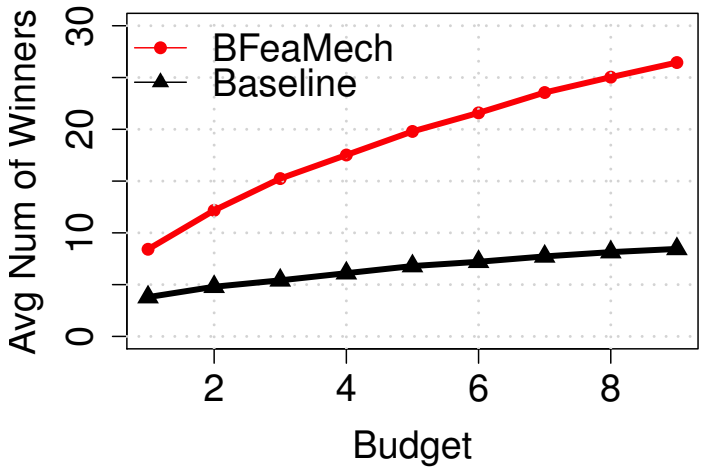

(a)

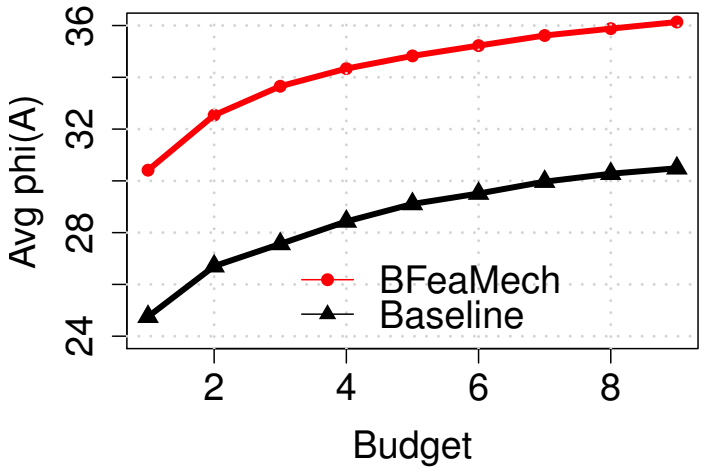

(b)

Figure 3.7: Impact of budget B on the performance of BFeaMech and the baseline mechanism. (a) Average number of purchased samples as a function of B. (b) Average $\phi(\mathcal{A})$ as a function of B. We observe that BFeaMech achieves an average $\phi(\mathcal{A})$ value 18.5%-22.3% higher than that of the baseline mechanism for different budgets.

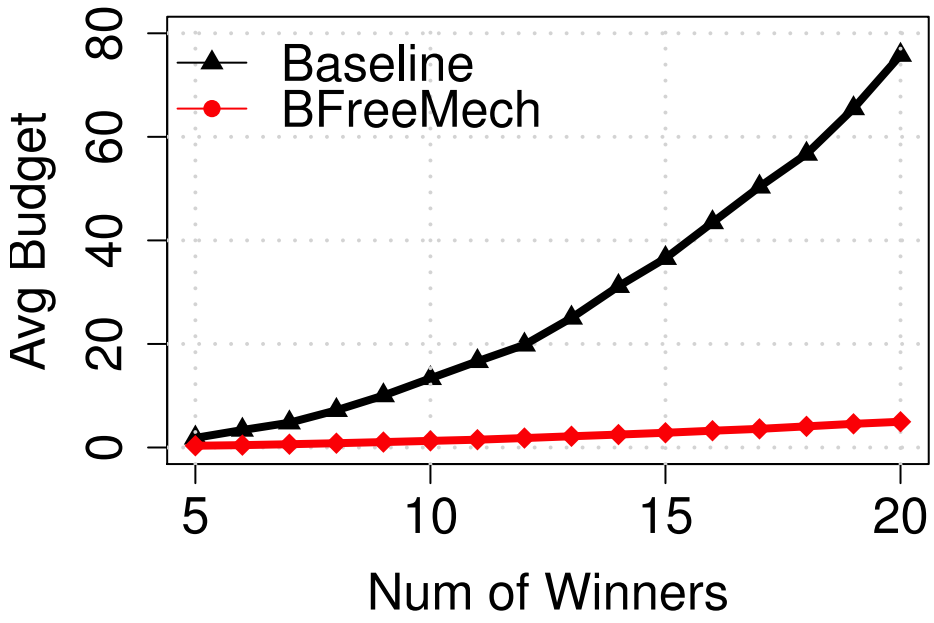

Figure 3.8: Average budget as a function of number of winners k for the baseline mechanism and BFreeMech. For the same number of winners, the average budget required by the baseline mechanism is higher than the average total payment given by BFreeMech.

Chapter 4

PRICING-BASED CROWDSENSING FOR SPATIAL-STATISTICS-BASED RADIO MAPPING

In the previous chapter, we considered the problem of designing an auction-based incentive mechanism for crowdsensed radio mapping based on spatial statistics (Kriging). We showed that the proposed mechanism is computationally efficient, individually rational, budget feasible, and truthful, and it outperforms the baseline mechanism in terms of maximizing the average prediction error reduction.

In this chapter, we employ Gaussian Process (GP) [68, 74] (a generalization of Kriging) as the underlying statistical interpolation technique and incorporate data quality into Mutual Information (MI) [68], a metric that measures the performance of radio mapping. We consider an alternative design of incentive mechanism based on *pricing* [75–77]. In this framework, the platform determines the *value* of a set of users based on location, data quality and its own preferences, which is the amount (of money) it is willing to pay. The platform then determines and send out one-time price offers to a set of selected users, who have only one chance to make a decision (either accept or reject) before the offer expires. If the *sensing cost* (i.e., sum of energy and opportunity costs) does not exceed the offered price, a *rational* user will accept the offer, perform sensing at the reported location, upload data, and receive the corresponding *payment*. Therefore, each set of users is associated with a *utility*, which is equal to the value minus the total payment. Due to possible offer expiration (due to network congestion etc.) and rejection, the platform wants to determine who to send offers to (i.e., *user selection*) and how much to offer (i.e., *price determination*), in order to maximize the *expected utility* (EU). We make the following specific contributions:

- We introduce EU and formulate pricing mechanism design as *EU maximization*. We

first propose *sequential offering*, where the platform sends out the best offer to the best user in each round and keeps offering until the next one is no longer profitable. Then we generalize it to *batched (i.e., single-batch and multi-batch) offering*, where a batch of multiple offers are made in each round.

- For batched offering, we show that EU is *submodular* in the discrete domain. We propose a pricing mechanism that first fixes the pricing rule, and selects users based on *Unconstrained Submodular Maximization* (USM); it compares different pricing rules to find the best batch of offers that maximizes EU (instead of the best-case utility) in each round. We adopt the linear-time deterministic USM algorithm that provides an 1/3 approximation guarantee [78] for user selection. In practice, however, EU is difficult to analytically evaluate and thus the Monte-Carlo estimated EU is fed to the algorithm. We show that its worst-case performance is degraded by estimation errors, and the reduced amount grows linearly in the number of users given the maximum estimation error (Theorem 4.1).

- We conduct extensive simulations to evaluate the proposed EU-maximization-based mechanisms and further compare them against baseline mechanisms that aim to find the best batch of offers that maximize the best-case utility in each round. Results show that our single-batch mechanism is better than the single-batch baseline mechanism with an improvement ranging from 8.5% to 40.5%. If more batches are allowed, our multi-batch mechanism achieves close performance with the multi-batch baseline mechanism, but requires much fewer batches (2.5 versus 7.7 batches on average) and thus a much smaller delay. Sequential offering works better than the single-batch baseline mechanism, but has a very large cumulative delay. Offer expiration adversely affected all mechanisms, but sequential and multi-batch offering are more robust.

The remainder of this chapter is organized as follows. Section 4.1 reviews related work and Section 4.2 provides a two-user tutorial example to illustrate pricing-based crowdsensed

radio mapping. Background on submodularity and our models are presented in Section 4.3. Our pricing mechanisms are presented in Section 4.4 and evaluated in Section 4.5. This chapter is concluded in Section 4.6.

4.1 Related Work

In recent years, spatial-statistics-based radio mapping has been proposed to better capture local radio environments to augment spectrum databases. In [50], Phillips *et al.* applied a statistical interpolation technique (Ordinary Kriging) to map the coverage of WiMax networks. Similar techniques have been applied to estimate the coverage area of single-transmitter [73] and multi-transmitter networks [46] in TV bands. See [79] for a more detailed discussion.

Radio mapping requires a large amount of sensing data, and incentivized crowd-sensing is considered as an economically viable option. A number of various incentive mechanisms have been proposed. In [62], Yang *et al.* studied a platform-centric incentive model, where users share the reward proportionally in a Stackelberg game. In mechanisms based on reserve auction [62, 65, 80], users bid for tasks and receive payments no less than bids when selected. One main goal for the platform is to design a truthful mechanism that motivates users to bid at their true private costs. In [81], Koutsopoulos designed an incentive mechanism to determine participation level and payment allocation to minimize platform's compensation cost with guaranteed service quality. Other models include all-pay auction [82], Bayesian models [81], Tullock contests [83] and posted pricing [75, 77, 84]. Some are proposed in an online setting with constraints like budget limits [84–86], where users arrive in a random order and a typical goal is to maximize a certain objective (e.g., revenue).

Incentive mechanisms are typically tailored to the crowd-sensing application being considered by incorporating factors like user location, data quality and user availability etc. As an example, in [65], each task has a specific location tag and each user can only compete for tasks within its service region. In [87], Peng *et al.* extended the well-known Expectation Maximization algorithm to estimate the quality of sensing data and incorporated it in determining rewards. In [77], Han *et al.* studied a quality-aware Bayesian pricing problem

where both users' sensing costs and qualities are random variables, drawn from known distributions. The goal is to choose an appropriate posted price to recruit a group of users with reasonable sensing quality, and minimize the total expected payment. If users need to move to designated sensing locations or are available at different time periods, then incentive mechanism design is closely coupled with task allocation [76] or scheduling [88].

In this study, we consider incentive mechanism design in an *offline* setting for crowdsensed radio mapping, in which the platform acquires data from a pool of users who are interested and available for sensing in each period, and measurements are taken at their current locations. We consider data quality in terms of hardware quality and incorporate it into the spatial statistical model (GP). Distinct from the auction-based incentive mechanism for crowd-sensed radio mapping [80], we are interested in *pricing mechanisms where the platform makes one-time price offers to a set of selected users* and collects data from those who accept offers. To select users and determine corresponding price offers, we define utility for the platform to trade the value it obtains from the resulting radio map generated based on the offered data against the total price (crowdsensing cost). We further introduce EU to account for possible offer expiration and rejection. We formulate the pricing mechanism design as EU maximization and propose mechanisms based on USM.

4.2 A Two-User Tutorial Example

In this section, we present our system architecture and provide a two-user tutorial example to illustrate the basic idea of pricing for crowdsensed radio mapping.

4.2.1 System Architecture

As shown in Figure 4.1, the platform acquires data periodically from users. At the beginning of each period, the platform broadcasts a sensing task to all users in the area of interest (AoI) with specific sensing parameters (e.g., center frequency, sampling rate, and FFT bin size) to ensure a consistent sensing procedure across different hardware. Note that the task does not specify sensing locations for two reasons. First, there is no need since the platform will take a

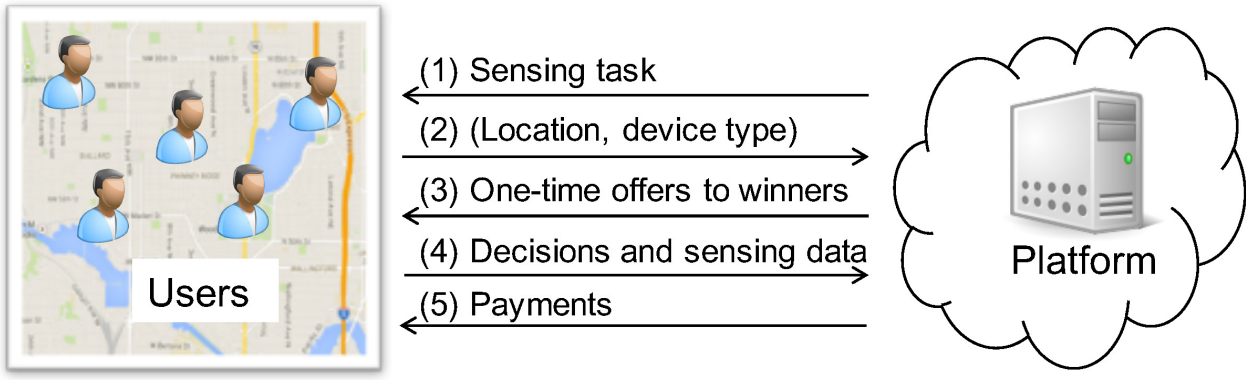

Figure 4.1: Pricing-based crowdsensing system. (1) In each period, the platform first broadcasts a sensing task to users in the area of interest. (2) Users who are interested and available for sensing in the current period report location and device type. (3) The platform determines and sends out one-time offers to selected users. (4) If a selected user decides to accept the offer, it performs the required sensing task. All selected users will inform the platform of their decisions (and upload the data) before the deadline. (5) The platform pays users who contribute data.

sampling approach, that is, selecting a subset of users *after they provide their locations*. This is consistent with the underlying spatial statistical model, where only the relative positioning (instead of absolute locations) that matters for the resulting radio map quality. Second, it requires extra time and costs for users to move to target sensing locations, which means extra incentivization costs for the platform and added complexity for mechanism design[1]. To avoid excessive delay due to communication delay or failure, network congestion etc., each offer has a deadline, by which a decision has to be received by the platform (along with the data if accepted); otherwise, the offer will be expired.

In this study, we assume no entry or other overhead costs, that is, a user does not incur a fee to communicate with the platform. We consider users of low mobility (e.g., pedestrians),

[1]See [76] for more discussions on allocation of tasks with specific locations.

who are honest in providing their information and following the protocol. We assume small displacements between reported locations and eventual sensing locations. We will leave the high-mobility case and security considerations as future work.

4.2.2 A Two-User Scenario

Figure 4.2 illustrates the topology of the two-user example. The goal of the platform is to estimate the RSSI $Z(x)$ (in dBm) at each location $x \in U$, where U represents the discretized AoI. There are two users $S = \{1, 2\}$ at x_1 and x_2 in the AoI. In each period, each user will incur a *sensing cost* $c_i > 0$ and receive an *offer* $p_i > 0$, when selected by the platform. We assume *rational* users, who accept the offer if $c_i \leq p_i$, and reject it otherwise. In the following discussion, we assume no expired offers and will consider them later in Section 4.4.

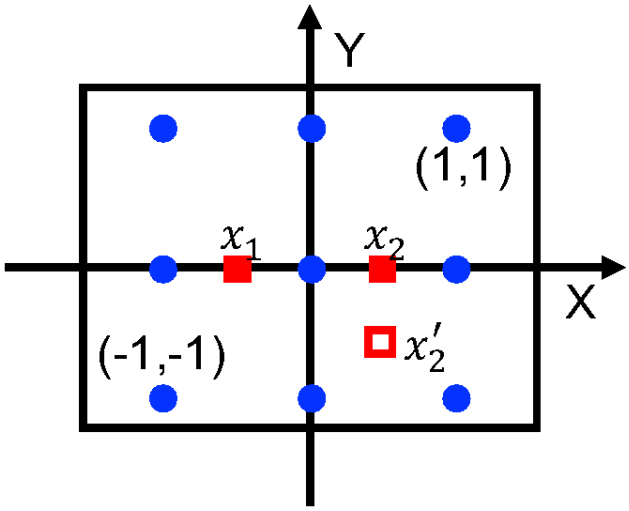

Figure 4.2: Topology of the two-user example. The area of interest is discretized into a mesh grid of 9 points (blue dots). User 1 is at $(-0.5, 0)$, and user 2 is at $(0.5, 0)$ or $(0.5, -0.5)$.

The platform has a *valuation* function $v : 2^S \mapsto \mathbb{R}_+$ and a *pricing* function $p : 2^S \mapsto \mathbb{R}_+$. For each set of users A, there is an associated *value* $v(A)$ and a total price of all offers $p(A) = \sum_{i \in A} p_i$ (i.e., crowdsensing cost for the platform), assuming that each offer is unexpired and

accepted. It makes sense for the platform, as a rational decision maker, to maximize its *utility* (or profit), that is,

$$\max_{A \subseteq S} u(A) = \max_{A \subseteq S} \left(v(A) - p(A) \right), \tag{4.1}$$

which is an important and widely used concept in economics (e.g., rational choice theory [89]) and measures the platform's preference over the set of users A. For convenience, we also write $v(A)$, $p(A)$, and $u(A)$ as v_A, p_A, and u_A, respectively.

In practice, however, the probability that an offer is accepted (and data is uploaded to the platform) by the deadline is less than 1, due to possible expiration and rejection. Hence, only a subset of users in A accept offers, and $u(A)$ is essentially the *best-case* utility. In this case, it makes more senses for the platform to maximize the average-case or *expected utility* (EU). More will be discussed later in this example.

4.2.3 How to Valuate Users

In this example, two RSSI data models are considered: one ignoring shadowing and noise, and the other one is our GP-based model that accounts for both. Both models assume that any small-scale fading over small distances and time has been averaged out via sensing.

Model I – Shadowing-Free, Noise-Free

This model assumes a constant but unknown path-loss-impaired RSSI at any location within the AoI. When there are no measurements, both users are equally valuable, since either can provide accurate estimation. Once one is recruited, a second user has zero marginal value. Hence, we have $v(\{1\}) = v(\{2\}) = v(\{1,2\}) = v_0$, where v_0 is the value (perceived by the platform) of estimating RSSIs at U. We set $v_0 = 4$ for later calculations.

Model II (GP) – Shadowing-Aware, Noise-Aware

Under this model, $Z(x)$ for $x \in U$ is the sum of path-loss-impaired average RSSI $\mu(x)$ and spatially correlated shadowing $\delta(x) \sim N(0, \sigma_x^2)$ with a covariance function $\mathcal{K}(d)$, where d is

the distance between two locations. $Z(x_i)$ for $x_i \in S$ represents the noisy RSSI measured by user i, which includes additional hardware noise $\epsilon_i \sim (0, \sigma^2_{\epsilon_i})$ that is independent of shadowing. Hence, RSSI at each location is modeled as a Gaussian random variable, and RSSIs at $S \cup U$ form a Gaussian random vector, whose joint distribution (Eq. (4.8)) is defined by a mean vector and a covariance matrix (Eq. (4.9)). More details about the model will be provided in Section 4.3.2. Mutual information $MI(A)$ (Eq. (4.12)) is used to quantify radio mapping quality of any subset of users $A \subseteq S$, and the valuation function $v(A)$ defined in Eq. (4.14) (with $\alpha = 0$) is used to translate MI to value that is comparable to payments.

We consider two cases under this model:

- Case 1: Users have different locations but provide data of the same quality. Suppose $x_1 = (-0.5, 0)$, $x_2 = (0.5, 0.5)$ and $\sigma^2_{\epsilon_1} = \sigma^2_{\epsilon_2} = 0.5$.

- Case 2: Users have equally good (i.e., symmetric) locations but provide data of different quality. Suppose $x_1 = (-0.5, 0)$, $x_2 = (0.5, 0)$ and $\sigma^2_{\epsilon_1} = 0.5 > \sigma^2_{\epsilon_2} = 0.2$.

For illustration, we set $\mathcal{K}(d) = 15.5 \cdot \exp(-\frac{d}{0.7})$ [73] (which is consistent with our later simulations in Section 4.5) and set the currency κ in $v(A)$ to 10. Valuation of users under both models is summarized in Table 4.1.

The above highlights a few things. First, apart from the platform's preferences (e.g., choice of valuation function and parameters like κ), the RSSI data model plays an important role. Second, for a reasonable RSSI data model that considers both shadowing and noise, user locations are important (e.g., Case 1 of Model II); data quality also matters and affects valuation (e.g., Case 2 of Model II).

4.2.4 How to Select and Pay Users

At this point, $v(\cdot)$ is available to the platform (Table 4.1). The next step is to select a subset of users and determine their price offers. This process is called "incentivizing".

	$v(\emptyset)$	$v(\{1\})$	$v(\{2\})$	$v(\{1,2\})$
Model I	0	4	4	4
Model II - Case 1	0	2.18	1.76	3.48
Model II - Case 2	0	2.18	2.23	3.82

Table 4.1: Valuation of users in the two-user example.

Deterministic Cost

If user devices are treated as specialized spectrum sensors, then sensing costs are dominated by *energy (or battery)* costs [90]. In this case, it is reasonable to assume deterministic sensing costs, which can be inferred from the task and device type. Since the platform knows $\{c_i\}$, it can set $p_{\{i\}} = c_i$ to minimize payments while guaranteeing offer acceptance, and search for the best set of users.

Suppose $c_1 = 2$ and $c_2 = 1.5$. Then $p_{\{1\}} = 2$, $p_{\{2\}} = 1.5$ and $p_{\{1,2\}} = 3.5$. It is easy to see that $A^* = \{2\}$ leads to the maximum utility in each case. If $c_1 = c_2 = 1.5$, we have $p_{\{1\}} = p_{\{1\}} = 1.5$ and $p_{\{1,2\}} = 3$. Under Model I, selecting either user will lead to a maximum utility of 2.5 but not both. In Case 1 of Model II, the platform is better off with $A^* = \{1\}$, while it better selects both in Case 2 of Model II. Hence, selecting more users does not necessarily leads to a higher utility, since it also means a higher cost for the platform.

Random Cost with Known Distributions

In crowdsensing, however, a user incurs an additional *opportunity cost*, i.e., the loss of potential gain when the user decides to spend resources on sensing instead of other tasks. It depends on the task and device status that varies over time. Hence, the perceived sensing cost in each period consists of a deterministic energy cost and a random opportunity cost.

In this case, it makes sense to model user i's sensing cost as a continuous random variable C_i in $[\underline{c}_i, \bar{c}_i]$, where $\bar{c}_i \geq \underline{c}_i > 0$ and $\underline{c}_i$ is the minimum energy cost. Random variables $\{C_i\}$ are independent of each other. Since device status is considered sensitive information, C_i

is private and only user i knows its realization in each period, c_i, by evaluating the task and current device status[2]. We assume that the platform has only *a priori* probabilistic knowledge of C_i. Let $f_{C_i}(c_i)$ and $F_{C_i}(c_i)$ be the probability density function (PDF) and corresponding cumulative density function (CDF), respectively. The PDF and $\underline{c}_i$, $\bar{c}_i$ could be learned by the platform from the empirical distribution out of prior cost declarations by users of the same device type, or from its long-term interaction with users (e.g., whether or not accept an offer with a known price). If such prior information is absent, C_i may be assumed to be uniformly distributed over $[\underline{c}_i, \bar{c}_i]$. Hence, it is reasonable to assume that the platform can infer $f_{C_i}(c_i)$ or $F_{C_i}(c_i)$ based on the reported device type.

Since the platform does *not* know $\{c_i\}$, it needs to consider possible offer rejections. For $A = \{1\}$ or $\{2\}$, the uncertainty in user decisions implies the following utility,

$$u_{\{i\}} = \begin{cases} v_{\{i\}} - p_{\{i\}}, & \text{if user } i \text{ accepts the offer} \\ 0, & \text{otherwise} \end{cases}, \tag{4.2}$$

which is a Bernoulli random variable and the acceptance probability is $\Pr(c_i \leq p_{\{i\}}) = \int_{\underline{c}_i}^{p_{\{i\}}} f_{C_i}(c_i)dc_i = F_{C_i}(p_{\{i\}})$. In this case, it makes more sense to consider the EU,

$$EU_{\{i\}} = \mathbb{E}[u_{\{i\}}] = (v_{\{i\}} - p_{\{i\}})F_{C_i}(p_{\{i\}}), \tag{4.3}$$

and the platform wants to find $p^*_{\{i\}}$ that maximizes $EU_{\{i\}}$, that is, *EU maximization*. For $A = \{1, 2\}$, the EU is given by

$$\begin{aligned} EU_{\{1,2\}} =& (v_{\{1,2\}} - p_{\{1\}} - p_{\{2\}})F_{C_1}(p_{\{1\}})F_{C_2}(p_{\{2\}}) \\ &+ (v_{\{1\}} - p_{\{1\}})F_{C_1}(p_{\{1\}})(1 - F_{C_2}(p_{\{2\}})) \\ &+ (v_{\{2\}} - p_{\{2\}})(1 - F_{C_1}(p_{\{1\}}))F_{C_2}(p_{\{2\}}). \end{aligned} \tag{4.4}$$

[2]In practice, we would expect a crowd-sensing application to be installed and running on users' mobile devices, which has some function that estimates the perceived sensing cost in each period based on the needed resources for the sensing task and the current device status. Designing such a function for sensing cost estimation will be of practical importance, not only to this work, but also to many other crowd-sensing applications (e.g., [81]). But this topic is out of the scope of this paper, and will be left as future work.

and the goal is to find $\mathbf{p}^* = [p^*_{\{1\}},\ p^*_{\{2\}}]$ that maximizes $EU_{\{1,2\}}$. Note that in general the platform does not have to send out offers all at once and stop; it can send more backup based on the knowledge of outcomes of previous offers.

Suppose that $C_1 \sim U[1,2]$ and $C_2 \sim U[0.5,1.5]$, where $U[\cdot,\cdot]$ denotes the uniform distribution. For pricing, the platform's first thought could be setting $p_{\{i\}} = \bar{c}_i$. Then the following reasoning is the same with the deterministic-cost case. A natural generalization is to choose a desired probability of acceptance[3] $\gamma \in [0,1]$ and set $p_{\{i\}} = F^{-1}_{C_i}(\gamma)$ for each user i, where $F^{-1}_{C_i}(\cdot)$ is the inverse CDF. Given γ, prices are fixed and the platform wants to maximize the EU.

Taking Case 2 of Model II and $\gamma = 0.95$ as an example, we have $p_{\{1\}} = 1.95$, $p_{\{2\}} = 1.45$, $p_{\{1,2\}} = 3.4$, and $A^* = \{2\}$ is the best with $EU_{\{2\}} = (2.23 - 1.45) \cdot 0.95 = 0.74$ by Eq. (4.3) and (4.4). Note that the platform may further consider user 1, if user 2 rejects the offer. Then the overall EU with multi-batch offering would be $EU_{\{2\}} + (1-\gamma)EU_{\{1\}} > EU_{\{2\}}$.

Given A, γ can also be optimized in each batch. Taking Case 2 of Model II as an example, when $A = \{1\}$, $EU_{\{1\}} = (2.18 - (1+\gamma))\gamma$ and $\gamma^* = 0.59$, $EU^*_{\{1\}} = 0.35$. Similarly, for $A = \{2\}$, $EU_{\{2\}} = (2.23 - (0.5+\gamma))\gamma$ and $\gamma^* = 0.865$, $EU^*_{\{2\}} = 0.75$. When $A = \{1,2\}$, we have $EU_{\{1,2\}} = -2.59\gamma^2 + 2.91\gamma$ and $\gamma^* = 0.56$, $EU^*_{\{1,2\}} = 0.82$. In this case, instead of using the same γ, the platform can also choose $\{\gamma_i\}$ for each user separately, and maximizing Eq. (4.4) leads to $\gamma^*_1 = 0.37, \gamma^*_2 = 0.76$ and the resulting $EU^*_{\{1,2\}} = 0.87$.

As we can see, the notation of utility accounts for locations, data quality and sensing costs, and the notation of EU further considers possible offer rejections. We can also see that user selection and price determination are closely coupled in a pricing mechanism. More will be discussed in Section 4.4.

---

[3]Compared to choosing the same desired price for all users, it makes more sense to choose the same desired probability for all users, since users have different cost distributions in general. If all user devices are of the same type, then these two approaches are the same.

4.3 Preliminaries and Our Model

In this section, we provide background on submodularity. We then present our spatial statistical model and define the metric for measuring radio mapping performance. Finally, we present our valuation model and explore its properties.

4.3.1 Preliminaries

The submodularity property is formally defined as follows.

Definition 4.1 (Submodularity)**.** *Let Ω be a finite set. A function $f : 2^{\Omega} \mapsto \mathbb{R}$ is submodular if for any $A, B \subseteq \Omega$,*

$$f(A) + f(B) \geq f(A \cup B) + f(A \cap B). \tag{4.5}$$

Equivalently [91], a function f is submodular if, for any $A \subseteq B \subseteq \Omega$ and any $i \in \Omega \setminus B$,

$$f(A \cup \{i\}) - f(A) \geq f(B \cup \{i\}) - f(B). \tag{4.6}$$

The notion of submodularity captures *diminishing returns* behaviors: adding a new element increases f more, if there are fewer elements so far, and less, if there are more elements.

Definition 4.2 ((Approximately) monotonic function)**.** *Let Ω be a finite set. A function $f : 2^{\Omega} \mapsto \mathbb{R}$ is said to be monotone (or monotonic), if $f(A \cup \{i\}) - f(A) \geq 0$ for any $A \subseteq \Omega$ and any $i \in \Omega \setminus A$; f is said to be α-approximately monotonic, if $f(A \cup \{i\}) - f(A) \geq -\alpha$ for some small $\alpha > 0$, and for any $A \subseteq \Omega$ and any $i \in \Omega \setminus A$.*

One of the most basic submodular maximization problems is USM, which is formally defined as follows.

Definition 4.3 (USM)**.** *Given a nonnegative submodular fucntion $f : 2^S \mapsto \mathbb{R}_+$, $\max_{A \subseteq S} f(A)$ is called Unconstrained Submodular Maximization.*

It is well known that USM is NP-hard [91,92] and thus heuristic-based algorithms are often used to find approximate solutions. One state-of-art *linear-time* deterministic algorithm

Algorithm 3 `USM`

Input: S – ground set, f – nonnegative submodular function

Output: A_n (or B_n) – selected subset

$A_0 \leftarrow \emptyset$, $B_0 \leftarrow S$
for $i = 1$ to n **do**
  $a_i \leftarrow f(A_{i-1} \cup \{u_i\}) - f(A_{i-1})$
  $b_i \leftarrow f(B_{i-1} \setminus \{u_i\}) - f(B_{i-1})$
  if $a_i \geq b_i$ **then**
    $A_i \leftarrow A_i \cup \{u_i\}$, $B_i \leftarrow B_{i-1}$
  else
    $A_i \leftarrow A_{i-1}$, $B_i \leftarrow B_{i-1} \setminus \{u_i\}$
  end if
end for
return A_n (or equivalently B_n)

is proposed in [78] and provided in Algorithm 3 for reference in the rest of this work. It is essentially a greedy algorithm, and achieves a 1/3-approximation, i.e., the algorithm obtains a solution A with the guarantee that $f(A) \geq \frac{1}{3} f(OPT)$, where OPT is the optimal solution.

4.3.2 Spatial Statistical Model – Gaussian Process

In this study, we employ GP [68, 74] (a generalization of Kriging) for radio mapping. Let the set of n interested users be S, and the finely discretized AoI be U, where $|U| \gg |S| = n$, where $|\cdot|$ is the cardinality operator. Define $V = S \cup U$ and each index $i \in V$ corresponds to a location x_i. Since the platform obtains *noisy* RSSI measurements at S and wants to estimate *noiseless* front-end RSSIs at U, the RSSI $Z(x_i)$ or Z_i is modeled as a Gaussian

random variable in GP,

$$Z(x_i) = \begin{cases} \mu(x_i) + \delta(x_i), & \text{for } i \in U \\ \mu(x_i) + \delta(x_i) + \epsilon_i, & \text{for } i \in S \end{cases}, \qquad (dBm) \tag{4.7}$$

where $\mu(x_i)$ is path-loss-impaired RSSI, $\delta(x_i) \sim N(0, \sigma_{x_i}^2)$ is spatially correlated shadowing and $\epsilon_i \sim N(0, \sigma_{\epsilon_i}^2)$ is hardware noise of user i's device.

Define a kernel (or covariance) function $\mathcal{K}(\cdot, \cdot)$ such that $\mathcal{K}(i, j)$ is the covariance between $\delta(x_i)$ and $\delta(x_j)$. In GP, the RSSIs at V form a Gaussian random vector $Z_V = [Z(x_i)]_{i \in V}$ with a joint distribution of

$$f_{Z_V}(z_V) = \frac{1}{(2\pi)^{n/2}|\Sigma_{VV}|} e^{-\frac{1}{2}(z_V - \mu_V)^T \Sigma_{VV}^{-1}(z_V - \mu_V)}, \tag{4.8}$$

where $z_V = [z(x_i)]_{i \in V}$ is a realization of Z_V, $\mu_V = [\mu(x_i)]_{i \in V}$ is the mean vector and Σ_{VV} is the covariance matrix. For any pair of indices $i, j \in V$, their covariance σ_{ij} is the (i, j)-th entry of Σ_{VV}, which is given by

$$\sigma_{ij} = \begin{cases} \mathcal{K}(i, j), & \text{if } i \neq j \\ \mathcal{K}(i, j) \text{ or } \sigma_{x_i}^2, & \text{if } i = j \in U \\ \mathcal{K}(i, j) + \sigma_{\epsilon_i}^2 \text{ or } \sigma_{x_i}^2 + \sigma_{\epsilon_i}^2, & \text{if } i = j \in S \end{cases} \tag{4.9}$$

Given a set of measurements Z_A where $A \subseteq S$, $Z(x_i)$ is a conditional Gaussian random variable with a mean $\mu_{Z(x_i)|Z_A}$ (or simply $\mu_{i|A}$) and a variance of $\sigma_{Z(x_i)|Z_A}^2$ (or simply $\sigma_{i|A}^2$),

$$\mu_{i|A} = \mu(x_i) + \Sigma_{Ai}^T \Sigma_{AA}^{-1}(z_A - \mu_A), \tag{4.10}$$

$$\sigma_{i|A}^2 = \sigma_{ii} - \Sigma_{Ai}^T \Sigma_{AA}^{-1} \Sigma_{Ai}. \tag{4.11}$$

Note that the posterior variance in Eq. (4.11) only depends on Σ_{VV}, not the actual measured values z_A.

Estimating $\mathcal{K}(\cdot, \cdot)$ can be difficult in practice, and it is often assumed that $\mathcal{K}(\cdot, \cdot)$ is stationary (i.e., a function of location displacement) and isotropic (i.e., a function of distance). In other words, $\mathcal{K}(i, j) = \mathcal{K}_\theta(||x_i - x_j||)$, where θ is a set of parameters. That being said,

our following discussions do not assume stationarity or isotropy, and thus can be applied to general kernel functions. But we do assume both mean and kernel functions have been estimated from previous measurements[4] and available in the current period.

4.3.3 Mutual Information for Uncertainty Reduction

To measure radio mapping performance, we adopt the MI metric [68] as defined below,

$$MI(A) = I(Z_A; Z_{V\setminus A}) = H(Z_{V\setminus A}) - H(Z_{V\setminus A}|Z_A), \tag{4.12}$$

which is the amount of uncertainty reduction about RSSIs at unmeasured locations given measurements at A.

Note that the platform is interested in $Z_{V\setminus A}$, which includes RSSIs at $S\setminus A$ (i.e., locations with confirmed user presence) and U (i.e., locations with possible user presence). As implicitly assumed in [68], $Z(x_i)$ includes noise for $i \in S \setminus A$ in the definition of MI, which is not a big issue, since noise is relatively small. Compared to the entropy criterion $H(Z_{V\setminus A}|Z_A)$, MI tends to not select users along the boundaries and avoids the "waste" of information.

Denote by $MI(i|A)$ the marginal MI of an additional user $i \in S \setminus A$ given A, which is

$$\begin{aligned} MI(i|A) &= MI(\{i\} \cup A) - MI(A) \\ &= H(Z_i|Z_A) - H(Z_i|Z_{V\setminus(A\cup\{i\})}), \end{aligned} \tag{4.13}$$

where $H(Z_i|Z_A) = \frac{1}{2}\log(2\pi e\sigma^2_{i|A})$ is the conditional entropy, which can be easily computed from Eq. (4.11). It was shown in [68] that $MI(A)$ is both submodular and α-approximately monotone[5]. For any given $\alpha > 0$, a discretization level exists so that $MI(A)$ is approximately monotone.

---

[4]In [50], authors used a predictive (empirical) path loss model to estimate the mean process $\mu(x)$. This procedure is called *detrending*. In the same paper as well as [73], authors estimated an empirical semivariogram $\gamma(\cdot)$ (isotropic and stationary) from real measurements and fitted it with parametric models. The relationship between $\gamma(\cdot)$ and $\mathcal{K}(\cdot,\cdot)$ is $\mathcal{K}(i,j) = c_0 - \gamma(||x_i - x_j||)$ for $i \neq j$, where c_0 is some constant.

[5]Intuitively, $MI(A)$ is monotone under the condition that $|V| \gg |S| \geq |A|$ and thus adding one more user increases the MI. Otherwise, consider the example that $S = \{1,2\}$ and $|V| = |S|$, then $MI(\emptyset) = MI(\{1,2\}) = 0$ but $MI(\{1\}) > 0$ and $MI(\{2\}) > 0$, which means that MI first increases then decreases as more users are selected. Its monotonicity is approximate due to the extreme case where there exist two (or

4.3.4 Valuation Function

We consider the following valuation function $v : 2^S \mapsto \mathbb{R}_+$ for the platform,

$$v(A) = \kappa \cdot \log(1 + MI'(A)), \tag{4.14}$$

where $\kappa > 0$ is a constant and $MI'(A) = MI(A) + \alpha|A|$. Intuitively, κ is the currency that reflects the platform's preference over per unit MI (in log scale). Commonly used in economics, $\log(\cdot)$ further emphasizes the diminishing returns behavior. We introduce $\alpha|A|$ to ignore the extreme case where some users are arbitrarily close to each other, which rarely occurs and/or can be avoided in practice (see Footnote 5).

We show that there exists useful structural properties like submodularity and monotonicity in $v(A)$.

Lemma 4.1. *The valuation function $v(\cdot)$ in Eq. (4.14) is monotone submodular.*

Proof. Consider two sets A, B such that $A \subseteq B \subseteq S$ and any $i \in S \setminus B$. Let $f(A) = 1 + MI'(A)$. We know that $f(A)$ is submodular from the submodularity of $MI(A)$, since

$$\begin{aligned} f(A \cup \{i\}) - f(A) &= MI(A \cup \{i\}) - MI(A) + \alpha \\ &\geq MI(B \cup \{i\}) - MI(B) + \alpha \\ &= f(B \cup \{i\}) - f(B). \end{aligned} \tag{4.15}$$

We also know that $f(\mathcal{A})$ is monotone, since $MI(A)$ is α-approximately monotone and thus

$$f(A \cup \{i\}) - f(A) = MI(A \cup \{i\}) - MI(A) + \alpha \geq 0. \tag{4.16}$$

Let $a = f(A)$, $b = f(A \cup \{i\})$, $c = f(B)$, and $d = f(B \cup \{i\})$. From the submodularity and monotonicity of $f(\cdot)$, we have $b - a \geq d - c \geq 0$ and $d \geq b$. Let $a' = b - (d - c) \geq a$. Since $\log(\cdot)$

more) users arbitrarily close to each other. If one is selected, selecting the other one will decrease MI. More discussions are available in [68]. In practice, the platform can avoid such extreme cases by considering only one of them. Also, a pricing mechanism that maximizes the (expected) utility should not select both, since the second user is not beneficial for radio mapping and not free-of-charge.

is non-decreasing concave, we have $\log(b) - \log(a) \geq \log(b) - \log(a') \geq \log(d) - \log(c) \geq 0$. Hence, $v(A \cup \{i\}) - v(A) \geq v(B \cup \{i\}) - v(B) \geq 0$, and $v(\cdot)$ is submodular monotone.

□

4.4 Pricing Mechanism

In this section, we formulate pricing mechanism design as EU maximization and propose two schemes: (1) sequential offering and (2) batched offering.

4.4.1 EU Maximization

Given S, $v(\cdot)$ and $\{F_{C_i}(c_i)\}$, the platform wants to determine a set of offers $(A, \mathbf{p})$, where $A \subseteq S$ are selected users and $\mathbf{p} = [p_i]_{i \in A}$ is the corresponding price vector. Let the decision of the i-the selected user be X_i, which is given by

$$X_i = \begin{cases} 1, & \text{if } c_i \leq p_i \text{ (i.e., offer is accepted)} \\ 0, & \text{else (i.e., offer is rejected)} \end{cases}. \tag{4.17}$$

It is a Bernoulli random variable (from the perspective of the platform), and $\Pr(X_i = 1) = \int_{\underline{c}_i}^{p_i} f_{C_i}(c_i) dc_i = F_{C_i}(p_i)$.

As mentioned in Section 4.2.1, an offer may be expired, and this event is modeled by a random variable X_i', i.e.,

$$X_i' = \begin{cases} 1, & \text{if offer is unexpired} \\ 0, & \text{if offer is expired} \end{cases}, \tag{4.18}$$

where $\rho_i = \Pr(X_i' = 1)$ is the probability of an unexpired offer. We assume that the platform can estimate ρ_i and that X_i' is independent of X_i.

Let Y_i be a random variable that represents whether a user is successfully *recruited* (i.e., offer is unexpired and accepted),

$$Y_i = \begin{cases} 1, & \text{if offer is unexpired AND accepted} \\ 0, & \text{if offer is expired OR rejected} \end{cases}, \tag{4.19}$$

where

$$\begin{aligned}\gamma_i &= \Pr(Y_i = 1) = \Pr(X_i' = 1, X_i = 1) \\ &= \Pr(X_i' = 1) \cdot \Pr(X_i = 1 | X_i' = 1) \\ &= \rho_i \cdot F_{C_i}(p_i) \in [0, \rho_i], \end{aligned} \tag{4.20}$$

is the probability that the i-th selected user is recruited.

Define $\mathbf{Y} = [Y_i]_{i \in A}$ and let $\mathbf{y}$ be the realization of $\mathbf{Y}$. Then $A_{\mathbf{y}} \subseteq A$ is the set of recruited users. Then the EU is given by

$$EU(A, \mathbf{p}) = \mathbb{E}_{\mathbf{Y}}[u(A_{\mathbf{y}}, \mathbf{p})] = \sum_{\mathbf{y}} \Pr(A_{\mathbf{y}}, \mathbf{p}) u(A_{\mathbf{y}}, \mathbf{p}), \tag{4.21}$$

where

$$\Pr(A_{\mathbf{y}}, \mathbf{p}) = \prod_{i \in A_{\mathbf{y}}} \gamma_i \cdot \prod_{i \notin A_{\mathbf{y}}} (1 - \gamma_i), \tag{4.22}$$

$$u(A_{\mathbf{y}}, \mathbf{p}) = v(A_{\mathbf{y}}) - \sum_{i \in A_{\mathbf{y}}} p_i, \tag{4.23}$$

are the probability and utility of $A_{\mathbf{y}}$ given $\mathbf{p}$, respectively.

The platform's goal is to design a *pricing mechanism* based on *EU maximization*, i.e.,

$$\max_{A \subseteq S, \mathbf{p}} EU(A, \mathbf{p}). \tag{4.24}$$

Hence, we can see from Eq. (4.24) that a pricing mechanism consists of a *selection rule* and a *pricing rule*, which is joint optimization in the discrete and continuous domains.

4.4.2 Sequential Offering

We first consider a special case of EU maximization, where $|A| = 1$. That is, the platform only selects one best user with its best offer in each round, and waits for its decision before making the next offer. We call it *sequential (individual) offering*. Formally, the task in each round is

$$\max_{i \in S \setminus A, p_i} EU(A \cup \{i\}, [\mathbf{p},\ p_i] | \mathbf{Y} = \mathbf{y}), \tag{4.25}$$

Algorithm 4 `Sequential_Offering`

Input: S – set of users, $v(\cdot)$ – valuation function, $\{F_{C_i}(\cdot)\}$ – cost distributions, $\{\rho_i\}$ – probabilities of unexpired offers, τ – threshold

Output: A – selected users, $\mathbf{p}$ – prices, $\mathbf{y}$ – outcomes

$A \leftarrow \emptyset$, $\mathbf{p} \leftarrow NULL$, $\mathbf{y} \leftarrow NULL$
while $A \neq S$ **do**
  for each user i in $S \setminus A$ **do**
    $p_i^* \leftarrow \arg\max_{p_i \in [\underline{c}_i, \bar{c}_i]} [v(i|A_{\mathbf{y}}) - p_i] \cdot F_{C_i}(p_i)$
    $EU_i \leftarrow [v(i|A_{\mathbf{y}}) - p_i^*] \cdot \rho_i \cdot F_{C_i}(p_i^*)$
  end for
  $i^* \leftarrow \arg\max_{i \in S \setminus A} EU_i$
  while $EU_{i^*} > \tau$ **do**
    Send the offer $(i^*, p_{i^*}^*)$ and observe y_{i^*} $A \leftarrow A \cup \{i^*\}$, $\mathbf{p} \leftarrow [\mathbf{p}, p_{i^*}^*]$, $\mathbf{y} \leftarrow [\mathbf{y}, y_{i^*}]$
    if $y_{i^*} = 1$ **then**
      break
    else
      $i^* \leftarrow \arg\max_{i \in S \setminus A} EU_i$
    end if
  end while
end while
return A, $\mathbf{p}$, $\mathbf{y}$

where $\mathbf{y}$ represents the outcomes of offers that have been sent and is known to the platform.

The algorithm for sequential offering is described in Algorithm 4. The idea is as follows: The platform first determines an optimum price p_i^* tailored to each i that maximizes EU_i. Then it picks the index i^* that maximizes among the EU_i, and offers to that user the corresponding $p_{i^*}^*$.

Price Determination (Lines 3-6)

Depending on whether user $i \in S \setminus A$ is successfully recruited, the utility is

$$u(A_{\mathbf{y}} \cup \{i\}_{Y_i}, [\mathbf{p},\ p_i]) = u(A_{\mathbf{y}}, \mathbf{p}) + \begin{cases} v(i|A_{\mathbf{y}}) - p_i, & \text{if } Y_i = 1 \\ 0, & \text{otherwise,} \end{cases} \tag{4.26}$$

where $v(i|A_{\mathbf{y}}) = v(\{i\} \cup A_{\mathbf{y}}) - v(A_{\mathbf{y}})$ is the marginal value of i given $A_{\mathbf{y}}$. The task is to find

$$\begin{aligned} p_i^* &= \arg \max_{p_i \in [\underline{c}_i, \bar{c}_i]} \mathbb{E}_{Y_i}[u(A_{\mathbf{y}} \cup \{i\}_{Y_i}, [\mathbf{p},\ p_i])] \\ &= \arg \max_{p_i \in [\underline{c}_i, \bar{c}_i]} [v(i|A_{\mathbf{y}}) - p_i] \cdot \Pr(Y_i = 1) \\ &= \arg \max_{p_i \in [\underline{c}_i, \bar{c}_i]} [v(i|A_{\mathbf{y}}) - p_i] \cdot F_{C_i}(p_i). \end{aligned} \tag{4.27}$$

Note that ρ_i in $\Pr(Y_i = 1)$ in Eq. (4.20) is a constant and does not impact the choice of p_i^*. If $f_{C_i}(c_i) = F'_{C_i}(c_i)$ is differentiable and non-increasing, the objective function in Eq. (4.27) will be concave in p_i, and p_i^* can be obtained with efficient algorithms (e.g., gradient descent). If $F_{C_i}(c_i)$ is twice continuously differentiable, techniques like interval analysis may be used to find p^* [93].

User Selection (Line 7)

The best user i^* that maximizes the EU is found,

$$i^* = \arg \max_{i \in S \setminus A} [v(i|A_{\mathbf{y}}) - p_i^*] \cdot \rho_i \cdot F_{C_i}(p_i^*). \tag{4.28}$$

Note that the above selection also takes ρ_i into account. If the user is recruited (Lines 10), the algorithm will go to Line 3 to recompute best prices for remaining users; otherwise, it

sends out the next best offer immediately until one is accepted (Lines 8-15). To enable fast convergence, the platform can set a minimum threshold $\tau > 0$ (e.g., 0.01) for the marginal EU (Line 8). The platform stops making offers when there are (1) no remaining users or (2) none of the remaining users leads to a non-trivial marginal EU.

Complexity Analysis

If we assume $\mathcal{O}(1)$ for computing the best price for a single user, the overall computational complexity of Algorithm 4 is $\mathcal{O}(n^2)$, since it takes $\mathcal{O}(n)$ to compute best prices for all remaining users and may select up to n users in the worst case. The inner while-loop does not require re-computation of best prices and is dominated by the for-loop. Note that $\mathcal{O}(n^2)$ is very conservative, since the algorithm may stop much earlier based on the configuration.

4.4.3 Batched Offering

As we can see, sequential offering is intuitive and straightforward, but its main drawback is the (possibly) large delay accumulated over multiple rounds of offering. Hence, a natural generalization is to make multiple offers (i.e., a batch) in each round and continue offering for multiple rounds. We refer to it as *(sequential) batched offering*.

In batched offering, the platform is faced with the general case of EU maximization in Eq. (4.24) in each round. Unfortunately, joint optimization can be difficult in practice, mainly because $EU(A, \mathbf{p})$ is a multi-variate function in the continuous domain of $\mathbf{p}$ given A, and there may not exist structural properties like concavity in general to enable efficient computation of the global optimum. Exhaustive search is prohibitive as the space of $\mathbf{p}$ is huge. Fortunately, $EU(A, \mathbf{p})$ has a useful structural property (i.e., submodularity) in the discrete domain of A as a set function, which inspires our following pricing mechanism design.

Lemma 4.2. Given $\mathbf{p}$, $EU(A, \mathbf{p})$ is submodular in A.

Proof. We notice that $u(A_{\mathbf{y}}, \mathbf{p})$ is submodular in $A_{\mathbf{y}}$ given $\mathbf{p}$, since $v(\cdot)$ is submodular

(Lemma 4.1) and

$$u(A_{\mathbf{y}} \cup \{i\}, \mathbf{p}) - u(A_{\mathbf{y}}, \mathbf{p}) = v(i|A_{\mathbf{y}}) - p_i \geq v(i|B) - p_i$$
$$\geq u(B \cup \{i\}, \mathbf{p}) - u(B, \mathbf{p}) \tag{4.29}$$

for $A_{\mathbf{y}} \subseteq B \subseteq S$ and any $i \in S \setminus B$. Since the class of submodular functions are closed under taking expectations, it follows that $EU(A, \mathbf{p})$ is submodular in A given $\mathbf{p}$. □

The basic idea of our pricing mechanism is to first fix the pricing rule and then focus on user selection to exploit the submodularity property. As mentioned in Section 4.3.1, if a set function f is nonnegative submodular and the problem is $\max_{A \subseteq S} f(A)$, there exist heuristic-based algorithms (e.g., Algorithm 3) that provide solutions with performance guarantee at low complexity. Next, we will present our pricing mechanisms for single-batch and multi-batch offering.

Single-Batch Offering

As mentioned in Section 4.2, we consider the following pricing rule in this work: the platform chooses a desired probability of recruitment $\gamma \in (0, 1]$ such that $\gamma_i = \min(\gamma, \rho_i)$ for any $i \in S$ and determines corresponding prices, i.e.,

$$p_\gamma(A) = \sum_{i \in A} p_\gamma(\{i\}) = \sum_{i \in A} F_{C_i}^{-1}\left(\min(\gamma/\rho_i, 1)\right). \tag{4.30}$$

Given $p_\gamma(\cdot)$, user selection then becomes

$$\max_{A \subseteq S} EU_\gamma(A) = \max_{A \subseteq S} \sum_{\mathbf{y}} \Pr_\gamma(A_{\mathbf{y}}) u_\gamma(A_{\mathbf{y}}), \tag{4.31}$$

where $\Pr_\gamma(A_{\mathbf{y}}) = \prod_{i \in A_{\mathbf{y}}} \gamma_i \cdot \prod_{i \notin A_{\mathbf{y}}} (1 - \gamma_i)$ and $u_\gamma(A_{\mathbf{y}}) = v(A_{\mathbf{y}}) - p_\gamma(A_{\mathbf{y}})$. By Lemma 4.2, $EU_\gamma(A)$ is submodular.

However, the USM formulation also requires the objective function to be nonnegative, but $EU_\gamma(A)$ can be negative. To bypass this issue, one straightforward way is to define

$$EU'_\gamma(A) = EU_\gamma(A) + p_0 \tag{4.32}$$

where

$$p_0 = \sum_{i \in S} \gamma_i p_\gamma(\{i\}) \tag{4.33}$$

is a constant that represents the maximum expected price, and adding a constant preserves submodularity. It is easy to see that $EU'_\gamma(A)$ is both submodular and nonnegative, and $\max_{A \subseteq S} EU'_\gamma(A)$ is equivalent to $\max_{A \subseteq S} EU'_\gamma(A)$.

Another issue is due to the difficulty of analytically evaluating $EU_\gamma(A)$ (or $EU'_\gamma(A)$), since it involves an exponentially growing number of terms due to the summation in Eq. (4.31). In practice, the Monte-Carlo (MC) method [94] can be used to obtain estimates of $\hat{EU}_\gamma(A)$ as well as $\hat{EU}'_\gamma(A)$ (by adding the constant p_0 to $\hat{EU}_\gamma(A)$). We show that $\texttt{USM}(S, \hat{EU}'_\gamma)$ has the following performance.

Theorem 4.1. *If $|\hat{EU}'_\gamma(A) - EU'_\gamma(A)| \leq \epsilon$ for some small $\epsilon > 0$ for any $A \subseteq S$, $\texttt{USM}(S, \hat{EU}'_\gamma)$ (or equivalently $\texttt{USM}(S, \hat{EU}_\gamma)$) returns a solution A with the following performance,*

$$EU'_\gamma(A) \geq \frac{1}{3} EU'_\gamma(OPT) - \frac{1}{3}(2n+2)\epsilon, \text{ and} \tag{4.34}$$

$$EU_\gamma(A) \geq \frac{1}{3} EU_\gamma(OPT) - \frac{2}{3} p_0 - \frac{1}{3}(2n+2)\epsilon, \tag{4.35}$$

where OPT is the optimal solution for $\max_{A \subseteq S} EU'_\gamma(A)$ as well as $\max_{A \subseteq S} EU_\gamma(A)$, $p_0 = \sum_{i \in S} \gamma_i p_\gamma(\{i\})$ and $n = |S|$.

Proof. Before proving Theorem 4.1, we first prove the following lemma.

Lemma 4.3. *Given a nonnegative submodular function $f : 2^S \mapsto \mathbb{R}_+$ and its estimate $\hat{f}$ with $|\hat{f}(A) - f(A)| \leq \epsilon$ for any $A \subseteq S$ and some small $\epsilon > 0$, $\texttt{USM}(S, \hat{f})$ returns a solution A with the following performance guarantee,*

$$f(A) \geq \frac{1}{3} f(OPT) - \frac{1}{3}(2n+2)\epsilon \tag{4.36}$$

where $OPT = \arg\max_{A \subseteq S} f(A)$ and $n = |S|$.

Proof. Our proof of Lemma 4.3 is inspired by the proof in [78]. Let us start with Lemma 4.4.

Lemma 4.4. *For every* $1 \leq i \leq n$, $a_i + b_i \geq -4\epsilon$, *where* $a_i = \hat{f}(A_{i-1} \cup \{u_i\}) - \hat{f}(A_{i-1})$ *and* $b_i = \hat{f}(B_{i-1} \setminus \{u_i\}) - \hat{f}(B_{i-1})$.

Proof. Since $|\hat{f}(A) - f(A)| \leq \epsilon$, $\forall A \subseteq S$, we have

$$f(A) - \epsilon \leq \hat{f}(A) \leq f(A) + \epsilon, \ \forall A \subseteq S. \tag{4.37}$$

Notice that $(A_{i-1} \cup \{u_i\}) \cup (B_{i-1} \setminus \{u_i\}) = B_{i-1}$, $(A_{i-1} \cup \{u_i\}) \cap (B_{i-1} - u_i) = A_{i-1}$. Based on both observations and submodularity of f, we get

$$\begin{aligned} a_i + b_i &= [\hat{f}(A_{i-1} \cup \{u_i\}) - \hat{f}(A_{i-1})] + [\hat{f}(B_{i-1} \setminus \{u_i\}) - \hat{f}(B_{i-1})] \\ &\geq [f(A_{i-1} \cup \{u_i\}) + f(B_{i-1} \setminus \{u_i\})] - [f(A_{i-1}) + f(B_{i-1})] - 4\epsilon \geq -4\epsilon. \end{aligned}$$

Hence, Lemma 4.4 is true. □

Define $OPT_i \triangleq (OPT \cup A_i) \cap (B_i)$. Therefore, $OPT_0 = OPT$ and the algorithm outputs $OPT_n = A_n = B_n$. Examine the sequence $f(OPT_0)$, ..., $f(OPT_n)$, which starts with $f(OPT)$ and ends with the f value of the output of the algorithm. The idea is to bound the total loss of value along this sequence.

Lemma 4.5. *For every* $1 \leq i \leq n$, *we have*

$$f(OPT_{i-1}) - f(OPT_i) \leq [\hat{f}(A_i) - \hat{f}(A_{i-1})] + [\hat{f}(B_i) - \hat{f}(B_{i-1})] + 2\epsilon.$$

Proof. W.L.O.G., we assume that $a_i \geq b_i$, i.e., $A_i \leftarrow A_{i-1} \cup \{u_i\}$, $B_i \leftarrow B_{i-1}$ (the other case is analogous). Notice that in this case $OPT_i = (OPT \cup A_i) \cap B_i = OPT_{i-1} \cup \{u_i\}$, $B_i = B_{i-1}$ and $\hat{f}(B_i) = \hat{f}(B_{i-1})$. Hence, the inequality we need to prove is that

$$f(OPT_{i-1}) - f(OPT_{i-1} \cup \{u_i\}) \leq [\hat{f}(A_i) - \hat{f}(A_{i-1})] + 2\epsilon = a_i + 2\epsilon.$$

We now consider two cases. If $u_i \in OPT$, then the left-hand of the inequality is 0, and all we need to show is that $a_i \geq -2\epsilon$. This is true since $a_i + b_i \geq -4\epsilon$ by Lemma 4.4, and we

assumed $a_i \geq b_i$. If $u_i \notin OPT$, then also $u_i \notin OPT_{i-1}$, and thus

$$\begin{aligned} f(OPT_{i-1}) - f(OPT_{i-1} \cup \{u_i\}) &\leq f(B_{i-1} \setminus \{u_i\}) - f(B_{i-1}) \\ &\leq \hat{f}(B_{i-1} \setminus \{u_i\}) - \hat{f}(B_{i-1}) + 2\epsilon \\ &= b_i + 2\epsilon \leq a_i + 2\epsilon. \end{aligned}$$

The first inequality follows by submodularity: $OPT_{i-1} = ((OPT \cup A_{i-1}) \cap B_{i-1}) \subseteq (B_{i-1} \setminus \{u_i\})$ (recall that $u_i \in B_{i-1}$ and $u_i \notin OPT_{i-1}$). The second and third inequalities follow from Eq. (4.37) and our assumption that $a_i \geq b_i$, respectively. □

Summing up Lemma 4.5 for every $1 \leq i \leq n$, we have

$$\sum_{i=1}^{n} [f(OPT_{i-1}) - f(OPT_i)] \leq \sum_{i=1}^{n} [\hat{f}(A_i) - \hat{f}(A_{i-1})] + \sum_{i=1}^{n} [\hat{f}(B_i) - \hat{f}(B_{i-1})] + 2n\epsilon.$$

The above sum is telescopic and we have

$$\begin{aligned} f(OPT_0) - f(OPT_n) &\leq [\hat{f}(A_n) - \hat{f}(A_0)] + [\hat{f}(B_n) - \hat{f}(B_0)] + 2n\epsilon \\ &\leq \hat{f}(A_n) + \hat{f}(B_n) + 2n\epsilon \leq f(A_n) + f(B_n) + (2n+2)\epsilon \end{aligned} \tag{4.38}$$

By our definition, $OPT_0 = OPT$ and $OPT_n = A_n = B_n$. Then we obtain that $f(OPT) \leq 3f(A_n) + (2n+2)\epsilon$ and $f(A_n) = f(B_n) \geq \frac{1}{3} f(OPT) - \frac{1}{3}(2n+2)\epsilon$. This completes the proof of Lemma 4.3. □

Now let us prove Theorem 4.1. By Lemma 4.3, we have $EU'_\gamma(A) \geq \frac{1}{3} EU'_\gamma(OPT) - \frac{1}{3}(2n+2)\epsilon$, where $OPT = \arg\max_{A \subseteq S} EU'_\gamma(A)$, which is also the optimal solution to $\max_{A \subseteq S} EU_\gamma(A)$. By definition of $EU'_\gamma(A)$, we obtain

$$EU_\gamma(A) + p_0 \geq \frac{1}{3}[EU_\gamma(OPT) + p_0] - \frac{1}{3}(2n+2)\epsilon,$$

and thus we have

$$EU_\gamma(A) \geq \frac{1}{3} EU_\gamma(OPT) - \frac{2}{3} p_0 - \frac{1}{3}(2n+2)\epsilon.$$

This completes the proof of Theorem 4.1. □

Algorithm 5 `Single_Batch_Offering`

Input: S – set of users, f – $\hat{EU}'_\gamma(\cdot)$ (or equivalently $\hat{EU}_\gamma(\cdot)$, $\Gamma = [\gamma_1, ..., \gamma_l]$ – candidate γ values where $\gamma_1 < \gamma_2 < ... < \gamma_l$, $p_\gamma(\cdot)$ – pricing rule

Output: A – selected users, $\mathbf{p}$ – prices, γ^* – best probability of recruitment

$A \leftarrow \emptyset$, $\mathbf{p} \leftarrow NULL$, $\gamma^* \leftarrow 0$
for γ in $[\gamma_1, ..., \gamma_l]$ **do**
  $A_\gamma \leftarrow \texttt{USM}(S, f)$
  if $A_\gamma = \emptyset$ **then**
    break
  end if
  if $\hat{EU}_\gamma(A_\gamma) > \hat{EU}_\gamma(A)$ **then**
    $A \leftarrow A_\gamma$, $\gamma^* \leftarrow \gamma$
  end if
end for
for each user i in A **do**
  $\mathbf{p} \leftarrow [\mathbf{p}, p_{\gamma^*}(\{i\})]$
end for
return A, $\mathbf{p}$, γ^*

Algorithm 5 describes the algorithm for single-batch offering. Since each γ leads to a different solution A_γ, it is better for the platform to search through a list of l candidate γ values (e.g. $\{0.1, 0.2, ..., 1.0\}$) to find the best one that maximizes $\hat{EU}_\gamma(A_\gamma)$. As `USM` takes $\mathcal{O}(n)$ time, the overall complexity of Algorithm 5 is $\mathcal{O}(ln)$.

Multi-Batch Offering

In the case of expired or rejected offers in the previous batch, the platform may send out more batches until the next batch is no longer profitable.

Denote by $EU_\gamma(B|A_\mathbf{y})$ the marginal EU of additional offers B conditioned on the set of recruited users $A_\mathbf{y}$,

$$EU_\gamma(B|A_\mathbf{y}) = \mathbb{E}_{\mathbf{Y}'}[u_\gamma(B_{\mathbf{y}'}|A_\mathbf{y})], \tag{4.39}$$

where $u_\gamma(B_{\mathbf{y}'}|A_\mathbf{y}) = u_\gamma(B_{\mathbf{y}'} \cup A_\mathbf{y}) - u_\gamma(A_\mathbf{y}) = v(B_{\mathbf{y}'}|A_\mathbf{y}) - p_\gamma(B_{\mathbf{y}'})$ is the marginal utility of $B_{\mathbf{y}'}$ given $A_\mathbf{y}$. We can see from Lemma 4.2 that $EU_\gamma(B|A_\mathbf{y})$ is again submodular in B.

The algorithm for multi-batch offering is provided in Algorithm 6. Starting from the second batch, the marginal EU function is passed as an input to `Single_Batch_Offering` (Line 3). If the (estimated) marginal EU of B is higher than a preset threshold $\tau > 0$ (e.g., 0.01), then it is profitable on average to send out the next batch of offers (Lines 5). The platform will then wait for the results and update A, $\mathbf{p}$, $\mathbf{y}$ accordingly (Line 6). The offering process stops when (1) there are no more users to consider (Line 2), or (2) the next batch is no longer profitable on average (Line 4).

4.5 Evaluation

In this section, we conduct extensive simulations to evaluate proposed pricing mechanisms based on EU maximization and compare them against baseline mechanisms based on (best-case) utility maximization. We also study the impact of offer expiration on the proposed pricing mechanisms.

Algorithm 6 `Multi_Batch_Offering`

Input: S – set of users, f – $\hat{EU'}_\gamma(\cdot)$ (or equivalently $\hat{EU}_\gamma(\cdot)$), $\Gamma = [\gamma_1, ..., \gamma_l]$ – candidate γ values where $\gamma_1 < \gamma_2 < ... < \gamma_l$, $p_\gamma(\cdot)$ – pricing rule, τ – threshold

Output: A – selected users, $\mathbf{p}$ – prices, $\mathbf{y}$ – outcomes

$A \leftarrow \emptyset$, $\mathbf{p} \leftarrow NULL$, $\mathbf{y} \leftarrow NULL$
while $A \neq S$ **do**
  $(B, \mathbf{p}_B, \gamma^*) \leftarrow$`Single_Batch_Offering`$(S \setminus A, f(\cdot|A_\mathbf{y}), \Gamma, p_\gamma(\cdot))$
  if $\hat{EU}_{\gamma^*}(B|A_\mathbf{y}) > \tau$ **then**
    Send out offers $(B, \mathbf{p}_B)$ and observe $\mathbf{y}_B$
    $A \leftarrow A \cup B$, $\mathbf{p} \leftarrow [\mathbf{p}, \mathbf{p}_B]$, $\mathbf{y} \leftarrow [\mathbf{y}, \mathbf{y}_B]$
  else
    break
  end if
end while
return $\mathcal{A}$, $\mathbf{p}$, $\mathbf{y}$

4.5.1 Simulation Setup

Figure 4.3(a) is a sample topology of 60 users, whose locations are randomly generated from the spatial Poisson process. The AoI is a 6km-by-6km region, which is discretized into a total of 169 points with a resolution of 450 meters. We assume an exponential kernel function $\mathcal{K}(d) = 15.5 \cdot \exp(-\frac{d}{0.7})$, as shown in Figure 4.3(b), which is adapted from the semivariogram fitted from real measurements [73]. Given the above settings, negative marginal MI values are not observed and α is set to 0.

The domain of C_i is $[\underline{c}_i, \underline{c}_i + \Delta c]$, where $\Delta c > 0$ and $\underline{c}_i$ is randomly generated from $U[0.1, 0.2]$, where $U[\cdot, \cdot]$ denotes the uniform distribution. We consider two types of distributions: uniform (UN) and truncated normal (TN) distributions. TN is the normal distribution $N(\underline{c}_i, (\Delta c/3)^2)$ truncated to $[\underline{c}_i, \underline{c}_i + \Delta c]$. Compared to UN, TN represents the situation where the majority of users have sensing costs closer to the energy costs $\underline{c}_i$, despite of opportunity costs. The same set of noise variances independently drawn from $U[0.5, 1]$ is used throughout our simulation.

Baseline Mechanisms

As mentioned in Section 4.2, an alternative to design a pricing mechanism is to maximize the best-case utility as in Eq. (4.1), assuming no expired or rejected offers. In this simulation, we consider single-batch and multi-batch offering based on utility maximization as baseline mechanisms. That is, instead of passing $\hat{EU}'_\gamma(\cdot)$ into `USM` in each batch (Line 3 of Algorithm 5), we pass $u'_\gamma(\cdot)$ (a nonnegative submodular function) into `USM`, where $u'_\gamma(A) = u_\gamma(A) + p_\gamma(S)$ and $u_\gamma(A) = v(A) - p_\gamma(A)$. Compared to $EU'_\gamma(\cdot)$, the objective function $u'_\gamma(\cdot)$ does not require the MC method and is easy to evaluate.

For convenience, we refer to EU-maximization-based mechanisms by feeding $\hat{EU}'_\gamma(\cdot)$ to `USM` as USM-EU, and baseline mechanisms by feeding $u'_\gamma(\cdot)$ to `USM` as USM-u.

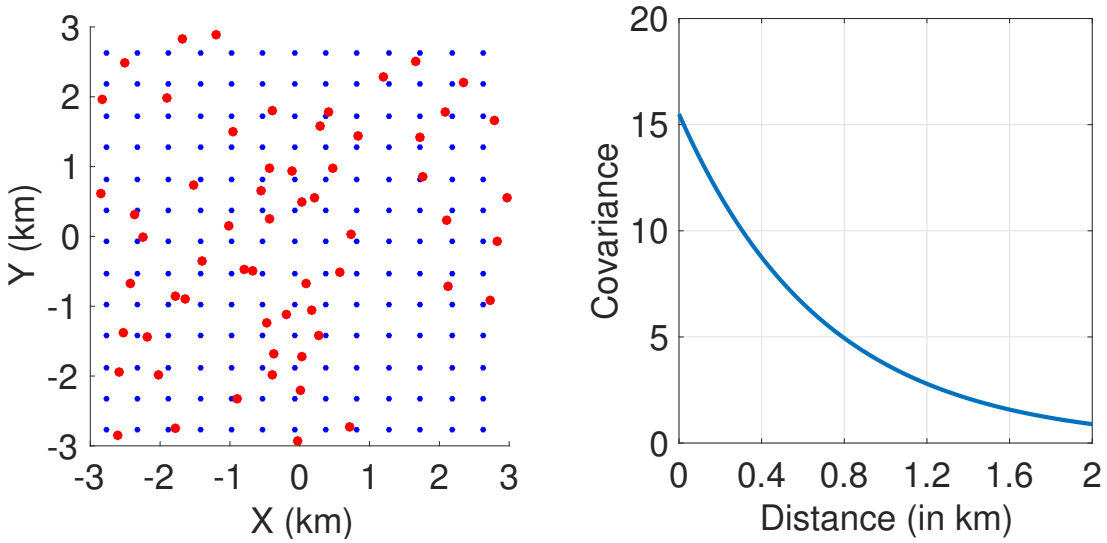

(a) Sample topology (b) Kernel function

Figure 4.3: (a) Sample topology of 60 users (in red) in a 6km-by-6km area that is discretized into a mesh grid of 169 points (in blue). (b) The kernel function $\mathcal{K}(d) = 15.5 \cdot \exp(-\frac{d}{0.7})$.

4.5.2 USM-EU vs. USM-u in Single-Batch Offering

In this experiment, we compare the performance of USM-EU and USM-u in singe-batch offering. $E\hat{U}'_\gamma(\cdot)$ is obtained by averaging over 50 iterations of MC simulations. We randomly select 30 or 60 users, and set κ in $v(\cdot)$ (Eq. (4.14)) to 4 or 8, and Δc to 0.1 or 0.5. We assume no expired offers and set $\rho_i = 1$ for each user i. We will study the impact of offer expiration later in Section 4.5.3. A total of 30 iterations are conducted, and a different seed is used for generating users and cost distributions in each iteration. In the i-th iteration, however, the same set of users and cost distributions are used across different γ and mechanisms for fair comparison. Results are provided in Figure 4.4.

In Figure 4.4(a), we first observe that γ^* achieving the maximum averaged EU is less than 1 for both USM-EU and USM-u under both UN and TN distributions. Intuitively, with a smaller γ, the platform can save money per user and send out more offers. Although each

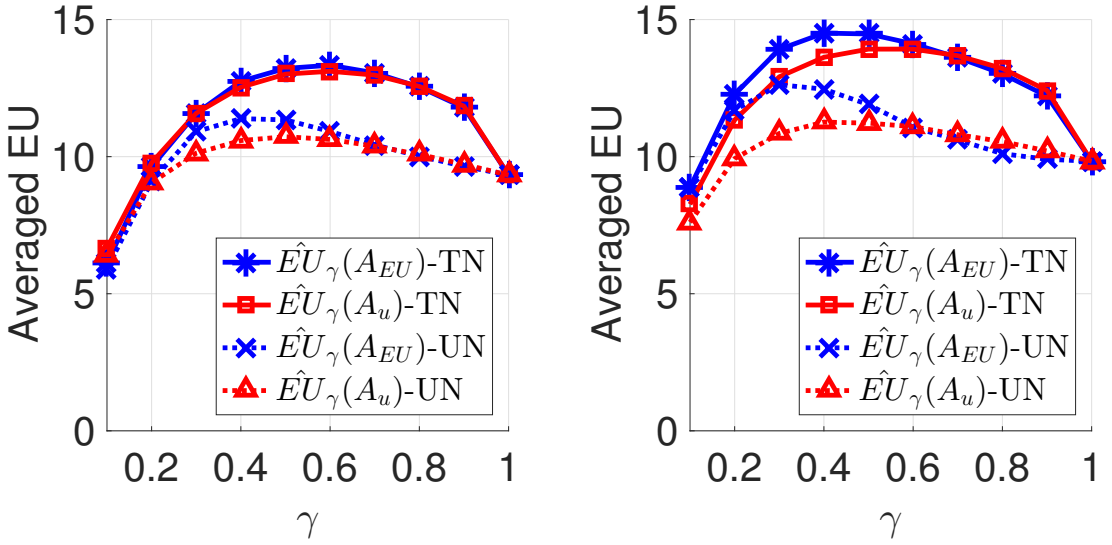

(a) $n = 30$, $\kappa = 8$, $\Delta c = 0.5$

(b) $\boldsymbol{n = 60}$, $\kappa = 8$, $\Delta c = 0.5$

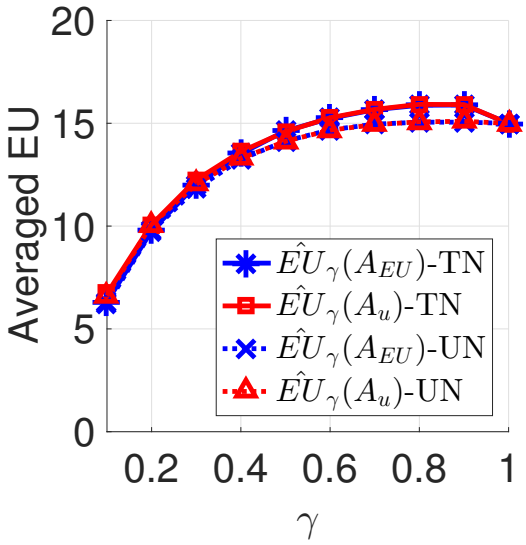

(c) $n = 30$, $\kappa = 8$, $\boldsymbol{\Delta c = 0.1}$

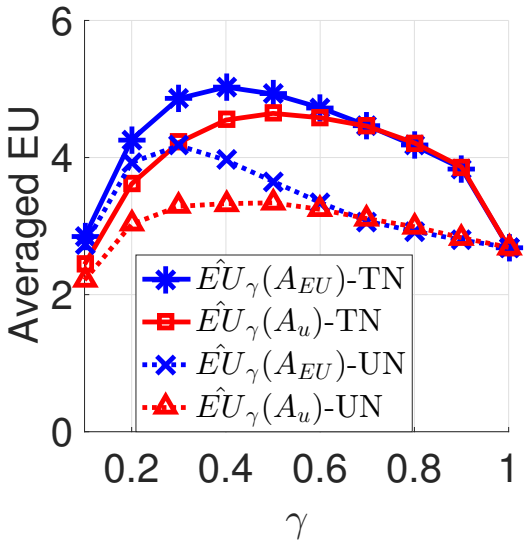

(d) $\boldsymbol{n = 30}$, $\kappa = 4$, $\Delta c = 0.5$

Figure 4.4: Average EU achieved by USM-u and USM-EU for UN and TN cost distributions under different settings.

offer is less likely to be accepted, the platform achieves a greater EU on average. Second, at $\gamma = \gamma^*$, USM-EU achieves a higher EU than USM-u, especially for UN. Besides, the fact that more money is saved per user under TN than UN with the same γ explains the observation that both USM-EU and USM-u achieve a larger EU under TN than UN.

Similar behaviors are observed in Figures 4.4(b) and 4.4(d). But in Figure 4.4(c) when Δc is changed from 0.5 to 0.1, the uncertainty in opportunity costs is reduced and energy costs become more dominant. In this case, the platform will not save much per user with a small γ and should choose a larger γ. Besides, we do not observe the advantage of USM-EU.

Furthermore, as shown in Figure 4.4(a), USM-EU is slightly better than USM-u with γ between 0.3 and 0.6 under UN, but their performance is very close for $\gamma \leq 0.2$ under UN and for all γ values under TN. This is mainly because in those cases, both mechanisms will send out offers to more or all users (30 max. in this setting) and thus achieve very close EU. When there are more users (Figure 4.4(b)), USM-EU is better than USM-u under both UN and TN for $\gamma < 0.6$. With smaller Δc (Figure 4.4(c)), USM-EU is less advantageous. With smaller κ (Figure 4.4(d)), each user is less valuable and USM-u selects fewer users, since it assumes no expired or rejected offers. In contrast, USM-EU considers the average-case utility and is more aggressive in user selection, which explains its better performance than USM-u with the same small γ.

4.5.3 Batched Offering vs. Sequential Offering

In this simulation, we compare the following mechanisms:

- SB-u/EU: single-batch offering with USM-u or USM-EU;
- MB-u/EU: multi-batch offering with USM-u or USM-EU;
- SE: sequential offering.

We randomly select n out of 60 users, and generate a set of noise variances and cost distributions, which are used in all iterations for each n. In the i-th iteration, a different

set of sensing costs is independently generated from the cost distributions and used across different mechanisms for fair comparison. We set $\Delta c = 0.5$, and varied n, κ or $\{\rho_i\}$ to study their impacts on the average utility achieved by the platform. All results are averaged over 50 iterations. Due to space limit, only results for UN distributions are reported, but similar observations exist for TN distributions.

Impact of n (number of users)

We first set $\kappa = 4$ and $\rho_i = 1$ for each user i (i.e., no expired offers). n is varied from 10 to 60, and results are provided in Figure 4.5(a). First, we observe that all mechanisms achieve a higher utility on average as n increases. Second, if only one batch/round is allowed, USM-EU achieves the highest utility, since it accounts for possible expiration and rejection and thus makes more offers in the first batch. The improvement of USM-EU (i.e., SB-EU) over USM-u (i.e., SB-u) varies from 8.5% with $n = 10$ to 40.5% with $n = 60$ (Figure 4.5(a)), which means the advantage of SB-EU (over SB-u) is more obvious with more users. SE performs the worst, since it only sends out one offer in the first round.

When more batches are allowed (Figure 4.5(b)), all mechanisms perform better, since it is always beneficial to send out more batches to make up for expired or rejected offers in the previous batch. Since USM-EU is very generous in making offers in the first batch, following batches become less profitable. If the maximum number of batches is unlimited, USM-u (i.e., MB-u) eventually achieves very close performance with USM-EU (i.e., MB-EU), but the price is a much larger cumulative delay. For instance, when $n = 60$, MB-EU and MB-u make 2.5 and 7.7 batches of offers on average. The number is 24.9 for SE, which is the worst.

Impact of κ (currency in Eq. (4.14))

We then fix $n = 30$ and vary κ from 1 to 6. We set $\rho_i = 1$ for each user i. As shown in Figure 4.5(c), the average utility obtained by each mechanism increases as κ increases, because the platform values per unit MI (log-scaled) more and is able to recruit more users. Besides, SB-EU is still better than SB-u for different κ, but its advantage is less obvious

when κ gets larger. For instance, the improvement is 127.1% with $\kappa = 1$, but reduces to 13.4% with $\kappa = 6$. Moreover, multi-batch offering is better than single-batch offering for both USM-EU and USM-u, but the improvement is more significant for USM-u.

Impact of ρ (probability of unexpired offers)

We set $n = 30$ and $\kappa = 4$. For simplicity, we assume $\rho_i = \rho$ for each user i and vary ρ from 0.2 to 1. Results are provided in Figure 4.5(d). First, we observe that all mechanisms are adversely affected when ρ decreases. Even though the platform knows ρ and adjusts the price as in Eq. (4.30) to achieve γ, i.e., increasing the acceptance probability to offset the high expiration probability, it implies higher prices for users and consequently reduced utility. As mentioned earlier in Section 4.4.2, the best price for each user in SE does not depend on ρ, but the resulting marginal EU does. Nevertheless, SE observes the outcome of the previous offer and continues offering, which explains why it (as well as multi-batch offering) is more robust against offer expiration than single-batch offering.

4.6 Conclusion and Future Work

In this work, we proposed a crowdsensing system for spatial-statistics-based radio mapping and developed pricing mechanisms, i.e., sequential and batched offering, based on EU maximization. We conducted extensive simulations to evaluate proposed mechanisms. Our results show that if only one batch is allowed, the proposed mechanism based on EU maximization is significantly better than the utility-maximization-based baseline mechanism. If multiple batches are permitted (and the number of batches is unlimited), the proposed mechanism achieves close performance with the baseline mechanism, but requires much fewer batches and thus a much smaller delay. Sequential offering works better than the single-batch baseline mechanism, but has a much larger cumulative delay. Offer expiration adversely affected all mechanisms, but sequential and batched offering are relatively more robust.

There are several future directions that could be explored. First, it would be very interesting to apply spatio-temporal statistics to also model temporal correlations and capture

temporal variations in radio environments. Second, it would be of practical importance to investigate the problem in an online setting, where users arrive in random order and one-time price offer has to be made upon each user's arrival. Such an online pricing mechanism would better handle high user mobility and minimize actual displacements between reported and sensing locations. Last but not the least, we would like to enhance security and protect user privacy of our system.

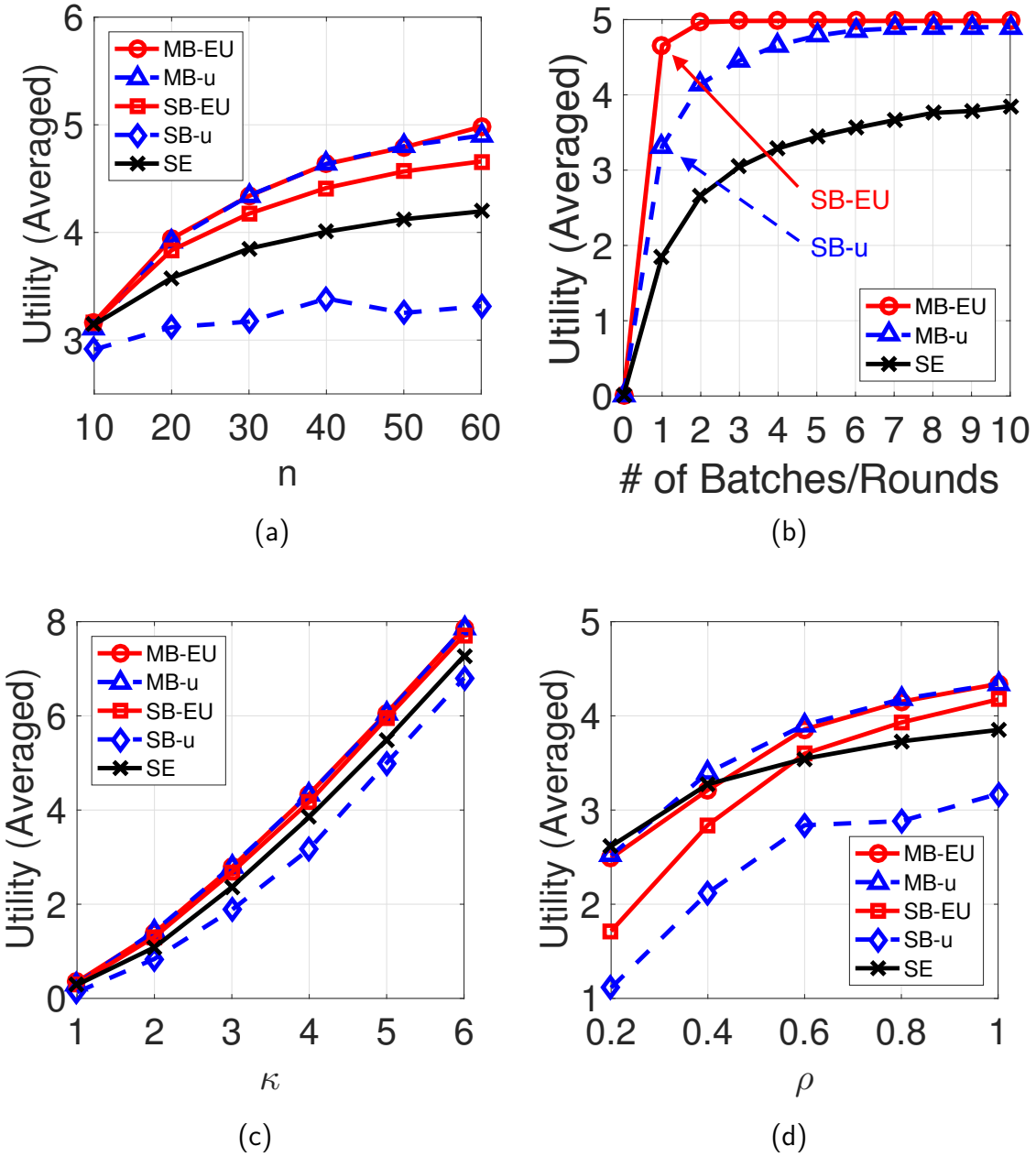

Figure 4.5: Comparison of SB-u, MB-u, SB-EU, MB-EU and SE. (a) Impact of n ($\kappa = 4$, no expired offers). (b) Utility vs. number of batches of offers ($n = 60$, $\kappa = 4$, no expired offers). (c) Impact of κ ($n = 30$, no expired offers). (d) Impact of ρ ($n = 30$, $\kappa = 4$, $\rho_i = \rho$ for each user i).

Chapter 5

SAS-ASSISTED COEXISTENCE-AWARE DYNAMIC CHANNEL ASSIGNMENT

In this previous chapter, we studied the problem of designing a pricing-based incentive mechanism for crowdsensed radio mapping. We showed that the proposed pricing mechanism based on expected utility maximization outperforms the baseline utility-maximization-based baseline mechanism.

Up to this point, we have discussed the application of spatial statistics (Kriging) to radio mapping (Chapter 2) and the design of incentive mechanisms including auctions (Chapter 3) and pricing (Chapter 4) for crowdsensed radio mapping, in complementary to the traditional radio prorogation models for identifying white space opportunities in shared spectrum. After estimating coverage/protection regions and identifying WS (available channels), it is crucial to assign the channels to SUs so as to optimize the network performance. In this chapter, we study dynamic channel assignment through a centralized entity in the 3.5 GHz CBRS band.

Following unlicensed use of TV spectrum [19], the FCC targeted the release of 3550-3700 MHz CRBS band for small cell deployment [25, 95–97], which is currently used by high-power Department of Defense shipborne radars and non-federal FSS earth stations. The CBRS adopts a three-tiered spectrum access framework that consists of three service tiers: IA, PA, and GAA (Figure 5.1). PA and GAA devices are also referred to as Citizens Broadband Radio Service Devices (CBSDs), which are fixed stations or networks of such stations operating on a PA or GAA basis. End user devices are not considered as CBSDs.

The above framework highlights the hierarchical spectrum access rights: Incumbents, including authorized federal and FSS users, would be protected from harmful interference from all other users, by forbidding CBSD transmissions within and close to the activated *Dynamic*

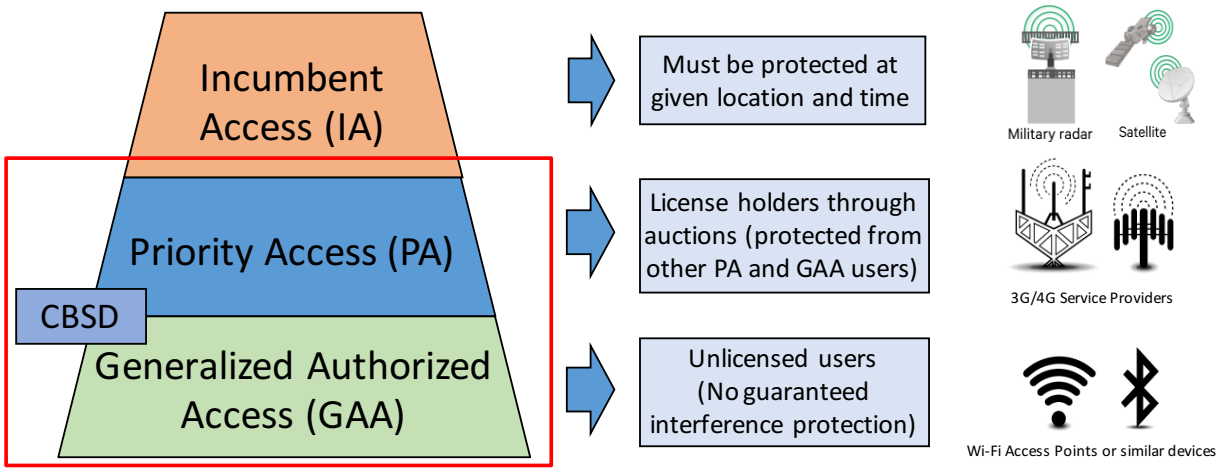

Figure 5.1: Three-tiered spectrum access framework in the 3.5 GHz CBRS band. Incumbents have the highest priority and must be protected at any given location and time. PA users obtain licenses via competitive bidding and are protected from other PA and GAA users. GAA users shall not expect any interference protection and are expected to coexist.

Protection Areas (DPAs). PA users such as hospitals and public safety entities with critical quality-of-service needs would be authorized to operate at specific locations with interference protection. But they need to purchase PA licenses (PALs) via competitive bidding, each of which guarantees the authorized and protected use of a 10 MHz channel in a census tract. In contrast, GAA CBSDs (or GAA nodes) would be authorized to opportunistically access the band within designated geographic areas, but they should expect no interference protection and avoid causing interference to incumbents and PA users. In the center of the CBRS ecosystem lies a centralized entity called SAS (Spectrum Access System) that authorizes and manages use of spectrum for the CBRS. In this work, we study the SAS-assisted dynamic channel assignment (CA) for PA and GAA tiers.

In order to provide a flexible, scalable, practically deployable bandwidth for high data rate technologies, the 3.5 GHz band is divided into 15 orthogonal 10-MHz channels. Up to seven channels can be reserved for PALs in a *license area* (i.e., a census tract), and a licensee

is allowed to aggregate up to four channels by stacking multiple channels in a *service area* that consists of one or multiple contiguous license areas. Although each PAL guarantees one assigned channel, the exact channel assignment is not fixed and would be determined by the SAS. Since the FCC requires the SAS to assign *contiguous channels to geographically contiguous PALs*, it imposes a major challenge to the design of a PA CA scheme.

To improve spectrum utilization, a PAL channel is made available for GAA use at locations outside the PAL protection areas (PPAs) and their vicinities, under the "use-it-or-share-it" rule. As a result, *channel availability* becomes location dependent and may vary significantly among GAA nodes. Moreover, a GAA node may also request multiple *contiguous channels* to meet its capacity demand or support network operations. For instance, a Wi-Fi-based node would require at least two contiguous channels in the CBRS.

In this work, we are interested in co-channel coexistence enabled by Wi-Fi like MAC protocols, such as CSMA/CA [98] or LBT in LTE-LAA [32]. Hence, the pairwise relationship of GAA nodes can be classified into three cases: 1) no conflict, 2) type-I conflict – two interfering nodes are hidden from each other and cannot detect possible interference at end user devices (or clients) without their feedbacks (e.g., packet loss or throughput degradation), or 3) type-II conflict – two interfering nodes are within each other's carrier-sensing (CS) or energy-detection (ED) range and can resolve the conflict through contention. Since GAA nodes are able to harmoniously share the same channel under type-II conflicts, the SAS can exploit such *coexistence opportunities* to accommodate more devices in a dense network.

Despite that dynamic CA has been studied in the context of spectrum sharing from various perspectives such as graph coloring [99–102] and game theory [103–105], the aforementioned challenges (i.e., channel and geographic contiguity, spatially varying channel availability, and coexistence awareness) differentiate the dynamic CA in the CBRS from previous work. In this work, we make the following specific contributions:

- We define the *node-channel pair* (NC pair) that assigns a set of contiguous and available channels to a node (i.e., a PA service area or a GAA CBSD) and introduce the *NC-pair*

conflict graph, in which each vertex is a NC pair and each edge represents a conflict.

- With the proposed conflict graph, we formulate PA CA as *max-cardinality CA*. For GAA CA with binary conflicts, we extend NC pairs to *super-NC pairs* to exploit type-II conflicts, where each super-node consists of a set of GAA nodes that can detect each other's transmission. We define a reward function to capture the preferences of (super-)NC pairs and formulate binary GAA CA as *max-reward CA*. To further enhance coexistence awareness, we introduce a penalty function and extend binary conflicts to non-binary. The non-binary GAA CA is then formulated as *max-utility CA* to trade off rewards against penalties.

- We propose a super-node formation algorithm based on clique searching and bin packing to identify super-nodes. The max-cardinality CA and max-reward CA are mapped to the problem of finding the maximum (weighted) independent set, and approximate solutions are obtained through a heuristic-based algorithm. For max-utility CA, we show that the utility function is submodular, and our problem is an instance of matroid-constrained submodular maximization. We propose a polynomial-time algorithm based on (approximate) local search that provides a provable performance guarantee.

- We conduct extensive simulations to evaluate the proposed algorithms, using a real-world dataset that contains Wi-Fi hotspot locations in the New York City (NYC) [106]. For PA CA, our results show that the proposed algorithm consistently serves over 93.0% of service areas and outperforms the baseline algorithm by over 30.0%. For binary GAA CA, the proposed algorithm with linear rewards is able to accommodate 10.2% more nodes and serve 10.4% more demand on average than the baseline algorithm. Besides, enabling coexistence awareness can effectively improve the performance of the proposed algorithms. For non-binary GAA CA, the proposed algorithm achieves 29.5% more utility while keeping the total interference much smaller than the baseline.

The remainder of this chapter is organized as follows. Section 5.1 reviews related work on

CA. Section 5.2 summarizes CA scenarios and presents the SAS-based architecture. Conflict graphs and problem formulations are presented in Section 5.3, and proposed algorithms are provided in Section 5.4. Section 5.5 presents simulation results and Section 5.6 concludes this study.

5.1 Related Work

Dynamic CA has been studied in various contexts such as cellular networks [107], mesh networks [108] and cognitive radio networks [109]. Among the proposed approaches, graphs are widely adopted for CA modeling. In [102, 110–112], authors considered CA under the channel availability and interference constraints using vertex-weighted interference/conflict graphs, where each vertex represents a user with a color (channel) list, and each edge denotes a binary conflict due to co-channel interference. The problem is then formulated as graph multi-coloring (i.e., assign conflict-free colors to users and obtain rewards on vertices) and a typical objective is to maximize the total reward or utility (derived from rewards). Such conflict-free CA algorithms are suitable for sparse networks.

In order to capture the interference with greater granularity, non-binary conflicts using an edge-weighting or penalty function may be introduced, and typical objectives include minimizing the total interference or penalty via graph coloring [99, 100, 113] or maximizing the total reward subject to the aggregate interference limit at each user [102, 114]. However, the vast majority of existing works do *not* consider geographic and channel contiguity constraints and thus are not applicable to CA in the CBRS. In [101], Subramanian *et. al.* introduced the notion of channel graph to enforce channel contiguity, where each vertex is a channel consisting of several contiguous primitive channels and each edge indicates overlapping channels. In Section 5.5.2, we will show that our proposed algorithm outperforms the algorithm in [101] in terms of accommodating more users and meeting greater demand.

In this work, we incorporate the contiguity constraints by introducing (super)NC-pair conflict graphs, which can also be used to represent channel availability and enhance coexistence awareness. Besides, the proposed conflict graph allows us to relate the PA CA and

binary GAA CA to the classic the maximum (weighted) independent set problem [115–117] and adopt a widely used heuristic-based algorithm that runs in polynomial-time with a performance guarantee. To further enhance coexistence awareness, we consider non-binary GAA CA and formulate the problem as utility maximization. We then prove the submodularity of the utility function and propose a polynomial-time algorithm based on local search with a provable performance guarantee.

5.2 Channel Assignment in CBRS

In this section, we describe CA scenarios for PA and GAA tiers based on the FCC rules [25, 95, 96, 118]. In particular, we highlight CA challenges and opportunities in the CBRS: geographic and channel contiguity, spatially varying channel availability, flexible demands, and coexistence awareness. Then we present the architecture of SAS from the perspective of dynamic CA.

5.2.1 PA CA Scenario

As per the FCC rules, up to 7 out of 10 channels in the 3550-3650 MHz band can be reserved for PALs, and up to four channels can be aggregated by the same licensee in each license (or service) area. Each deployed PA CBSD has an associated PPA with a default protection contour that is calculated based on the signal level of -96 dBm/10 MHz, which cannot extend beyond the licensee's service area. A self-reported PPA contour is also acceptable, so long as it is within the default PPA contour. If PPAs for multiple CBSDs operated by the same licensee overlap, they would be merged into a single PPA. Note that interference protection is enforced for each active PPA, i.e., the aggregate co-channel interference from other PA or GAA CBSDs at any location within a PPA cannot exceed -80 dBm/10 MHz.

The FCC imposes two contiguity requirements for PA CA: 1) *geographic contiguity* – an SAS must assign geographically contiguous PALs held by the same PA licensee to the same channels in each geographic area, to the extent feasible; and 2) *channel contiguity* – an SAS must assign multiple channels held by the same PA licensee to contiguous channels

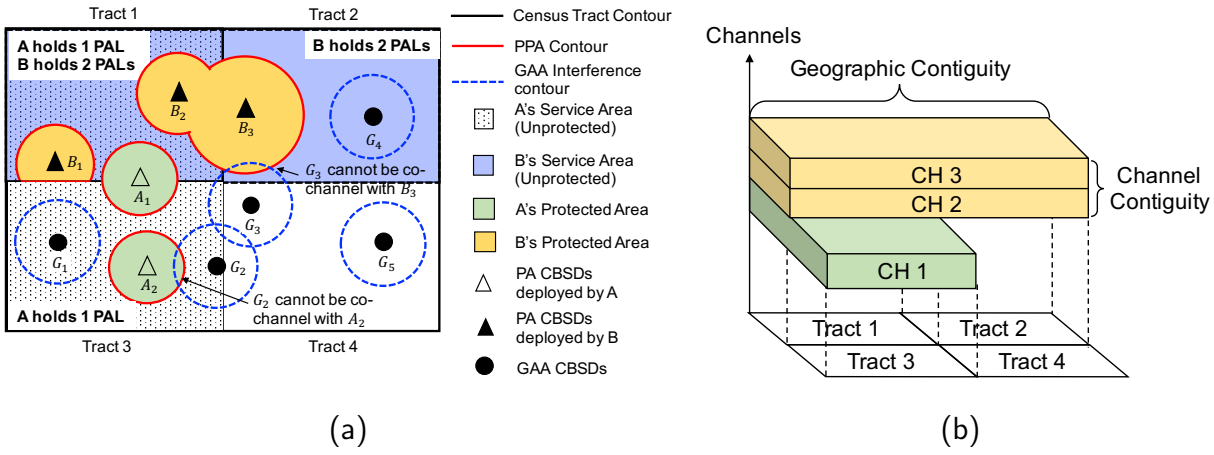

Figure 5.2: Illustration of the PA CA scenario. (a) A holds one PAL in its service area that consists of tracts 1 and 3, while B stacks two PALs in its service area that consists of tracts 1 and 2. Each PA CBSD deployed by the licensee has a PPA that cannot extend beyond its service area. GAA nodes may reuse assigned PAL channels at locations beyond the PPAs, subject to the interference constraint. (b) Given three PAL channels, the SAS can assign CH $\{1\}$ in tracts 1 and 3 to A's PALs and CH $\{2, 3\}$ in tracts 1 and 2 to B's PALs, so as to meet the geographic and channel contiguity requirements.

in the same license area, to the extent feasible. An example is provided in Figure 5.2 that illustrates the PA CA scenario[1].

5.2.2 GAA CA Scenario

GAA CA differs from PA CA in the following aspects. First, channel availability for GAA nodes can vary significantly depending on location. This is because a PAL channel is considered "in use" only within PPAs, and thus it may become available for GAA use at a location

[1]It is worth noting that in cases where two adjacent, non-overlapping service areas are assigned the same channel, locations close to the service area boundaries may not be suitable for PA CBSD deployment. Consider two PA CBSDs operated by different licensees are deployed close to the boundary. They can cause interference to each other that exceeds the -80 dBm/10 MHz interference limit, if they operate co-channel. While this issue may occur in practice, the SAS's objective for PA CA is to assign channels to PALs, and thus we do not consider addressing this issue as the SAS's responsibility.

beyond the PPAs (and their vicinities), if GAA transmission at that location does not cause excessive interference at any location within PPAs.

As illustrated in the example in Figure 5.2, GAA nodes G_1 and G_4 are located in the service area of PA licensees, but they are free to use all channels just like G_5, since they do not cause significant interference to any PA CBSD. In contrast, G_2 cannot operate co-channel with A_2, and G_3 cannot operate co-channel with B_3, due to the interference constraint. Although it is not desirable for G_2 and G_3 to operate co-channel as they would interfere with each other, it is indeed acceptable as per the FCC ruling.

Second, a GAA node may also request multiple contiguous channels (up to a certain limit such as four), and the demand could be rather flexible. For instance, a Wi-Fi-based node may request a minimum of two contiguous channels for network operations, but it would be very willing to receive four contiguous channels to obtain higher capacity. Although the SAS is not obligated to meet the maximum demands of all GAA nodes, it would be expected to maximize the number of assigned channels or the overall throughput with best efforts.

Third, GAA nodes are expected to coexist in the same frequency, space and time. In this work, we consider co-channel coexistence enabled by Wi-Fi like MAC protocols such as CSMA/CA in Wi-Fi [98] and LBT in LAA [32]. Traditional channel assignment techniques [110–112] typically model interference as a binary conflict and avoid assigning the same channel to any two conflicting nodes. However, two interfering nodes in close proximity are able to detect each other's transmission (no hidden nodes) and share the same channel(s) in the CSMA/CA fashion. Hence, the SAS may exploit such opportunities to accommodate more nodes in this case, especially when the spectrum is crowded. In this work, we further consider non-binary conflicts to enhance *coexistence awareness*.

5.2.3 Architecture of SAS-Assisted Dynamic CA

As illustrated in Figure 5.3, the SAS is a centralized entity that consists of incumbent, PA, and GAA managers. It communicates with the Environment Sensing Capability (ESC) component, FCC databases (DBs), and CBSDs. The PA manager receives information on

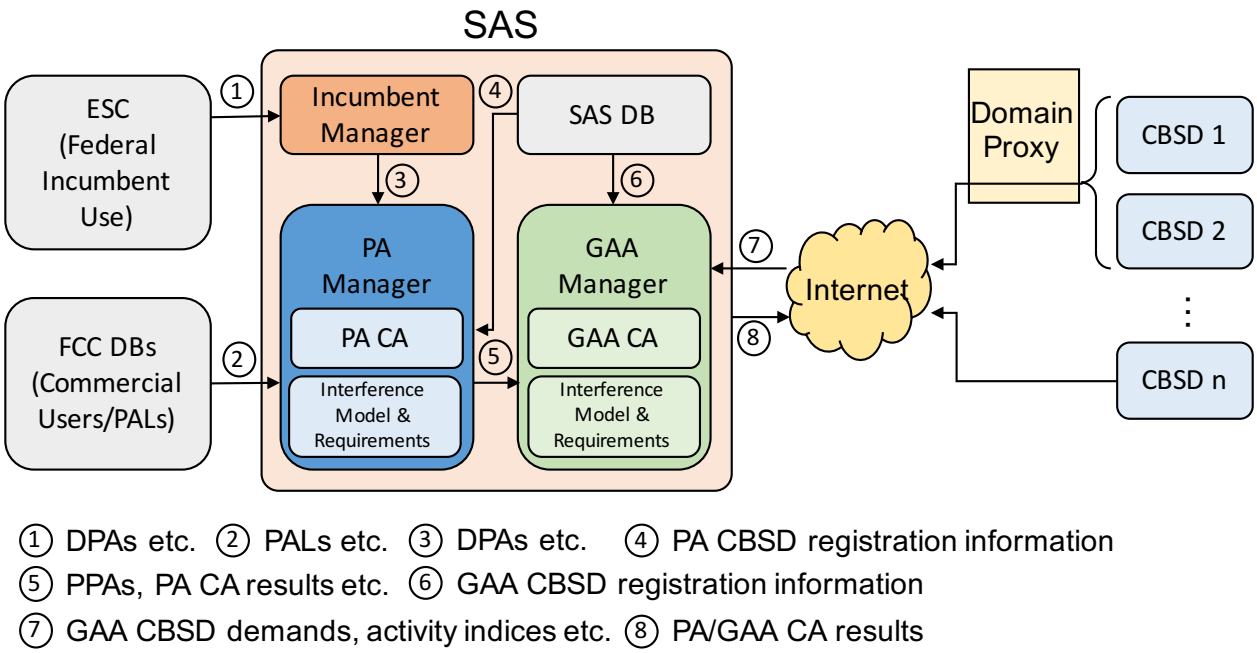

Figure 5.3: Architecture of SAS as a centralized entity from the perspective of dynamic CA. A centralized PA/GAA CA algorithm will be implemented in the PA/GAA manager within the SAS. Note that only data flows for PA/GAA CA purposes are highlighted.

DPAs and PALs, determines PAL channel availability based on the interference model and requirements, and executes the PA CA algorithm to assign channels to PALs grouped by service areas. The GAA manager takes as input 1) the PPAs and PA CA results, 2) GAA CBSD registration information (e.g., location, transmit power, and antenna gain), 3) CBSD demands and activity indices (i.e., traffic load indicators), and 4) the interference model[2] and requirements. It then determines channel availability for GAA nodes and executes the GAA CA algorithm. Finally, the SAS will disseminate the PA and GAA CA results to individual CBSDs (e.g., within 10s of seconds).

[2]Radio propagation models, despite their limitations, are still widely used for initial network planning, but the interference relationship can also be determined from real measurements. Such measurement reporting is already supported by the WInnForum SAS-CBSD protocol [119].

According to the WInnForum SAS-CBSD protocol specifications [119], the protocol exchange between the SAS and CBSDs already exists, including requests and responses for (de)registration, spectrum inquiry, grant (relinquishment) and heatbeat. Therefore, the SAS can readily leverage registration and regular heartbeat messages to collect inputs from CBSDs and use them for CA purposes, without introducing additional signaling overhead.

It is also important to note that the CA in the CBRS is indeed dynamic: changes in DPAs and PALs would trigger PA CA, which further trigger GAA CA along with other factors (e.g., changes in GAA CBSD demands). Since DPA and PAL changes are relatively infrequent, PA channel assignments will be expected to be quasi-stable, and channel reassignment occurs presumably in the order of hours or days. In contrast, the SAS may have to aggregate demands from all GAA nodes and perform GAA CA periodically (e.g., every 100s of seconds). Nevertheless, the SAS can always take a snapshot of the CBSD network at a given time instant and perform CA for PA and GAA tiers separately in a centralized fashion[3].

5.3 Novel Conflict Graphs and Problem Formulation

In order to incorporate channel availability and contiguity, we define a NC pair as a channel assignment that assigns a set of contiguous and available channels to a node, i.e., a PA service area or a GAA node. We further introduce NC-pair conflict graph, where each vertex is a NC pair and each edge indicates a conflict between two connected NC pairs due to the one-channel-assignment-per-node or interference constraint. In the rest of this section, we will describe conflict graph construction in detail and present our problem formulation for each CA scenario.

5.3.1 Conflict Graph for PA CA

Let us consider a geographic region with M PA licensees. Each licensee i holds N_i PALs in n_i service areas, and there are a total of $n = \sum_{i=1}^{M} n_i$ service areas in total. Let S_{ij} be the set

[3]The SAS itself may be implemented in a distributed cloud so as to exploit dedicated computing resources spread over multiple virtual machines to perform CA for a specific region.

of license areas that form the j-th service area of licensee i, and each license area in S_{ij} has N_{ij} PALs[4]. There are a total of 10 PAL channels in the CBRS, denoted as $\Omega = \{1, 2, ..., 10\}$. Due to the DPAs of incumbents, the set of available PAL channels for S_{ij}, denoted as $\Gamma(S_{ij})$, is a subset of Ω. Denote the set of valid channel assignments for S_{ij} as $\mathcal{C}_{ij}$. It means that each channel assignment $C \in \mathcal{C}_{ij}$ consists of contiguous channels and satisfies $C \in \Gamma(S_{ij})$ and $|C| = N_{ij}$. For instance, with $\Gamma(S_{ij}) = \{1, 2, 3\}$ and $N_{ij} = 2$, we have $\mathcal{C}_{ij} = \{\{1, 2\}, \{2, 3\}\}$.

In the proposed conflict graph $G = (V, E)$ for PA CA, each vertex is a NC pair (S_{ij}, C_{ij}) that assigns channel(s) C_{ij} to S_{ij}, and an edge exists between (S_{ij}, C_{ij}) and (S_{lk}, C_{lk}), if

- $i = j$ and $l = k$ (i.e., S_{ij} and S_{lk} refer to the same service area), and $C_{ij} \neq C_{lk}$, or
- $S_{ij} \cap S_{lk} \neq \emptyset$ and $C_{ij} \cap C_{lk} \neq \emptyset$.

The first constraint requires each service area to take at most one channel assignment, referred to as the *one-channel-assignment-per-node constraint*, while the second constraint prevents two overlapping service areas from being assigned overlapping channels, which is called the *conflict constraint*. It is worth noting that by selecting a vertex (S_{ij}, C_{ij}), i.e., assigning channel(s) C_{ij} to S_{ij}, the SAS can meet both the geographic and channel contiguity requirements. An example of the proposed conflict graph for PA CA is provided in Figure 5.4.

Since a conflict due to interference exists only for two NC pairs that represent two overlapping service areas with overlapping channels, a sparse conflict graph would be expected in practice. Therefore, adjacency lists would be preferred in general with a storage cost of $O(|V| + |E|)$. It takes $O(1)$ time to add a vertex or edge, $O(E)$ to remove a vertex, and $O(V)$ to remove an edge. More details are available in [120].

Problem Formulation: Given a conflict graph $G(V, E)$ for PA CA, the SAS wants to find a scheme $I \subseteq V$ so as to maximize the total number of served service areas without conflicts,

$$\max_{I \subseteq V} |I| \text{ s.t. } e(u, v) \notin E, \forall u, v \in I, \tag{5.1}$$

[4]The constraint that no more than seven PALs shall be assigned in any license area should have been enforced during the licensing stage and can be verified by checking $\sum_{i=1}^{M} \sum_{j=1}^{n_i} \mathbf{1}_{\{s \in S_{ij}\}} \cdot N_{ij} \leq 7$ for each license area s, where $\mathbf{1}_{\{s \in S_{ij}\}}$ is the indicator variable.

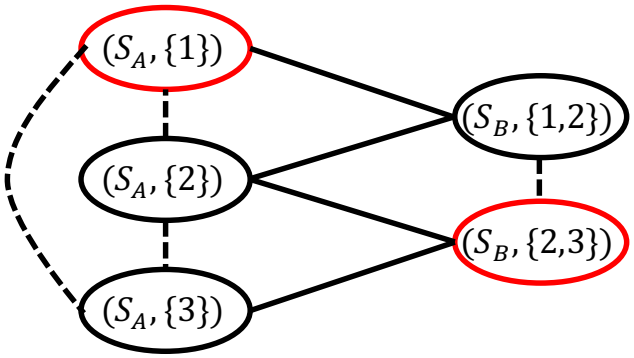

Figure 5.4: Conflict graph for the PA CA example in Figure 5.2. Dashed and solid edges are due to the one-channel-assignment-per-node and conflict constraints, respectively. The SAS aims to choose the largest set of conflict-free vertices. One possible CA scheme consists of two vertices in red, i.e, $(S_A, \{1\})$ and $(S_B, \{2, 3\})$. An alternative is $(S_A, \{3\})$ and $(S_B, \{1, 2\})$.

where $|\cdot|$ is the cardinality operator. We refer to the above problem as **Max-Cardinality CA**[5].

5.3.2 Conflict Graph with Binary Conflicts for GAA CA

Suppose that there are n GAA nodes at fixed locations in the same geographic region. The ground set of channels is $\Omega = \{1, 2, ..., 15\}$, and the SAS can determine the set of available channels $\Gamma(i) \subseteq \Omega$ for each GAA node i. In this paper, we focus on CA by assuming fixed transmit power for all nodes and leave joint channel and power assignment as future work.

Denote the demand set of node i as $\mathcal{D}(i) = \{d_{i1}, d_{i2}, ...\}$, where d_{ik} is the number of contiguous channels node i requests. For example, $\mathcal{D}(i) = \{2, 4\}$ means that node i requests for two or four contiguous channels. By default, the SAS may set $\mathcal{D}(i)$ to $\{1, 2, ..., L\}$, where L is the limit (e.g., $L = 4$). As a result, $\Gamma(i)$ and $\mathcal{D}(i)$ jointly determine the set of valid

[5]Due to the one-channel-assignment-per-node constraint, the maximum possible size of I is n. In practice, the PAL licensing process should ensure that a solution of size n can be found. When it is impossible to do so due to incumbent activities, the SAS may have to temporarily divide a large service areas to smaller ones that take non-contiguous channels.

channel assignments $\mathcal{C}(i)$. For example, with $\Gamma(i) = \{1, 4, 5\}$ and $\mathcal{D}(i) = \{1, 2\}$, we have $\mathcal{C}(i) = \{\{1\}, \{4\}, \{5\}, \{4, 5\}\}$.

In the proposed conflict graph $G(V, E)$ for binary GAA CA, each vertex is a NC pair (i, C_i) that assigns channel(s) $C_i \in \mathcal{C}(i)$ to node i, and an edge exists between (i, C_i) and (j, C_j) if

- $i = j$ and $C_i \neq C_j$, or
- $i \neq j$, $C_i \cap C_j \neq \emptyset$, and node i would conflict or interfere with node j when assigned the same channel based on the interference model.

The above two conditions correspond to the one-channel-assignment-per-node and conflict/interference constraints, respectively. Like the conflict graph for PA CA, the conflict graph for GAA CA is expected to be sparse and thus adjacency lists are generally preferred.

In the rest of this section, we will characterize pairwise interference relationship, discuss coexistence awareness under binary conflicts, and introduce a reward function to reflect preferences of NC pairs. Then we will present our problem formulation for binary GAA CA.

Characterization of Pairwise Interference

First of all, the SAS needs to determine whether two GAA nodes are causing interference to each other, which is a binary (yes-or-no) decision. According to the physical interference model [121], a successful reception at a client from the CBSD is possible, if the SINR at the client is greater than a certain threshold $SINR_{\min}$. If client locations are known, the SAS can use this criterion to determine the pairwise interference relationship. Otherwise, the SAS may consider the worst-case scenario where clients are located at the service region boundaries with respect to a certain signal level (denoted as γ_i) and determine if the interference from node j (denoted as γ_j) at the nearest boundary client exceeds $SINR_{\min}$, i.e., $\frac{\gamma_i}{\gamma_j + \sigma_n^2} \geq SINR_{\min}$, where σ_n^2 is the noise power. This determines the maximum allowable interference from node j, that is, $\gamma_j \leq \gamma_i / SINR_{\min} - \sigma_n^2$. In this work, we assume that

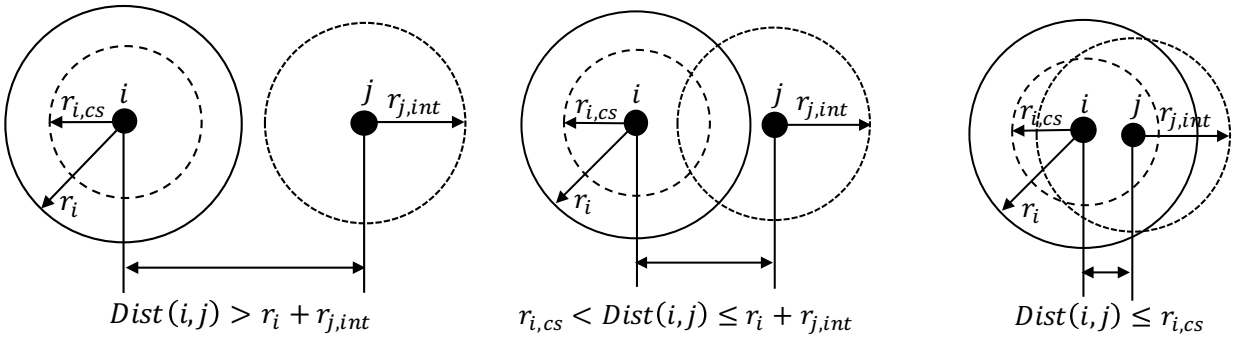

Figure 5.5: Impact of node j's interference on node i. (a) No conflict. Nodes i and j are free to reuse the same channel if j's interference region does not overlap with i's service region. (b) Type-I conflict. Node j causes non-negligible interference to i's clients located in the overlapping region, which cannot be detected by i without feedback from the clients such as packet loss or throughput degradation. (c) Type-II conflict. Node j is within i's CS or ED range, and its interference can detected by i.

the SAS no prior knowledge about client locations[6], and thus determining pairwise interference relationship translates into determining whether the service region of node i overlaps with the interference region of node j. Nevertheless, when information about client locations becomes available, the SAS can exploit this information to determine the interference relationship more accurately.

While the service and interference regions can be highly irregular in practice, we assume circular regions for illustration. Denote node i's service region as $\mathcal{R}_i$ of radius r_i, and node j's interference region as $\mathcal{R}_{j,int}$ of radius $r_{j,int}$. Then there exists no conflict between i and j due to j' interference, if the distance is larger than $r_i + r_{j,int}$, regardless of the positions of i's clients (Figure 5.5(a)). As nodes i and j get closer, $\mathcal{R}_{j,int}$ starts to overlap with $\mathcal{R}_i$, which means that j may cause interference to clients that are possibly located in the overlapping

[6]Clients or end user devices are not required to register with the SAS or report their locations.

region in the downlink. If the distance is smaller than $r_i + r_{j,int}$ but larger than i's CS/ED range $r_{i,cs}$, as shown in Figure 5.5(b), node j is said to be hidden from i, and the interference from j cannot be detected by i without feedback from i's clients. When the distance is less than $r_{i,cs}$ (Figure 5.5(c)), node i is able to detect j's transmission via CS or ED and achieve harmonious co-channel coexistence through contention. In order to distinguish the above cases, we call them type-I and type-II conflicts, respectively. Note that our interference model is very similar to the popular protocol models in literature (e.g., [121–123]), which can be easily implemented in the SAS using radio propagation models.

Coexistence Awareness

Ideally, two nodes should be assigned the same channel only when they do not conflict. Nevertheless, GAA nodes have the lowest spectrum access priority and are expected to coexist in the presence of conflicts. Compared with type-I conflicts, type-II conflicts can be handled more easily and thus may be considered as coexistence opportunities to the SAS. To that end, we introduce *super-NC pair* (S, C), where S is a *super-node* that consists of nodes that can coexist on channel C with two conditions: 1) channel C is available at all nodes in S and 2) nodes in S be within each other's CS/ED range so that all conflicts can be gracefully resolved. The super-node formation algorithm will be presented later in Section 5.4.1.

Figure 5.6 shows an example of the proposed conflict graph with and without coexistence awareness. Suppose that nodes B, C are within each other's CS/ED range. Then there are two super-NC pairs $(\{B, C\}, \{1\})$ and $(\{B, C\}, \{2\})$. As illustrated in Fig. 5.6(b), when a super-NC pair is identified, it is added to the graph and inherits the conflict relationship of its children RC pairs. Then edges among its children RC pairs are removed. For instance, removing the edge between $(B, \{2\})$ and $(C, \{2\})$ means that when $(B, \{2\})$ is selected, $(\{B, C\}, \{2\})$ will become invalid, but the SAS can still select $(C, \{2\})$, since B and C are able to coexist under type-II conflicts.

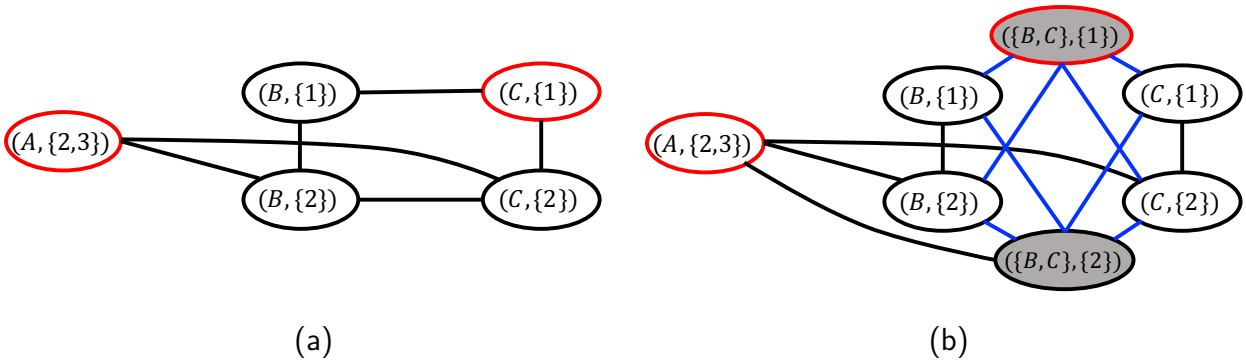

Figure 5.6: Example of (a) NC-pair conflict graph and (b) coexistence-aware NC-pair conflict graph. Suppose that A has two channels $\{2, 3\}$ available and requests for two contiguous channel, while B and C have two available channels $\{1, 2\}$ and each requests for one channel. A, B, and C are interfering with each other, but B and C are within each other's CS/ED range. Based on the conflict graph in (a), the SAS may assign CH $\{2, 3\}$ to A and CH $\{1\}$ to C. After realizing that B and C are able to coexist under type-II conflicts, the SAS may assign CH $\{1\}$ to both B and C based on the conflict graph in (b).

Rewards

In GAA CA, the basic objectives of the SAS would include accommodating more nodes and assigning more channels. As a result, NC pairs that assign more channels to more nodes are generally more preferred. To reflect such preference, the SAS can define a *reward (or vertex weighting) function* $R : V \mapsto \mathbb{R}^+$ that assigns a positive reward to each vertex $v = (S, C)$. If the SAS aims to meet more demand by assigning more channels, the *linear* reward function $R(v) = R(S, C) = |S| \cdot |C|$ may be used, which is equal to the total number of assigned channels at each vertex. If the SAS wants to prioritize the objective of accommodating more nodes, an alternative *log* reward function may be adopted, i.e., $R(v) = R(S, C) = |S| \cdot (1+\log(|C|))$, which captures the decreasing benefit of a node getting additional channels.

Problem Formulation: Given a vertex-weighted conflict graph $G(V, E, R)$ for n nodes for

binary GAA CA[7], the SAS wants to find a scheme $I \subseteq V$ so as to maximize the total reward, subject to the cardinality and conflict constraints, i.e.,

$$\max_{I \subseteq V} R(I), \text{ s.t. } \sum_{v \in I} |S(v)| = n; \ e(u,v) \notin E, \forall u, v \in I,$$

where $R(I) = \sum_{v \in I} R(v)$ is the total reward, and $S(v)$ is the set of nodes at vertex v.

In cases where the demand exceeds the supply, i.e., there are many more nodes than available channels, the SAS may not obtain a feasible solution to the above problem. Hence, the SAS may relax it to the following optimization problem.

Relaxed Problem Formulation: Given a vertex-weighted conflict graph $G(V, E, R)$, the SAS wants to find a scheme $I \subseteq V$ so as to maximize the total reward subject to the conflict constraint,

$$\max_{I \subseteq V} R'(I), \text{ s.t. } \ e(u,v) \notin E, \forall u, v \in I, \tag{5.2}$$

where $R'(I) = \sum_{v \in I} (R(v) + \lambda |S(v)|)$ and $\lambda \geq 0$ is the trade-off parameter chosen by the SAS. Intuitively, the SAS aims to assign as many channels and serve as many nodes as possible at the same time. We refer to the problem in (5.2) as **Max-Reward CA**.

5.3.3 Conflict Graph with Non-Binary Conflicts for GAA CA

In order to further exploit type-I conflicts, we extend the proposed conflict graph to incorporate non-binary conflicts and formulate the CA problem as a utility maximization problem.

We start with a conflict graph without any super-NC pair as constructed in Section 5.3.2. To differentiate and quantify the impacts of a conflict on two interfering nodes, we consider directed edges and use a *penalty (or edge weighting) function* $P : E \mapsto \mathbb{R}^+$ to assign a non-negative penalty to each directed edge. Let the penalty of $e(u,v) \in E$ as $P(e(u,v))$ or simply $P_{u,v}$, i.e., the penalty on v due to the interference from u. In general, we have $P_{u,v} \neq P_{v,u}$, and $P_{u,v} = 0$ if $e(u,v) \notin E$.

[7]In this work, we focus on the CBSD-centric graph representation and algorithms for GAA CA. Hence,

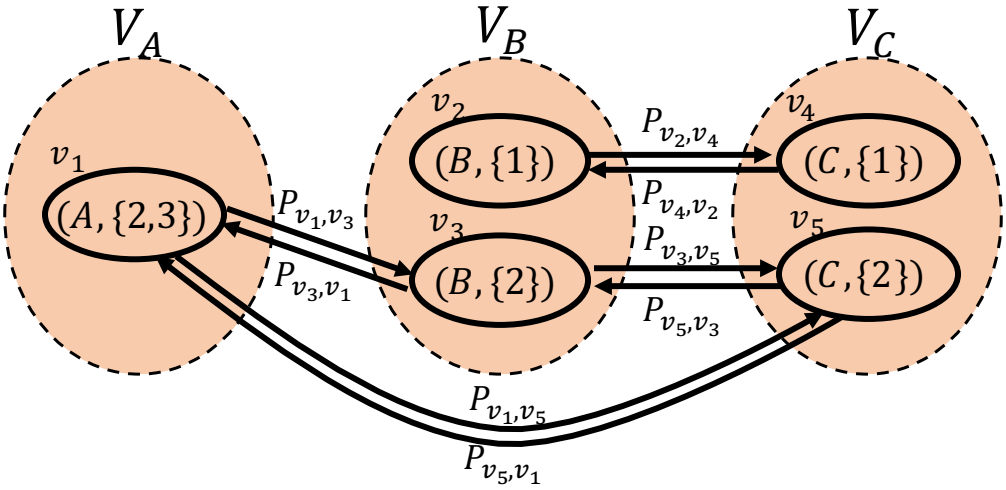

Figure 5.7: Example of NC-pair conflict graph with non-binary conflicts. Each vertex is associated with a reward and each directed edge has a penalty. Note that NC pairs belonging to the same node are grouped as a cluster and there are no intra-cluster edges.

Figure 5.7 illustrates the proposed non-binary conflict graph. In addition to the directed edges with penalties, the other main difference is that the set of NC pairs that belong to the same node are grouped as a cluster, and there are no edges within a cluster. The one-channel-assignment-per-node constraint is enforced instead by selecting at most one NC pair from each cluster.

Problem Formulation: Given a vertex- and edge-weighted conflict graph $G(V, E, R, P)$ for n nodes for non-binary GAA CA, the SAS wants to find a scheme $I \subseteq V$ so as to

$$\max_{I \subseteq V} U(I), \text{ s.t. } |I \cap V_i| \leq 1, \forall i = 1, 2, ..., n, \tag{5.3}$$

where

$$U(I) = \sum_{v \in I} R(v) - \lambda \cdot \sum_{u,v \in I} P_{u,v} \tag{5.4}$$

since GAA nodes are at fixed locations, the SAS does not need to consider node mobility. We will leave extending this work to client-centric and studying the impact of end user device mobility on the proposed algorithms as future work.

is the *utility function*, and $\{V_i\}$ are NC-pair clusters that form a partition of V, that is, $V = \bigcup_i V_i$ and $V_i \cap V_j = \emptyset$ for $i \neq j$. We refer to the above problem as **Max-Utility CA**.

5.4 Proposed Algorithms

In this section, we first present our super-node formation algorithm that identifies super-nodes and then present a greedy algorithm for max-cardinality and max-reward CA. Finally, we propose a local search based algorithm for max-utility CA, which exploits the structural property of the utility function and provides a performance guarantee.

5.4.1 Super-Node Formation

As mentioned in Section 5.3.2, the objective of super-node formation is to identify a set of super-nodes for a given channel C, i.e., nodes that have C available and that are within each other's CS/ED range. As shown in Algorithm 7, the main input is an undirected graph, where each vertex is a node with C available, and each edge connects two nodes that are within each other's CS/ED range. Since a super-node is a *clique* (i.e., a subgraph where every two distinct vertices are connected), the first task is to find all such cliques. In this work, we adopt the well-known Bron-Kerbosch algorithm [124], a recursive backtracking algorithm that lists subsets of vertices that are cliques, and no listed subset can have any additional vertex without breaking its complete connectivity. Even though a node can belong to multiple cliques, it randomly chooses a clique to join, since it cannot join two super-nodes at the same time.

Although nodes in each clique (and any of its subsets) are able to coexist, the SAS may want to divide them into smaller groups for load balancing. Denote the *activity index* of node i as $\alpha_i > 0$, which is the estimated total number of channels it demands. The activity index mapped to C is $\alpha_i(C) = \min(\alpha_i/|C|, 1) \in (0, 1]$. To avoid overcrowded super-nodes, the SAS can set a *sum activity index limit* $\bar{\alpha} > 0$ (e.g., $\bar{\alpha} = 1.0$) for each super node. As a result, the task of grouping nodes (i.e., items with weights) into fewer super-radios (i.e., bins with capacity of $\bar{\alpha}$) becomes the well-known one dimensional *bin packing problem* (BPP). In

Algorithm 7 Super-Node Formation

Input: CS graph on channel C, activity index limit $\bar{\alpha}$

Output: A set of super-NC pairs U on channel C

1: Run Bron-Kerbosch algorithm to find cliques $\mathcal{Q}$.
2: Each node in V that belongs to multiple cliques chooses one to join (e.g., randomly).
3: **for all** clique Q in $\mathcal{Q}$ **do**
4: Run FFD to identify super-nodes $\mathcal{S}$ w.r.t. $\bar{\alpha}$.
5: Add (S, C) for each $S \in \mathcal{S}$ s.t. $|S| > 1$ to U.
6: **end for**
7: **return** U

this work, we adopt a heuristic-based algorithm called *first fit decreasing* (FFD) [125]: it first creates a sequence of super-nodes (i.e., empty bins) and sorts nodes in non-increasing order of activity index; then it places each node into the lowest-indexed super-node with sufficient remaining space. Latest analysis has shown that FFD uses no more than 11/9 OPT + 6/9 bins, where OPT is the number of bins given by the optimal solution [126].

5.4.2 Algorithm for Max-Cardinality and Max-Reward CA

Our proposed graph representation enables us to map the max-cardinality CA in Eq. (5.1) to the classic *maximum independent set* (MIS) problem, and the max-reward CA in Eq. (5.2) to the generalized *maximum weighted independent set* (MWIS) problem. Formally, given a vertex-weighted graph $G(V, E, R)$, a subset $I \subseteq V$ is an *independent set* (IS) if for any two vertices $u, v \in I$, it holds that $e(u, v) \notin E$. The weight of a set I is $R(I) = \sum_{v \in I} R(v)$, and an IS I is maximum if there is no IS $I' \neq I$ such that $R(I) < R(I')$.

Since M(W)IS can be difficult[8], we adopt simple heuristic-based algorithms[9] like GMWIS (Algorithm 8) to obtain an approximate solution. Denote by $\theta(G)$ the weight of a maximum IS, and by $A(G)$ the weight of the solution obtained by algorithm A. The performance ratio is defined by $\rho_A = \inf_G \frac{A(G)}{\theta(G)}$. It has been shown in [116] that GMWIS outputs an IS of weight at least $\sum_{v \in V} \frac{R(v)}{\delta_G(v)+1}$, where $\delta_G(v)$ is the vertex degree of v and its performance ratio is $\frac{1}{\Delta_G}$, where Δ_G is the maximum vertex degree of G. Note that the computational complexity of Algorithm 8 is $O(|V|^2)$, since each iteration takes $O(|V|)$ operations and there are up to $|V|$ iterations.

Algorithm 8 Greedy algortihm for MWIS (GMWIS)

Input: Vertex-weighted undirected graph $G(V, E, R)$

Output: A maximal independent set I in G

1: Pick a vertex $v \in V$ that maximizes $\frac{R(v)}{\delta_G(v)+1}$.

2: Add v to I and remove v and its neighbors from V.

3: Repeat steps 1 and 2 until all vertices in V are removed.

4: **return** I

5.4.3 Proposed Algorithm for Max-Utility CA

In this section, we provide brief background on submodularity and matroids. We then show that the max-utility CA problem in Eq. (5.3) is matroid-constrained submodular maximization and proposed a polynomial-time algorithm with a provable performance guarantee.

[8]The M(W)IS problem on general graphs is known to be NP-hard [115], but it may become easy on simple classes of graphs. For instance, MWIS can be solved in linear time in any tree graph. Polynomial time algorithms exist for MWIS in other classes of graphs including bipartite graphs, line graphs, circle graphs, claw-free graphs and planar graphs. See [127] for a brief summary.

[9]Apart from GMWIS, there exist other algorithms for MWIS. For example, authors in [117] defined a metric called the weighted average degree and proposed greedy algorithms with provable performance. Randomized algorithms like Tabu search [128] may also provide good results for MWIS. In this study, we adopt GMWIS due to its simplicity and low computational complexity, but more sophisticated MWIS algorithms may be implemented in practice.

Background on Submodularity and Matroids

Submodularity is a property of set functions that captures the *diminishing returns* behavior, that is, adding a new element introduces greater incremental benefits, if there are fewer elements so far, and less, if there are more elements. The formal definition is as follows.

Definition 5.1 (Submodularity)**.** *Given a finite set V, a function $f : 2^V \mapsto \mathbb{R}$ is submodular if, for any subsets $S, T \subseteq V$,*

$$f(S) + f(T) \geq f(S \cap T) + f(S \cup T).$$

An equivalent definition is the following [91]. A set function is submodular if, for any sets $S \subseteq T \subseteq V$ and any $v \in V \setminus T$,

$$f(S \cup \{v\}) - f(S) \geq f(T \cup \{v\}) - f(T). \tag{5.5}$$

Definition 5.2 (Matroid)**.** *Let V be a finite set, and let $\mathcal{I}$ be a collection of subsets of V. A set system $\mathcal{M} = (V, \mathcal{I})$ is a matroid if the following three conditions hold: (i) $\emptyset \in \mathcal{I}$, (ii) if $B \in \mathcal{I}$, then $A \in \mathcal{I}$ for all $A \subseteq B$, and (iii) if $A, B \in \mathcal{I}$ and $|A| < |B|$, then there exists $v \in B \setminus A$ such that $(A \cup \{v\}) \in \mathcal{I}$.*

Given a matroid $\mathcal{M}$, $\mathcal{I}(\mathcal{M})$ is called the set of *independent sets* of $\mathcal{M}$. A sub-class of matroids called *partition matroids* is defined as follows.

Definition 5.3 (Partition Matroid)**.** *Let V be a finite set, and V_1, ..., V_m be a partition of V, that is, a collection of sets such that $V_1 \cup ... V_m = V$ and $V_i \cap V_j = \emptyset$ for $i \neq j$. Let k_1, ..., k_m be a collection of nonnegative integers. Define a set $\mathcal{I}$ by $A \in \mathcal{I}$ iff $|A \cap V_i| \leq k_i$ for all $i = 1, ..., m$. Then $\mathcal{M} = (V, \mathcal{I})$ is a matroid, called a partition matroid.*

Matroid-Constrained Submodular Maximization

As we can see, the constraint in the max-utility CA formulation in Eq. (5.3) defines a partition matroid,

$$\mathcal{M} = (V,\ \mathcal{I}),\ \text{where } \mathcal{I} = \{I : |I \cap V_i| \leq 1, \forall i = 1, 2, ..., n\} \text{ and } \{V_i\} \text{ is a partition of } V, \tag{5.6}$$

and we can show that the utility function in Eq. (5.4) is a submodular set function.

Lemma 5.1. *The utility function $U(\cdot)$ in Eq. (5.4) is submodular.*

Proof. See Appendix 5.7.1 for proof. □

Hence, the problem $\max\{U(I) : I \in \mathcal{I}(\mathcal{M})\}$ is an instance of matroid-constrained submodular maximization, where $\mathcal{M}$ is the partition matroid defined in Eq. (5.6).

Proposed Algorithm

Our algorithm `UM` (Algorithm 9) is based on the (approximate) local search procedure `LS` (Lines 6-16). It quickly finds an initial solution by iteratively adding the next element with the maximum incremental utility (Lines 6-10) and then searches for the locally optimal solution under the local delete (Line 12), add and swap (Line 13) operations subject to the matroid constraint. To achieve faster convergence, the parameter ϵ can be set to obtain an approximately locally optimal solution. Note that `LS` is called twice in `UM`: it first obtains I_1 for the original matroid $\mathcal{M}$ and then I_2 for the new matroid $\mathcal{M}'$, which corresponds to the partition $\{V_i'\}$ of V' (i.e., $V \setminus I_1$). The set, either I_1 or I_2, that yields a greater utility is returned.

Theorem 5.1 shows that `UM` (Algorithm 9) provides a performance guarantee.

Theorem 5.1. *Algorithm 9 returns a solution I with the following performance guarantee*

$$U(I) \geq \frac{1}{(4 + 2\epsilon)}[U(OPT) + 2U_{\min}], \tag{5.7}$$

Algorithm 9 Utility Maximization (UM)

Input: Partition matroid $\mathcal{M} = (V, \mathcal{I})$, utility function $U(\cdot)$, and parameter $\epsilon > 0$

Output: I – Selected NC pairs

$I_1 \leftarrow$ LS $(\mathcal{M}, U, \epsilon)$

$\mathcal{I}' \leftarrow \{I : |I \cap V_i'| \leq 1\}$, where $V_i' = V_i \setminus I_1, \forall i = 1, 2, ..., n$

Define $\mathcal{M}' = (V', \mathcal{I}')$, where $V' = \cup_i V_i'$

$I_2 \leftarrow$ LS $(\mathcal{M}', U, \epsilon)$

return $I \leftarrow \arg\max_{I \in \{I_1, I_2\}} U(I)$

Local Search Procedure (LS):

Input: Matroid $\mathcal{M} = (V, \mathcal{I})$, submodular function $f(\cdot)$, and parameter $\epsilon \geq 0$

Output: A selected subset I

$I \leftarrow \emptyset$, $v \leftarrow \arg\max\{f(u)|u \in V\}$, $N \leftarrow |V|$.

while $v \neq \emptyset$ and $f(I \cup \{u\}) > (1 + \frac{\epsilon}{N^2}) f(I)$ **do**

  $I \leftarrow I \cup \{v\}$

  $v \leftarrow \arg\max\{f(I \cup \{u\}) - f(I)|u \in V \setminus I$ and $I \cup \{u\} \in \mathcal{I}\}$

end while

while *true* **do**

  if there exists $d \in I$ s.t. $f(I \setminus \{d\}) \geq (1 + \frac{\epsilon}{N^2}) f(I)$ **then** $I \leftarrow I \setminus \{d\}$, **continue**

  if there exists $a \in V \setminus I$ and $d \in I \cup \emptyset$ s.t. $I \setminus \{d\} \cup \{a\} \in \mathcal{I}$ and $f(I \setminus \{d\} \cup \{a\}) \geq (1 + \frac{\epsilon}{N^2}) f(I)$ **then** $I \leftarrow I \setminus \{d\} \cup \{a\}$, **continue**

  break

end while

return I

where OPT is the optimal solution to $\max\{U(I) : I \in \mathcal{I}(\mathcal{M})\}$*, and* $U_{\min} = \min\{U(I) : I \in \mathcal{I}(\mathcal{M})\}$*. If* $U(\cdot)$ *is non-negative (i.e.,* $U_{\min} \geq 0$*), we have* $U(I) \geq \frac{1}{(4+2\epsilon)} U(OPT)$*.*

Proof. See Appendix 5.7.2 for proof. □

Proposition 5.1. *Algorithm 9 is in polynomial time with runtime bounded by* $O(\frac{1}{\epsilon} N^3 \log N)$*.*

Proof. See Appendix 5.7.3 for proof. □

5.5 Evaluation

We implemented the proposed algorithms in MATLAB and compare their performance against baseline algorithms via extensive simulations. A real-world Wi-Fi hotspot location dataset in NYC [106] is used to simulate a dense outdoor scenario. Our results demonstrate the advantages of the proposed graph representation and algorithms for dynamic CA in the CBRS band.

5.5.1 Evaluation of Max-Cardinality CA

For PA CA, we evaluate the proposed algorithm based on GMWIS (Algorithm 8) and compare it against a baseline algorithm called Non-Preemptive Sum Multi-Coloring (npSMC) [129]. To the best of our knowledge, npSMC is the only existing algorithm that explicitly considers channel contiguity, applicable to the PC CA scenario in the CBRS band.

Baseline: The algorithm npSMC was proposed in [129] for scheduling dependent jobs on a graph, where each vertex v is a job with a length or execution time $x(v)$ (i.e., required number of colors) and each edge indicates two dependent jobs that cannot be scheduled at the same time. Given a certain amount of time units or colors, the objective is to color as many vertices as possible, such that each vertex is assigned a desired amount of distinct contiguous colors and adjacent vertices are assigned disjoint sets of colors.

Given a graph $G(V, E, x)$, npSMC first puts vertices of the same length to the same group by adding an edge for each pair of vertices of different lengths, that is, $E' = E \cup \{(u, v) :$

$x(u) \neq x(v)\}$. This ensures that at any given time, vertices from the same group are being colored. Then it finds a maximal independent set (e.g., Algorithm 8) in the new graph $G' = (V, E')$ and color the selected jobs to completion non-preemptively in each iteration, until colors are exhausted.

Setup: We consider a square area of width m that consists of m^2 census tracts, as shown in Figure 5.8(a). We generate randomly located circular areas of radius r_s and consider census tracts that overlap with a circular area as a service area for PA CA purposes. The number of PALs held by the same PA licensee for each service area is uniformly selected from $[1, 4]$ at random. To simulate the worst case, we generate as many service areas as possible (up to 1000 trials) subject to the seven-PALs-per-census-tract limit. Since the maximum possible size of a solution I is equal to the total number of service areas n, we use the metric called *ratio of service areas served*, $p = |I|/n$ to measure the performance for PA CA.

Results: To simulate cities of different sizes, we set r_s to 1 and vary m from 5 to 30 with a step of 5. For instance, with an optimal size of $4,000$ people for a census tract, 100 census tracts ($m = 10$) corresponds to a medium-sized city. As mentioned in Section 5.2.1, there are a total of 10 PAL channels. Results are averaged over 100 iterations. In each iteration, the same seed is used for the baseline and proposed algorithms for fair comparison.

As shown in Figure 5.9(a), the proposed algorithm serves 93.7% of service areas on average, as compared to 70.1% achieved by npSMC, with an improvement of 33.7%. We observe that due to the grouping in npSMC, service areas with larger demands tend to have lower priorities and thus often obtain no channels, whereas the proposed algorithm considers all service areas equally.

We then set m to 10 and vary r_s from 0.4 to 1.4. As shown in Figure 5.9(b), the average p is 94.3% and 71.4% for the proposed algorithm and npSMC, respectively. The improvement is as high as 32.0%. To summarize, our results show that the proposed algorithm is able to consistently meet more than 93.0% of PA demands with a significant improvement over the baseline algorithm.

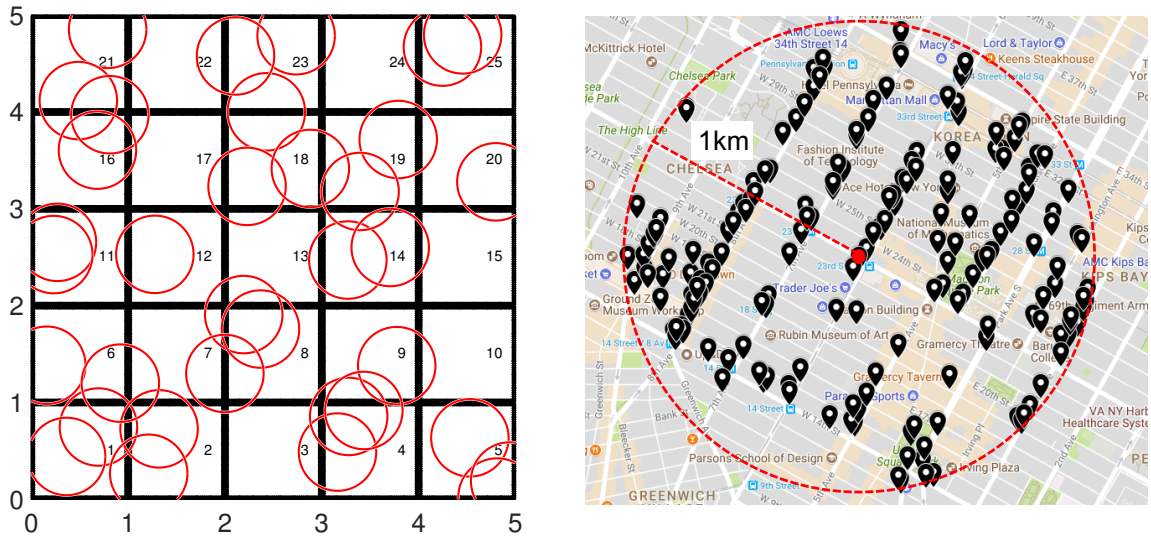

Figure 5.8: (a) Example of census tracts for PA CA. The set of census tracts that overlap with a red circle are treated as a service area for a PA licensee. In this example, each circle is of radius 0.4 and each service area contains up to four census tracts. (b) Examples of Wi-Fi hotspot locations in NYC treated as CBSDs locations for GAA CA. In this example, there are 190 GAA CBSDs inside the circle centered at the (randomly selected) location $(40.74, -73.99)$ with a radius of 1 km.

5.5.2 Evaluation of Max-Reward CA

In this section, we evaluate the proposed algorithm (Max-Reward) based on GMWIS (Algorithm 8) for binary GAA CA and compare it against the Max-Revenue Algorithm (MRA) in [101]. Note that npSMC is not applicable, as it requires the same set of contiguous available channels at each node and cannot handle flexible demands. We also evaluate Max-Reward with different settings to study the impact of reward function and coexistence awareness.

Baseline: MRA was proposed for bidding-based spectrum allocation in [101]. It selects a

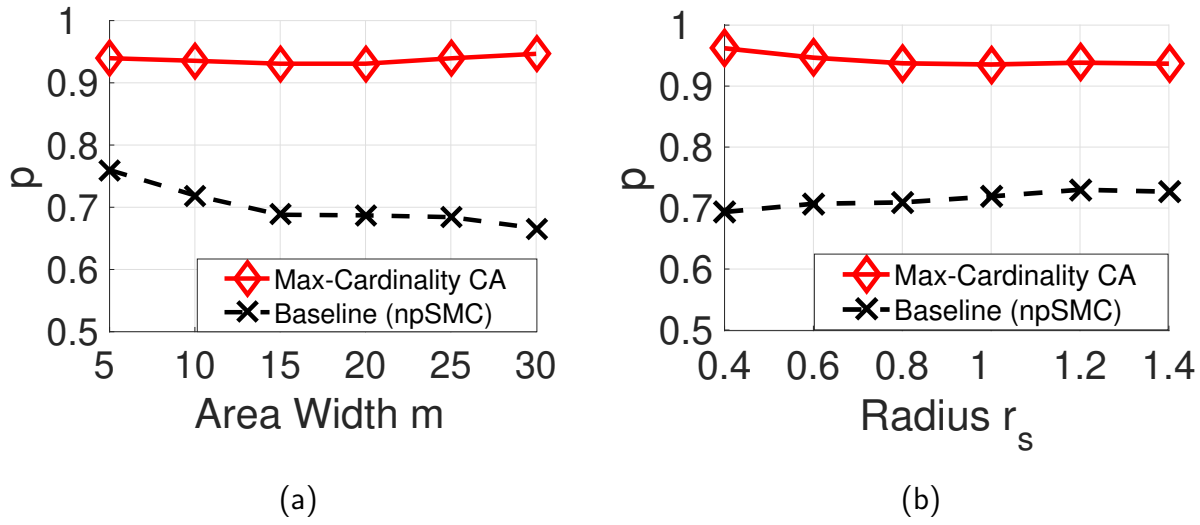

Figure 5.9: Performance of the proposed and baseline algorithms vs. (a) area width and (b) radius. The proposed algorithms consistently serves over 93.0% of PA demands for different area widths and radii with a significant improvement over the baseline algorithm.

set of non-conflicting NC pairs so as to maximize the total revenue, which corresponds to the total reward in our case. It is essentially a greedy algorithm that iteratively selects the next non-conflicting NC pair with the maximum incremental revenue. Note that MRA is coexistence unaware and it is unaffected by the choice of the reward function.

Setup: We consider a scenario where the SAS is serving a circular region of radius r (in km) that is randomly located in the densely populated Manhattan area of NYC, as illustrated in Figure 5.8(b). We import outdoor Wi-Fi hotspot locations within the circular region from a publicly available dataset [106] and treat them as GAA nodes.

In order to create location-dependent channel availability for GAA nodes, we consider two PA licensees that are assigned with CH 1-4 and CH 5-7, respectively, and generate 10 randomly deployed PA nodes for each licensee. A channel is considered available for a GAA

node, if its -80 dBm/10 MHz interference contour[10] does not overlap with any PA node's default PPA (Section 5.2.1). Each GAA node has a demand set $\mathcal{D} = \{1, 2, 3, 4\}$ and an activity index α in $U[0, 4]$. In this work, we adopt the PA interference protection rules for determining the interference relationship between two GAA nodes, that is, a GAA node j is said to be interfering with i, if its interference at any location within i's -96 dBm/10 MHz service contour is higher than -80 dBm/10 MHz. The CS/ED threshold is set to -75 dBm/10 MHz (adapted from -72 dBm/20 MHz in [32]). The transmit power is 30 dBm for each node, and transmit and receive antenna heights are 3 and 1.5 meters, respectively [118]. We adopt the widely used COST-231 Hata [130] as the propagation model. Two metrics are adopted to measure the performance: 1) *percentage of nodes served*, denoted as p_1, and 2) *percentage of demands served*, denoted as p_2, i.e., the ratio between the total number of assigned channels and the total demand.

Results: In order to study the performance of Max-Reward for regions with different sizes, we vary r from 0.4 km to 1.2 km. The trade-off parameter λ and the sum activity index limit $\bar{\alpha}$ are set to 0 and 1, respectively. Results are averaged over 30 iterations.

As shown in Figure 5.10, the size of the SAS's service region does not have a significant impact on the performance of a CA algorithm. Without coexistence awareness, Max-Reward-Linear and Max-Reward-Log achieve an average p_1 larger than 72.6% and 90.5% in all cases and outperform the baseline algorithm by 10.2% and 36.4% on average, respectively.

On the other hand, Max-Reward-Log has very close performance with the baseline algorithm in terms of average p_2, while Max-Reward-Linear outperforms the baseline by 10.4% on average. The above behaviors of Max-Reward are not surprising, since the log reward function encourages assigning a channel to nodes with fewer channels, leading to a larger p_1 but a smaller p_2.

---

[10]Strictly speaking, -80 dBm/10 MHz is the limit for the aggregate co-channel interference, and a lower limit may be chosen for pairwise co-channel interference. Nevertheless, the choice of this limit does not affect our evaluation, since the same set of available channels are used as input for both the proposed and baseline algorithms.

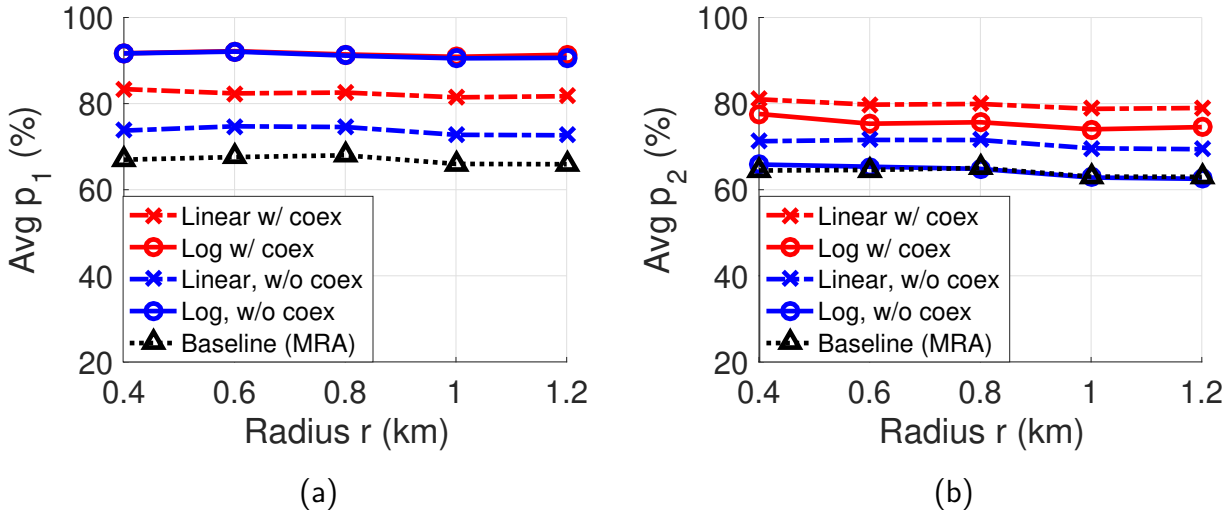

Figure 5.10: Performance of the proposed and baseline algorithms in terms of average p_1 in (a) and p_2 in (b) as function of n. The proposed algorithms outperform the baseline algorithm and this advantage is further enhanced by coexistence awareness.

We can also observe that coexistence awareness effectively improves the performance of Max-Reward-Linear in terms of average p_1 by 11.7% but has little effects on Max-Reward-Log. On the other hand, it is able to improve both Max-Reward-Linear and Max-Reward-Log in terms of average p_2 by 12.8% and 17.4% on average, respectively.

Impact of λ and $\bar{\alpha}$: In order to study the impact of λ, we set $r = 0.8$, $\bar{\alpha} = 1$, and vary λ from 0 to 8. As illustrated in Figures 5.11(a) and 5.11(b), there exists a trade-off between p_1 and p_2 when choosing λ for the proposed algorithm. With a larger λ, the proposed algorithm prioritizes the objective of serving more nodes by assigning more weight on the cardinality of the node set in each vertex, thus increasing p_1 but reducing p_2. We also see that that with a large λ, coexistence awareness does not help improve p_1 but is still able to effectively improve p_2.

We then set $r = 0.8$, $\lambda = 0$ and vary $\bar{\alpha}$ from 0 to 5. As shown in Figures 5.11(c) and 5.11(d), a larger $\bar{\alpha}$ value allows more nodes to form a super-node, thus increasing both p_1

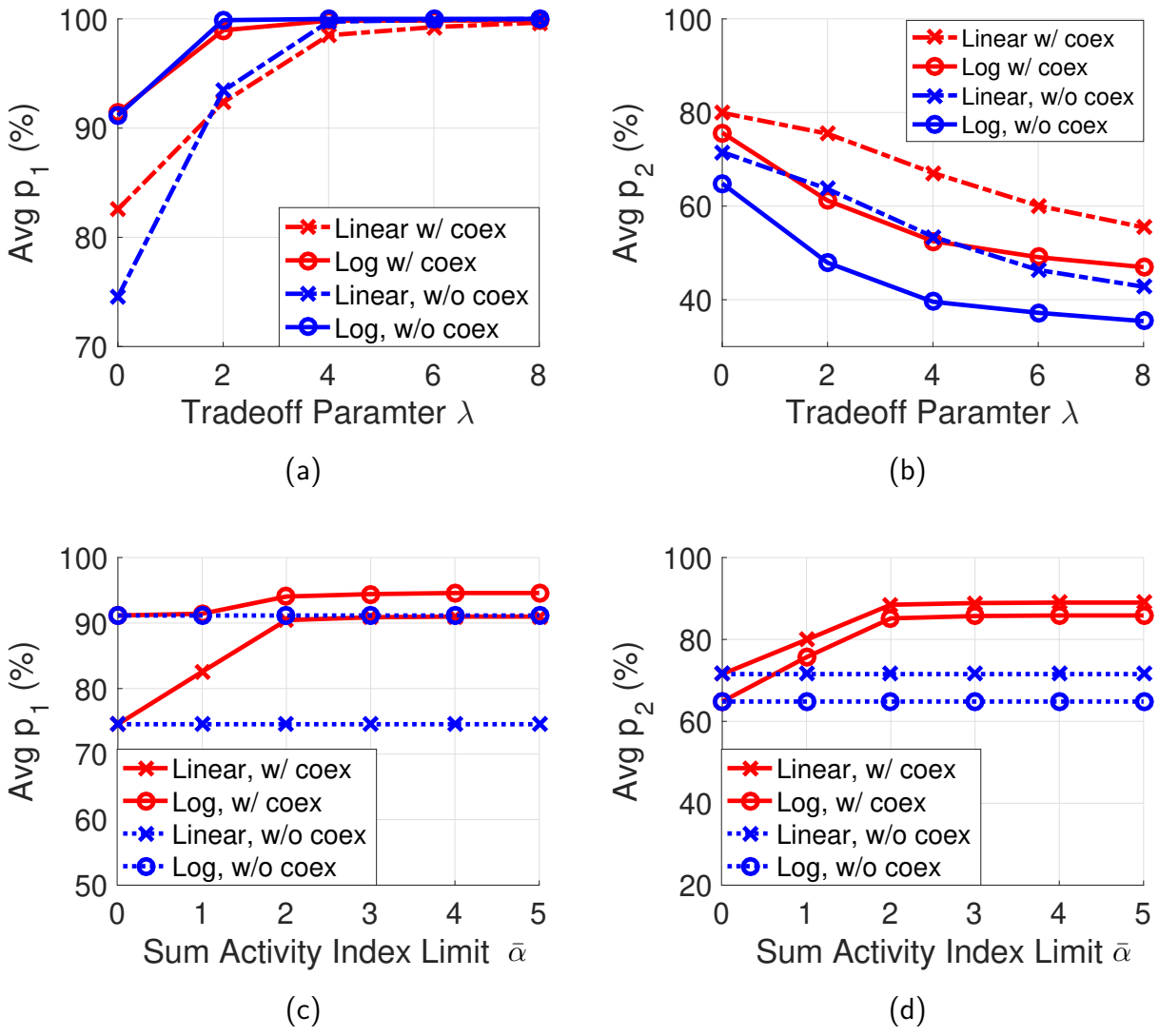

Figure 5.11: Impact of λ and $\bar{\alpha}$ on the performance of the proposed algorithm in terms of average p_1 and p_2. There exists a trade-off between p_1 and p_2 when choosing λ. In addition, increasing $\bar{\alpha}$ can improve both p_1 and p_2, but such improvements no longer exist when $\bar{\alpha}$ is large enough and all nodes in a clique are considered as a single super-node.

and p_2. But such improvement saturates at $\bar{\alpha} = 2$, at which point all nodes in a clique will be considered as a super-node and thus further increasing $\bar{\alpha}$ does not help any more.

5.5.3 Evaluation of Max-Utility CA

In this section, we evaluate the proposed Max-Utility algorithm `UM` (Algorithm 9) for non-binary GAA CA and compare its performance against a random selection-based algorithm, which randomly selects a NC pair from each cluster. It repeats the process multiple times (e.g., 10000) and returns the one with the maximum utility.

Setup: We use the same setup in Section 5.5.2 and set $\epsilon = 0$ for Algorithm 9. The linear reward function is used and represents the number of channels assigned to each node, which is proportional to the best-case capacity that can be achieved in the absence of interference.

There are many options for penalties from literature. For example, Padhye *et al.* defines the link interference ratio as the penalty [131], that is, the ratio of aggregate output of the links when they are active simultaneously, to the aggregate throughput when they are active individually. This penalty can be empirically measured via broadcast probes. In [132], Rei *et al.* improves the scalability of the previous approach by developing an interference model based on RSSI measurements. In [99], the penalty is defined as the number of clients associated with two interfering nodes that are affected if the two nodes are assigned the same channel. Due to the ease of practical implementation, we use the interference estimated from a radio propagation model as penalty as in [100, 133] (normalized by the maximum pairwise interference) in this work[11]. The performance is measured in terms of the achieved *utility* and *the total amount of interference*.

[11] While the number of assigned channels is used as the reward and the estimated pairwise interference is chosen as the penalty in this work, our proposed algorithm is not limited to the chosen reward or penalty function. For example, the capacity averaged over client device locations [17] (assuming no interference, i.e., best-case) can be adopted as the reward, and the amount of capacity reduction due to the interference introduced by the conflicting node as the penalty. In this case, the total utility ($\lambda = 1$) reflects the overall capacity under the pairwise interference relationship. Besides, λ can be adjusted to account for the difference between the actual capacity reduction and the capacity reduction under pairwise interference.

Results: We first set $\lambda = 1$ and vary the radius r from 0.4 km to 1.2 km. Results averaged over 30 iterations are provided in Figure 5.12. As we can see, Max-Utility is able to achieve a much greater utility than random selection, and the relative gains are more significant as SAS's service region becomes larger. The improvement in average utility is more than 29.5% in all cases and reaches 50.2% with $r = 1.2$ km. On the other hand, the total interference generated by Max-Utility is always smaller than random selection.

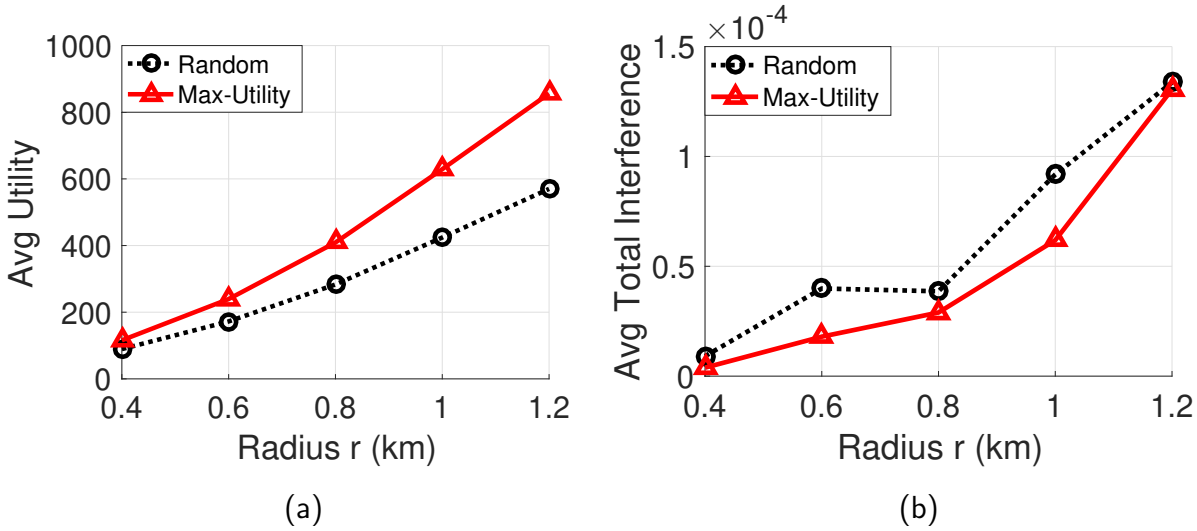

Figure 5.12: Performance of Max-Utility and random selection in terms of (a) averaged utility and (b) averaged total interference as a function of the radius of SAS's service region. Max-Utility achieves a much greater utility and smaller total interference than random selection.

In order to study the impact of λ, we set r to 0.8 and vary λ from 10^0 to 10^3. Results averaged over 30 iterations are shown in Figure 5.13. We observe that increasing λ reduces the achieved utility, but the decrease for Max-Utility is slower than random selection. This is because a larger λ implies a larger weight on the interference, which effectively makes Max-Utility avoid selecting NC pairs with larger interference. It also explains the decrease in the total interference for random selection. In all cases, Max-Utility achieves a much greater utility while keeping the total interference much smaller than random selection. Figure 5.14

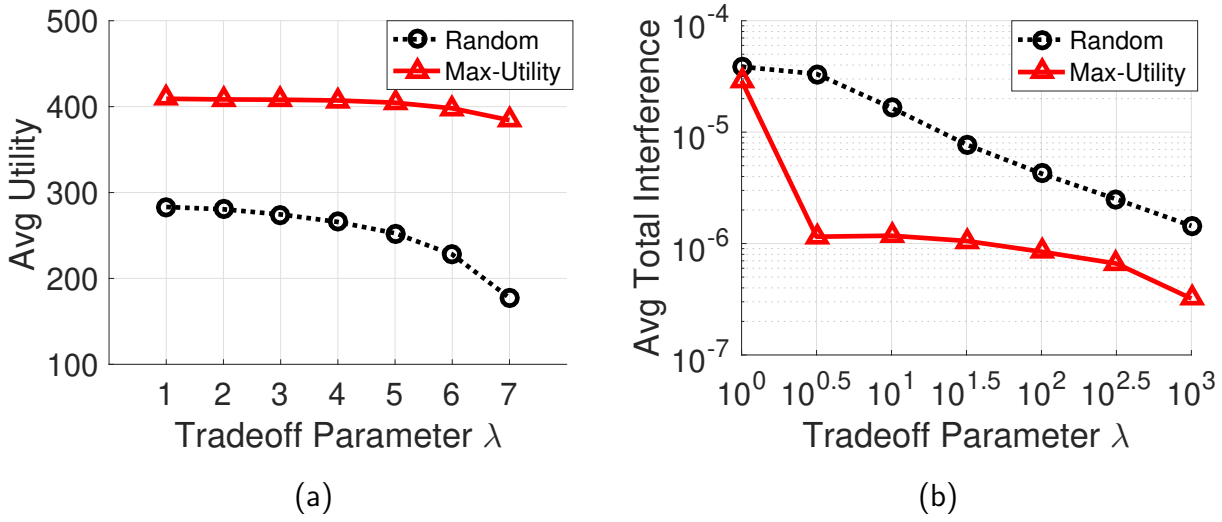

Figure 5.13: Performance of Max-Utility and random selection in terms of (a) averaged utility and (b) averaged total interference as a function of the trade-off parameter λ. We can see that increasing λ puts more weights on the interference, thus leading to less interference at the cost of reduced utility.

illustrates the performance of Max-Utility in terms of p_1 and p_2. We can see with non-binary GAA CA formulation, the SAS can serve almost all nodes and demands. As λ keeps increasing, p_1 and p_2 will decrease accordingly, because a large λ value forces the SAS to avoid assigning overlapping channel(s) to nodes that would cause significant interference to each other.

5.6 Conclusion and Future Work

In this paper, we studied SAS-assisted dynamic CA for the 3.5 GHz CBRS band. We proposed the NC-pair conflict graph to model pairwise interference, spatially varying channel availability and channel contiguity. We further introduced super-NC pairs to exploit coexistence opportunities under type-II conflict and proposed the super-node formation algorithm to identify super-nodes. The proposed conflict graph enables us to formulate PA CA as max-

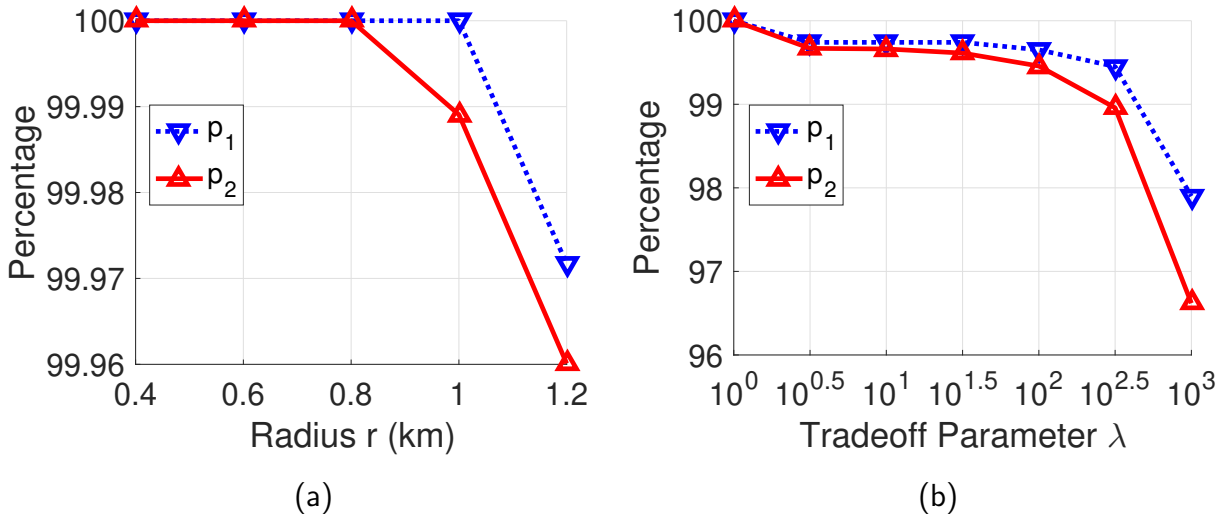

Figure 5.14: Performance of the proposed algorithm in terms of p_1 (percentage of nodes served) and p_2 (percentage of demands served) as a function of (a) radius with $\lambda = 1$ and (b) trade-off parameter with $r = 0.8$. We can see that p_1 and p_2 obtained by the proposed algorithm are close to 100% and do not decrease significantly as radius increases. In contrast, as λ increases, the SAS needs to avoid assigning the same channel(s) to conflicting nodes that generate large interference, thus leading to a decrease in both p_1 and p_2.

cardinality CA and GAA CA with binary conflicts as max-reward CA, and further map them to the classic maximum (weighted) independent set problem. We adopted a heuristic-based algorithm to obtain approximate solutions. To further enhance coexistence awareness, we extended binary conflicts to non-binary by assigning each conflict a penalty. Then we formulated non-binary GAA CA as utility maximization. We showed that the utility function is submodular and our problem is an instance of matroid-constrained submodular maximization. We proposed a polynomial-time algorithm based on local search for max-utility CA that provides a provable performance guarantee.

Our results based on a real-world dataset show that the proposed max-cardinality algorithm consistently serves over 93.0% of service areas and outperforms the baseline algorithm

by over 30.0% for PA CA. For binary GAA CA, the proposed max-reward algorithm with linear rewards can accommodate 10.2% more nodes and serve 10.4% more demand on average than the baseline algorithm, and coexistence awareness can effectively improve the performance of the proposed algorithm. For non-binary GAA CA, the proposed max-utility algorithm achieves 29.5% more utility with much less total interference compared to random selection.

There are several interesting directions that could be explored. First, it would be of practical importance to address possible implementation issues and generalize the current pairwise interference model to the physical interference model to account for accumulated interference. Second, it is very likely that there are multiple SASs operated by different operators. Therefore, it is an interesting question to perform multi-SAS channel assignment through the inter-SAS protocol while achieving desirable objectives such as fairness.

5.7 Appendix

5.7.1 Proof of Lemma 5.1

Proof. Consider any two sets S, T with $S \subseteq T \subseteq V$ and any $v \in V \setminus T$. Since $P_{u,v} \geq 0$, we any $u, v \in V$, we have

$$\begin{aligned} U(S \cup \{v\}) - U(S) &= R(v) - \lambda \cdot \sum_{u \in S} [P_{u,v} + P_{v,u}] \\ &\geq R(v) - \lambda \cdot \left(\sum_{u \in S} [P_{u,v} + P_{v,u}] + \sum_{u \in T \setminus S} [P_{u,v} + P_{v,u}] \right) \\ &= R(v) - \lambda \cdot \sum_{u \in T} [P_{u,v} + P_{v,u}] \geq U(T \cup \{v\}) - U(T), \end{aligned}$$

which establishes the submodularity of $U(\cdot)$ by the definition in Eq. (5.5). □

5.7.2 Proof of Theorem 5.1

Proof. Let $OPT_1 = OPT \cap V$, and $OPT_2 = OPT \cap V'$. Hence, we have $OPT_1 = OPT$. It has been shown in [134] that the `LS` procedure returns an approximately locally optimal

solution I such that $(2+\epsilon)f(I) \geq f(I \cup C) + f(I \cap C)$ for any $C \in \mathcal{I}$, where $\epsilon \geq 0$ is the parameter used in `LS`. The above result implies that

$$(2+\epsilon)U(I_1) \geq U(I_1 \cup OPT_1) + U(I_1 \cap OPT_1)$$
$$(2+\epsilon)U(I_2) \geq U(I_2 \cup OPT_2) + U(I_2 \cap OPT_2).$$

Using $U(I) \geq \max\{U(I_1), U(I_2)\}$, we have

$$\begin{aligned}(4+2\epsilon)U(I) &\geq [U(I_1 \cup OPT_1) + U(I_2 \cup OPT_2)] + U(I_1 \cap OPT_1) + U(I_2 \cap OPT_2) \\ &\geq U(I_1 \cup I_2 \cup OPT_1) + [U(OPT_2) + U(I_1 \cap OPT_1)] + U(I_2 \cap OPT_2) \\ &\geq U(I_1 \cup I_2 \cup OPT_1) + U(OPT_1) + U(I_2 \cap OPT_2) \\ &\geq U(OPT_1) + 2U_{\min} = U(OPT) + 2U_{\min}.\end{aligned}$$

The first inequality is obvious. The second inequality follows from submodularity, using $(I_1 \cup OPT_1) \cup (I_2 \cup OPT_2) = I_1 \cup I_2 \cup OPT_1$ and $(I_1 \cup OPT_1) \cap (I_2 \cup OPT_2) = OPT_2$. The third inequality is also follows from submodularity, using $OPT_2 \cup (I_1 \cap OPT_1) = OPT_1$ and $OPT_2 \cap (I_1 \cap OPT_1) = \emptyset$. Hence, we have $U(I) \geq \frac{1}{(4+2\epsilon)}[U(OPT) + 2U_{\min}]$. □

5.7.3 Proof of Proposition 5.1

Proof. Let the first element of I be v_1 (Line 6 in `LS`), and we have

$$f(OPT) \leq \sum_{s \in OPT} f(s) \leq |OPT| \cdot f(s^*) \leq N \cdot f(s^*) \leq N \cdot f(v_1)$$

where $s^* = \arg\max_{s \in OPT} f(s)$ and the first inequality is due to submodularity. Since $f(v_1) \geq \frac{f(OPT)}{N}$ and each local operation increases the value by a factor $(1 + \frac{\epsilon}{N^2})$, the maximum number of iterations is $\log_{1+\frac{\epsilon}{N^2}} \frac{f(OPT)}{\frac{f(OPT)}{N}} = O(\frac{1}{\epsilon}N^2 \log N)$. As each iteration requires at most N evaluations of the objective function $f(\cdot)$, it implies that the computational complexity of `LS` is $O(\frac{1}{\epsilon}N^3 \log N)$ in the worst case. Despite calling the procedure `LS` twice, the overall computational complexity of `UM` (Algorithm 9) is $O(\frac{1}{\epsilon}N^3 \log N)$, which is polynomial in N.

□

Chapter 6

MONITORING CHANNEL ACCESS TIME FAIRNESS FOR WI-FI/LTE-U COEXISTENCE

In this previous chapter, we studied the problem of SAS-assisted dynamic channel assignment in the 3.5 GHz CBRS band. We proposed novel graph representation to capture channel availability and contiguity constraints as well as the coexistence opportunities. We further proposed channel assignment algorithms and showed that they outperform the baseline mechanisms through extensive simulations.

In this chapter, we look at another resource allocation problem, that is, channel access time fairness among different radio access technologies in shared bands. As discussed in previous chapters, unlicensed devices and networks operating in shared bands usually have equal spectrum access priorities and are expected to coexist in the same frequency, time, and space. It is widely believed that Wi-Fi and LTE are among the most dominant technologies that will be deployed in shared bands in the next few years, which have different channel access mechanisms. With CSMA/CA, each Wi-Fi device senses the medium and allows others to finish transmission before attempting its own transmission. In contrast, LTE transmits continuously without sensing, as it traditionally operates exclusively in bands owned by operators. As a result, LTE would block Wi-Fi transmissions during coexistence, resulting in degraded Wi-Fi performance [35].

In order to achieve time-division-multiplexing based coexistence with Wi-Fi, two types of LTE have been proposed for unlicensed operations: LAA and LTE Unlicensed (LTE-U). The former employs LBT, while the latter is duty-cycle based and proposed for supplementary downlink. LTE-U exploits existing LTE functionality (almost blank subframes [40]) to create alternating ON/OFF periods so as to accommodate Wi-Fi transmissions. In this work, we

are interested in LTE-U that is intended for earlier commercialization in markets where regulations do not require LBT, such as China, Korea, India and the USA.

Wi-Fi/LTE-U coexistence has drawn growing attention from different aspects [33,39,40], and one important consideration is *fairness*. Since both are time-division-multiplexing based, one natural criterion is fair sharing in channel access time, i.e., fraction of LTE-U ON duration in each cycle (aka. duty cycle, a quantity between 0 and 1) should not be more than a limit. For example, when coexisting with a Wi-Fi network, the LTE-U AP[1] should not transmit for more than 50% of the time. In fact, this criterion has already been adopted by the LTE-U Forum as part of the coexistence specifications [38].

Although many researchers have studied LTE-U duty cycle adaptation design for fair sharing (e.g. [37,41,42]), a concerning fact has often been neglected: Wi-Fi nodes, as benign users, can only access the channel during LTE-U OFF time, while ON/OFF time is under unilateral control of LTE-U APs that are considered as new entrants to the unlicensed spectrum. Therefore, LTE-U APs, as self-interested users, will have incentives to *misbehave*, that is, transmitting with a larger duty cycle that exceeds the limit, so as to gain a greater share in channel access time and throughput. This is a realistic concern (from Wi-Fi operators and users), especially when LTE-U operators are not likely to disclose details of their proprietary duty cycle adaptation algorithms. Such concern persists, unless a proper fairness monitoring scheme is in place to enforce the coexistence specifications defined by the LTE-U Forum, and this need has also been acknowledged in [135].

In this work, we propose monitoring of Wi-Fi/LTE-U channel access time fairness as a responsibility the spectrum manager (e.g., DBA in TVWS and SAS in CBRS). Specifically, the spectrum manager assigns a reasonable duty cycle limit to a LTE-U AP, and estimates its duty cycle to see if it exceeds the assigned limit. For the above purpose, an energy detector may be deployed to measure the total ON duration and subtract the portion due to Wi-Fi activities (e.g., by detecting Wi-Fi preambles). In fact, such energy detector is already

[1]Throughput the paper, LTE-U eNB (Evolved Node B) is referred to as access point (AP) for the purpose of convenience.

available at each Wi-Fi device, which is able to measure ON duration with 1 μs granularity. It means that the spectrum manager can collect PHY layer observations from a Wi-Fi AP close to the target LTE-U AP and estimate its duty cycle to detect possible misbehavior. We make the following specific contributions:

- We consider coexistence between a LTE-U network and a Wi-Fi network and propose a scheme that allows the spectrum manager to estimate the LTE-U duty cycle in a cycle period based on observed busy periods from a local Wi-Fi AP without interrupting normal operations of the Wi-Fi network.

- We propose a thresolding scheme for misbehavior detection. We analyze its detection performance in terms of detection probability P_d and false alarm probability P_{fa}. Our analysis shows that smaller Wi-Fi packets and a larger LTE-U cycle period would improve P_d and reduce P_{fa}.

- We implement the proposed schemes in `ns3` [136] and evaluate their performance with extensive experiments. Our results show that for a typical LTE-U cycle period of 160ms with a 2ms idle gap every 20ms ON duration [37], the estimation error is within $\pm 1\%$ of the true duty cycle. Besides, the proposed scheme detects misbehavior with a duty cycle that is 2.8% larger than the limit with P_d at least 95% and P_{fa} less than or equal to 1%.

The remainder of this chapter is organized as follows. In Section 6.1, a brief review of related work is provided. Sections 6.2 and 6.3 present the system model and the proposed fairness monitoring schemes, respectively. Evaluation results are provided in Section 6.4 and this study is concluded in Section 6.6.

6.1 Related Work

Wi-Fi and LTE-U coexistence is being actively studied in the recent years. In [40], Almeida *et al.* implemented LTE-U duty cycles by modifying the almost blank subframe functionality.

Such duty cycle can be static as in [137], or adaptive as in Carrier Sensing Adaptive Transmission (CSAT), which was proposed by Qualcomm [37]. It allows a LTE-U AP to sense and measure medium utilization during OFF time, and adjust duty cycles accordingly. In [138], Cano *et al.* proposed a duty-cycle mechanism to achieve proportional fairness among LTE-U and WiFi, by selecting an appropriate probability to access the channel and transmission duration. Other techniques include Q-learning [41] and the multi-armed bandit approach [42], which dynamically adjust duty cycles based on channel usage.

In reality, duty cycle adaptation schemes are most likely to be proprietary, and their details would not be revealed by LTE-U operators. Therefore, without a proper duty cycle estimation and misbehavior detection scheme, fair sharing between Wi-Fi and LTE-U can only be at the mercy of LTE-U operators. In this work, we propose a scheme that allows the spectrum manager to estimate LTE-U duty cycle, and detects possible misbehavior.

6.2 System Model

In this section, we provide brief background on Wi-Fi and describe the duty cycled LTE-U model. We then formally define channel access time fairness and present our fairness monitoring architecture.

6.2.1 Wi-Fi Basics

The Wi-Fi standard [31] employs CSMA/CA that implements the Distributed Coordination Function (DCF) – a distributed slotted medium access scheme with an exponential back-off. In DCF, each node attempting to transmit must ensure the medium has been idle for a DIFS (DCF Interframe Spacing) period (i.e., 34μs). Then it selects a back-off (BO) counter uniformly at random from $[0, CW - 1]$, where CW is the contention window with an initial value of $CW_{\min}$. Each failed transmission doubles CW, up to $CW_{\max}$, and each successful transmission resets CW to $CW_{\min}$. After a DIFS idle period, the counter is reduced by one every BO slot (i.e., 9μs), if no other transmissions are detected during the countdown. Otherwise, the counter is frozen until the medium is once again idle for a DIFS period.

Each Wi-Fi node performs Clear Channel Assessment (CCA) to determine if medium is idle or busy. It has two functions:

- *Carrier sense* (CS): The ability to detect the preamble of a valid Wi-Fi transmission at a signal level equal to or greater than −82dBm/20MHz.

- *Energy detection* (ED): The ability to detect the energy of non-Wi-Fi transmissions (or Wi-Fi transmissions with missed preamble) at a signal level equal to or greater than −62dBm/20MHz.

A typical CSMA/CA access cycle is shown in Figure 6.1. When a packet is successfully received, the intended receiver will transmit an acknowledgement (ACK) after a SIFS (Short Interframe Space) period (i.e., 16μs).

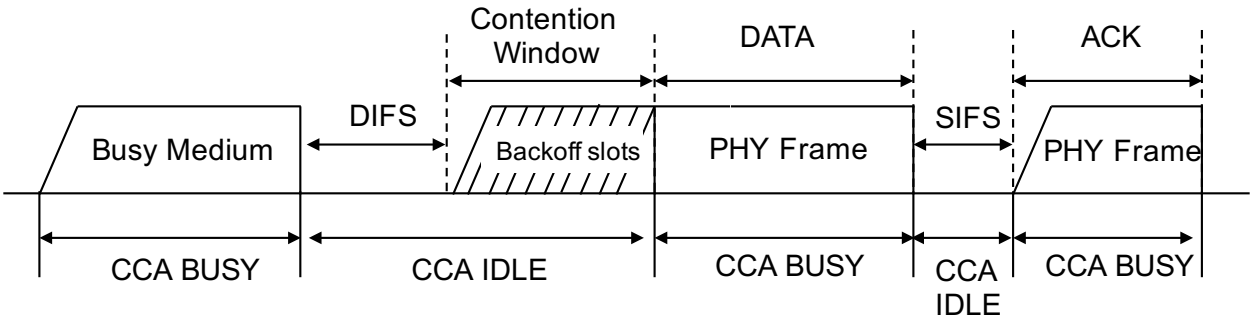

Figure 6.1: Typical CSMA/CA access cycle.

6.2.2 Duty Cycled LTE-U

Figure 6.2 illustrates the duty cycling behavior of a LTE-U AP as in CSAT [37]. It operates in the shared channel with a period of T (ms), ranging from 10s to 100s of ms (typical values are 80ms and 160ms, or as large as 640ms [37]). In each cycle, it transmits (i.e., ON) for a fraction of time $\alpha \in (0, 1)$, i.e., *duty cycle*, and stays OFF in the remaining time.

To protect Wi-Fi flush delay-sensitive data, frequent idle gaps (of few msec) are introduced in ON duration [37] such that the maximum *continuous* ON duration is no greater than a limit (e.g., 20ms) [38]. We assume that the minimum continuous ON time is larger than the maximum transmission time of Wi-Fi packets.

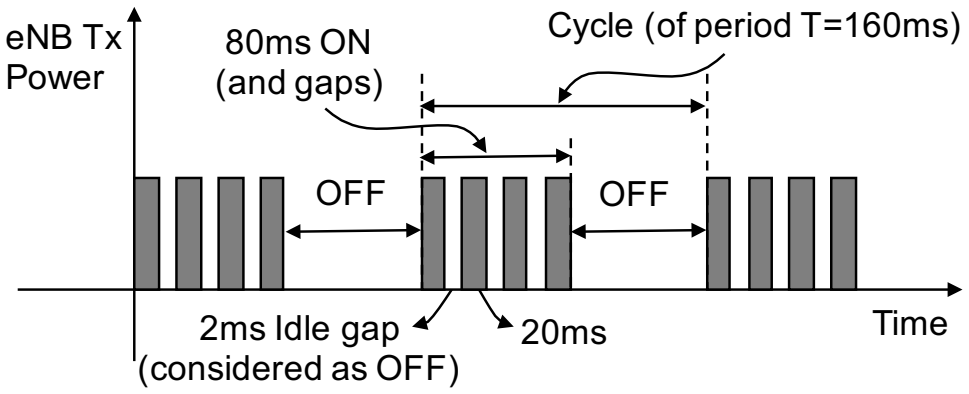

Figure 6.2: Example of duty cycled LTE-U with a cycle of 160ms and a duty cycle of 0.5 (i.e., 80/80ms ON/OFF). Idle gaps are introduced every 20ms ON duration.

6.2.3 Fairness in Channel Access Time

In this work, we are interested in fair sharing of channel access time between one LTE-U cell[2] and one Wi-Fi network that share one 20MHz channel. We assume that Wi-Fi nodes are interfered by the LTE-U AP (i.e., received LTE-U interference at each Wi-Fi node exceeds the CCA-ED threshold), and they are within each other's CS range. It is important to note that multiple Wi-Fi networks that are overlapping or in close range can be considered as a single larger network if we assume that no hidden nodes exist[3]. In this case, Wi-Fi nodes

[2]When multiple LTE-U cells are present, they may coordinate and transmit in different portions of the same cycle. For instance, with two LTE-U cells A and B, A only transmits in the first half of the cycle, while B only transmits in the second half. If so, LTE-U cells can be monitored separately.

[3]The impact of hidden Wi-Fi nodes is deterred for future work.

will sense LTE-U interference and deter their transmissions until LTE-U ON time is over; during OFF time, they will contend for the next transmission opportunity.

Given a cycle of period T, define ON_i as the i-th *continuous* ON duration, where $1 \leq i \leq n$. According to the coexistence specifications proposed by the LTE-U Forum [38], it is required that the duty cycle be less than or equal to a limit $\alpha_{\max}$, i.e.,

$$\alpha = \frac{1}{T} \sum_{i=1}^{n} ON_i \leq \alpha_{\max} \in (0, 1). \tag{6.1}$$

For instance, if a LTE-U cell is coexisting with a Wi-Fi network, $\alpha_{\max}$ may be set to 50%; with two Wi-Fi networks, $\alpha_{\max}$ may be set to 33% instead.

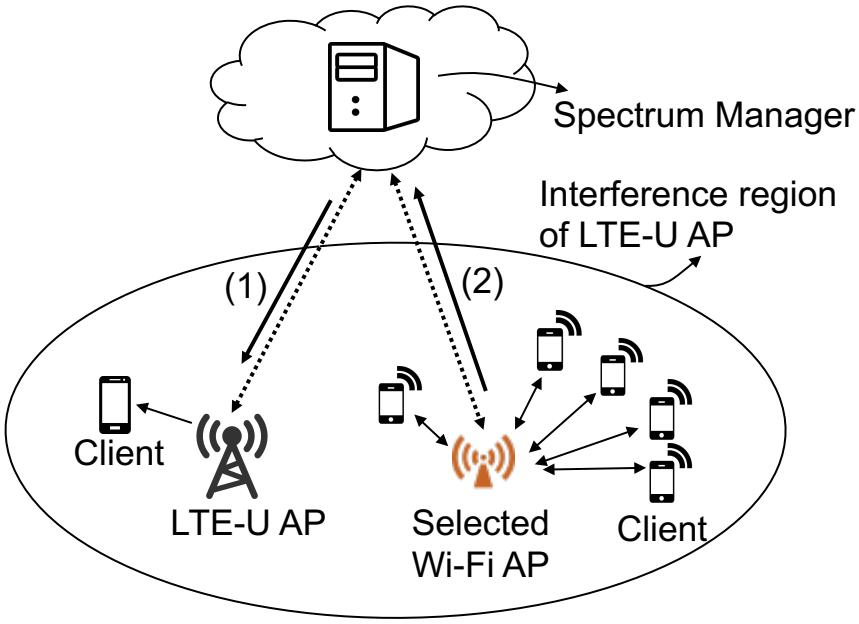

Figure 6.3: Co-channel deployment of a LTE-U cell and a Wi-Fi network. (1) The spectrum manager determines a reasonable duty cycle limit for the LTE-U AP. (2) Then it gathers PHY layer observations from a nearby Wi-Fi AP, so as to estimate the duty cycle of the LTE-U AP and detect any misbehavior.

6.2.4 Fairness Monitoring

In shared bands (e.g., TVWS and CBRS bands), there exists a spectrum manager that manages infrastructure-based LTE-U and Wi-Fi networks (Figure 6.3). Every AP is required to first register with the spectrum manager and obtain permission to operate. Moreover, they need to follow any instructions (like power/channel assignments) from the spectrum manager. Therefore, it is natural to propose fairness monitoring as part of the spectrum manager's extended functionality and responsibility.

The fairness monitoring procedure is as follows. First, the spectrum manager assigns a reasonable duty cycle limit to a LTE-U AP based on the current channel usage, which would serve as input to the duty cycle adaptation algorithm. Then the spectrum manager collects information from a local Wi-Fi AP for duty cycle estimation without interrupting its normal network operations. If it is decided that the LTE-U AP is misbehaving (i.e., violating the rule in Eq. (6.1)), it will be punished accordingly (e.g., temporary suspension)[4].

We assume that the selected Wi-Fi AP can be configured to always physically senses the medium (regardless of RTS/CTS messages sent by other nodes), and it tries to receive every Wi-Fi packet during the monitoring process. We also assume that it reports requested information honestly; robust duty cycle estimation against possible misreporting is left as future work. The start time and period of LTE-U cycles are honestly reported by LTE-U APs to the spectrum manager, since they have no incentives to misreport. But the actual duty cycle in each cycle is not reported due to signaling overhead, or can be easily misreported to avoid punishment.

6.3 Duty Cycle Estimation and Misbehavir Detection

In this section, we discuss the information collected by the selected Wi-Fi AP, and present our duty cycle estimation and misbehavior detection schemes.

---

[4]Designing an appropriate punishment scheme is out of the scope of this paper and left as future work.

6.3.1 PHY Layer Observations

We first discuss what a Wi-Fi AP (as the observer node) that is interfered by the target LTE-U AP would observe at the PHY layer. As shown in Figure 6.1, normal Wi-Fi operations are characterized by frequent idle periods (e.g., SIFS, DIFS and BO periods), which can only be seen during LTE-U OFF time. On the other hand, ON time will cause the observer node to detect busy medium for duration longer than any normal Wi-Fi packets. By physically sensing the medium, the observer node can easily observe idle/busy periods, which will be useful for duty cycle estimation.

Now let us take a closer look at the PHY layer state machine of the observer node. For duty cycle estimation, we are mainly interested in four PHY states: IDLE, CCA_BUSY, TX_BUSY and RX_BUSY, as shown in Figure 6.4. Transitions between the four states are triggered by medium busy/idle events as well as Tx/Rx events, and indicated by primitives that are already available at the MAC layer as per the Wi-Fi standard.

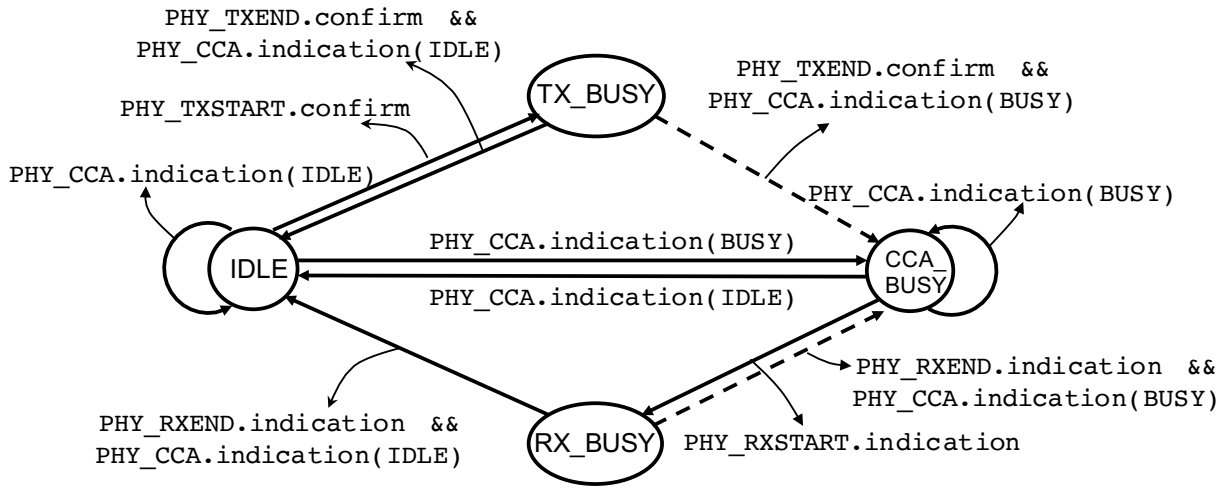

Figure 6.4: Wi-Fi PHY layer state machine. Transitions in dashed arrows are mainly caused by LTE-U transmissions.

Consider an observer node in IDLE. When it starts transmission, the `PHY_TXSTART.confirm`

primitive is issued, and it enters TX_BUSY; the end of transmission is indicated by `PHY_TXEND.confirm`. If other node transmits, the medium will become busy, and the `PHY_CCA.indication(BUSY)` primitive will be issued. The observer node will go to CCA_BUSY, looking for valid Wi-Fi preambles. If a valid Wi-Fi preamble and header are received, `PHY_RXSTART.indication` is issued, and the observer node goes to RX_BUSY. It stays there till the end of predicted duration (indicated by `PHY_RXEND.indication`). If the preamble or header is missed, it stays in CCA_BUSY for a period equal to the Wi-Fi packet transmission duration. Under normal conditions, the observer node is expected to return to IDLE after transmission or reception of a Wi-Fi packet. Note that it is possible that two Wi-Fi packets collide, and the node (i.e., the observer node) transmitting a shorter packet detects busy medium (CCA_BUSY) immediately after transmission (TX_BUSY). But this rare case can be ignored safely.

Since a LTE-U AP may transmit anytime without notifying Wi-Fi nodes, the PHY layer state machine is impacted in the following way. If ON time starts when the medium is idle, the observer node will immediately transit from IDLE to CCA_BUSY, and stay there till the end of ON time, since no Wi-Fi preamble or header will be received. If ON time starts during TX_BUSY or RX_BUSY, the observer node operates as usual, since it cannot immediately detect the presence of LTE signals. But it enters CCA_BUSY instead of IDLE after Tx/Rx is over, since ON time is longer than a Wi-Fi packet.

As we can see, the observer node can indeed observe idle ($\mathcal{I}$) and busy ($\mathcal{B}$) periods that appear alternately very easily, as well as Tx/Rx duration, by keeping track of related primitives available at the MAC layer. Although the time spent in the three busy states (i.e., CCA_BUSY, TX_BUSY and RX_BUSY) is counted towards busy periods, a busy period will be labeled differently with $\mathcal{B}_{tx}$ or $\mathcal{B}_{rx}$, if TX_BUSY or RX_BUSY is visited.

In practice, when a Wi-Fi AP receives a monitoring request from the spectrum manager, it starts recording observed busy periods for the requested time window chronologically. Let the i-th observed busy period be $(t_i, label_i, d_i, d_i')$, where t_i is the start time, $label_i \in \{\mathcal{B}, \mathcal{B}_{tx}, \mathcal{B}_{rx}\}$ is the label, d_i is the duration of that busy period, and d_i' is the time spent in TX_BUSY or RX_BUSY, if $label_i = \mathcal{B}_{tx}$ or $\mathcal{B}_{rx}$ (otherwise 0). Note that in each busy period, either

TX_BUSY or RX_BUSY may be visited at most once, since it is not possible for a Wi-Fi node to transit directly from TX_BUSY to RX_BUSY (or vice versa) without visiting IDLE. Finally, this Wi-Fi AP reports observed busy periods to the spectrum manager for duty cycle estimation.

6.3.2 Duty Cycle Estimation

Since the spectrum manager knows the start time and period of LTE-U cycles, it can focus on duty cycle estimation for each individual cycle of period T. Although a busy period may be caused by either Wi-Fi or LTE-U transmissions, an *abnormal* busy period with duration that is much longer than a Wi-Fi packet must contain a continuous LTE-U ON period. In fact, it may also contain a portion of a Wi-Fi packet (Figure 6.5), due to LTE-U/Wi-Fi collision.

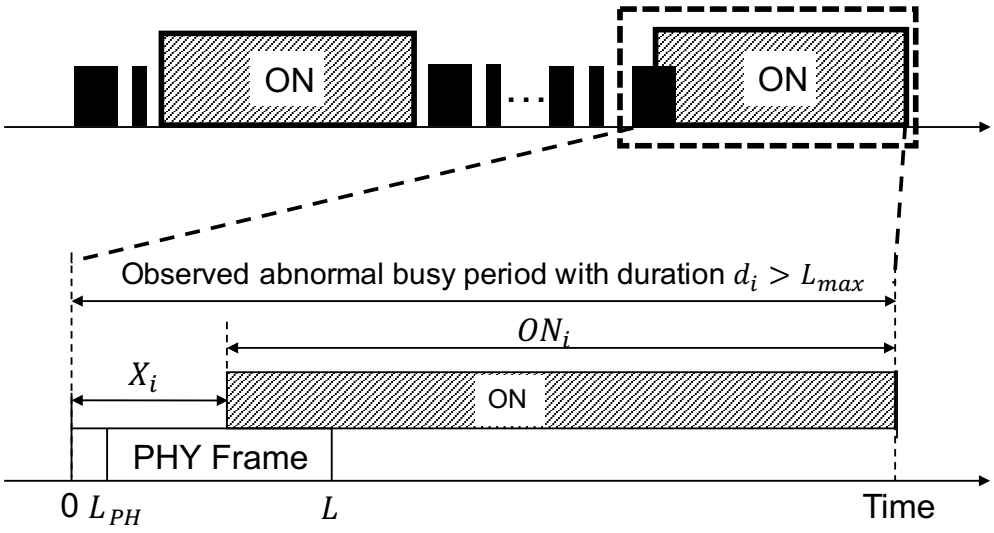

Figure 6.5: In addition to a continuous LTE-U ON period, an abnormal busy period may contain a portion of a Wi-Fi packet due to collision.

Denote the set of abnormal busy periods in a cycle as $S' = \{(t_i, label_i, d_i, d_i') : label_i \in \{\mathcal{B}, \mathcal{B}_{tx}, \mathcal{B}_{rx}\}, d_i > L_{\max}\}$, where $|S'| = m$ and $L_{\max}$ is the maximum transmission duration

of Wi-Fi packets. For convenience, elements in S' are relabeled from 1 to m. As mentioned earlier, LTE-U ON time may or may not overlap with an ongoing Wi-Fi transmission (Fig. 6.5). If the LTE-U AP starts transmission before any Wi-Fi node transmits during an idle period, the observer node will sense the medium to be busy and back off. In this case, the observed abnormal busy period contains only CCA_BUSY duration[5], which is equal to the ON duration. In other words, we have $ON_i = d_i$, if $label_i = \mathcal{B}$.

However, if ON time starts during an ongoing Wi-Fi transmission, then the observed abnormal busy period includes a portion of the Wi-Fi packet at the beginning, followed by an ON period. There exist two cases here. In the first case, the observer node is currently transmitting a packet of duration L. In the second case, the observer node has detected a valid Wi-Fi preamble and header (of length L_{PH}), and is currently receiving the payload of predicted duration $(L - L_{PH})$ (which can be inferred from the LENGTH field in the header). In both cases, it will stay in TX_BUSY or RX_BUSY for duration L before going to CCA_BUSY.

Denote the portion of the Wi-Fi packet that is not overlapping with the ON period as X_i. We can see that

$$ON_i = d_i - X_i,$$

where $X_i \in [0, L]$ if $label_i = \mathcal{B}_{tx}$, and $X_i \in [L_{PH}, L]$ if $label_i = \mathcal{B}_{rx}$. Due to lack of information about X_i, we model it as a uniform random variable when $label_i$ is $\mathcal{B}_{tx}$ or $\mathcal{B}_{rx}$. Then we have

$$ON_i \sim \begin{cases} d_i, & \text{if } label_i = \mathcal{B} \\ Unif[d_i - L, d_i], & \text{if } label_i = \mathcal{B}_{tx} \\ Unif[d_i - L, d_i - L_{PH}], & \text{if } label_i = \mathcal{B}_{rx}, \end{cases}$$

where $L = d'$ in our model. It is reasonable to assume that $\{X_i\}$ are independent of each

[5]Note that it is possible that the ON period overlaps with the Wi-Fi preamble and header, or with two Wi-Fi packets that happen to collide, in which case RX_BUSY is not visited, and the observer node stays in CCA_BUSY. In the first case, we still have $ON_i \approx d_i$, since the Wi-Fi preamble and header length (in 10s of μs) is much smaller than the ON period (in 10s of ms). We intentionally ignore the second case, since the probability is small (especially when RTS/CTS is enabled).

other. The spectrum manager adopts the following estimator for ON_i,

$$\hat{ON}_i = \begin{cases} d_i, & \text{if } label_i = \mathcal{B} \\ d_i - \frac{1}{2}d'_i, & \text{if } label_i = \mathcal{B}_{tx} \\ d_i - \frac{1}{2}(d'_i + L_{PH}), & \text{if } label_i = \mathcal{B}_{rx} \end{cases},$$

and $\mathbb{E}[\hat{ON}_i] = ON_i$, which means that $\hat{ON}_i$ is an unbiased estimator. The spectrum manager estimates the duty cycle $\hat{\alpha}$ as follows,

$$\hat{\alpha} = \frac{1}{T}\sum_{i=1}^{m} \hat{ON}_i,$$

which is also an unbiased estimator, since $\mathbb{E}[\hat{\alpha}] = \alpha$.

Note that although in practical LTE systems, one subframe of 1ms duration is usually the minimum time unit for resource allocation, we do not make this assumption, and stay with the general case. Nevertheless, such knowledge can potentially increase estimation accuracy, and our logic is still applicable to this special case.

6.3.3 Misbehavior Detection

After obtaining $\hat{\alpha}$, the spectrum manager needs to determine whether the LTE-U AP violates the rule in Eq. (6.1). The detection scheme is as follows,

$$Result = \begin{cases} \text{Violated}, & \text{if } \hat{\alpha} > (1+\gamma)\alpha_{\max} \\ \text{Not violated}, & \text{Otherwise} \end{cases},$$

where $\gamma \geq 0$ is a parameter set by the spectrum manager.

Its performance is measured by *probability of detection* P_d and *probability of false alarm* P_{fa}, i.e.,

$$P_d(\alpha, \gamma) = \Pr(\hat{\alpha} > (1+\gamma)\alpha_{\max} | \alpha > \alpha_{\max})$$
$$P_{fa}(\alpha, \gamma) = \Pr(\hat{\alpha} > (1+\gamma)\alpha_{\max} | \alpha \leq \alpha_{\max}).$$

To understand P_d and P_{fa}, we consider the example in Figure 6.2, in which the LTE-U AP transmits continuously for $ON_{\max}$ of 20 ms and pauses for a short period of 2 ms, before transmitting again for another duration equal to (or less than) $ON_{\max}$. We set $\alpha_{\max}$ to 0.5. We consider the worst case that each ON period overlaps with a Wi-Fi packet of length $L_{\max}$, and ignore L_{PH} when $label_i = \mathcal{B}_{rx}$ for simplicity. Then we have

$$\begin{aligned}\hat{\alpha} &= \frac{1}{T}\sum_{i=1}^{m}\left(d_i - \frac{1}{2}L_{\max}\right) = \frac{1}{T}\sum_{i=1}^{m}\left(ON_i + X_i - \frac{1}{2}L_{\max}\right) \\ &= \alpha + \frac{1}{T}\left(\sum_{i=1}^{m} X_i - \frac{1}{2}mL_{\max}\right),\end{aligned}$$

where $X_i \in Unif[0, L_{\max}]$ and $m = \lceil \frac{\alpha T}{ON_{\max}} \rceil$.

Define $X_i' = \frac{X_i}{L_{\max}} \in Unif[0,1]$. Then the sum of m i.i.d. random variables $Y = \sum_{i=1}^{m} X_i'$ follows the Irwin-Hall (or uniform sum) distribution, that is,

$$F_Y(y) = \Pr(Y \le y) = \frac{1}{m!}\sum_{k=0}^{\lfloor y \rfloor}(-1)^k \binom{m}{k}(y-k)^m, \tag{6.2}$$

and it has a mean of $\frac{m}{2}$ and a variance of $\frac{m}{12}$. When m is large, the distribution of Y can be well approximated by a Gaussian distribution $N(\frac{m}{2}, \frac{m}{12})$. But m may be small in our case, and we will use Eq. (6.2). Then the probability of $\hat{\alpha} > (1+\gamma)\alpha_{\max}$ is given by

$$\begin{aligned}\Pr\left\{\hat{\alpha} > (1+\gamma)\alpha_{\max}\right\} &= \Pr\{\alpha + \frac{L_{\max}}{T}\left(Y - \frac{m}{2}\right) > (1+\gamma)\alpha_{\max}\} \\ &= 1 - F_Y\left(\frac{m}{2} + \frac{T}{L_{\max}}[(1+\gamma)\alpha_{\max} - \alpha]\right).\end{aligned} \tag{6.3}$$

Note that if the true duty cycle α is greater than $\alpha_{\max}$, the probability in Eq. (6.3) is P_d; otherwise, it becomes P_{fa}. For instance, with $L_{\max} = 0.5$ ms, $T = 160$ ms and $\gamma = 0$ (i.e., the black curve in Figure 6.6), if the LTE-U AP transmits with a duty cycle of 0.498, the probability of mistakenly identifying that AP as misbehaving is 14.0%. If $\alpha = 0.502$, the probability of correctly detecting that misbehaving user is 83.4%.

Next we study the impact of γ, $L_{\max}$ and T on Eq. (6.3). In Figure 6.6, the setting with $L_{\max} = 0.5$ ms, $T = 160$ ms and $\gamma = 0$ is considered as the baseline. When γ is increased

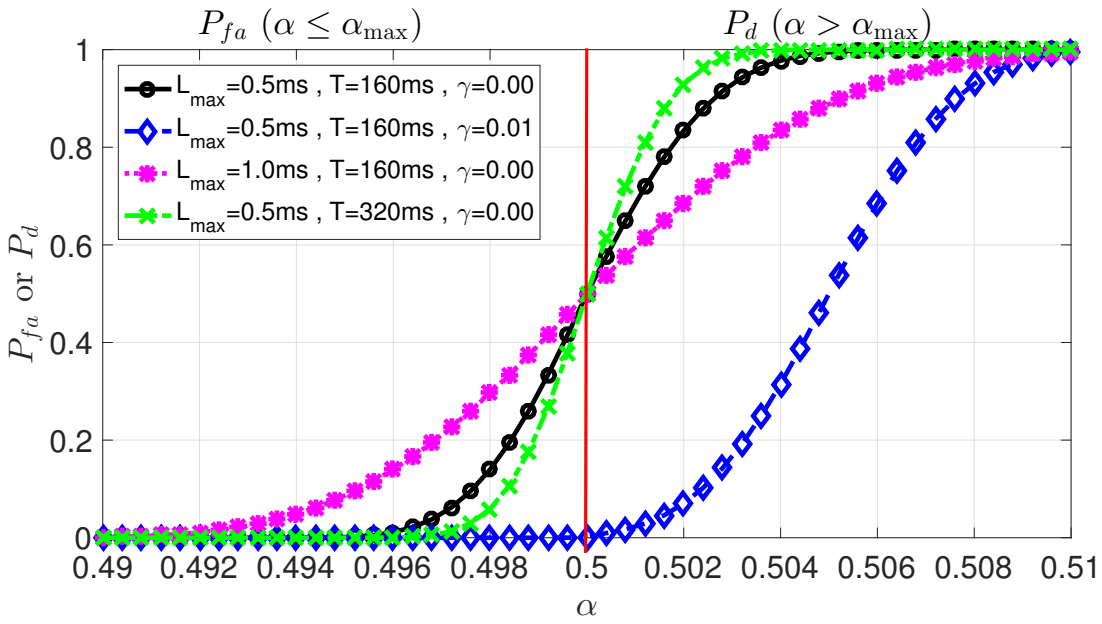

Figure 6.6: P_d and P_{fa} as function of α with different values of γ, $L_{\max}$ and T, where $\alpha_{\max} = 0.5$. We observe that increasing λ shifts the curve (in black) to the right (the one in blue), which implies a trade-off between P_d and P_{fa}. We also observe that increasing L_{max} adversely affects the detection performance, i.e., reducing P_d and increasing P_{fa}, while increasing T can improve the detector performance (for a given true α).

to 0.01, the curve is shifted to the right, which implies smaller P_{fa} for any $\alpha \leq \alpha_{\max}$ but also smaller P_d for any $\alpha > \alpha_{\max}$. Hence, it implies a tradeoff between P_d and P_{fa} when adjusting γ.

Then we increase $L_{\max}$ to 1.0 ms while keeping other parameters the same with the baseline. We can see an increase in P_{fa} and a decrease in P_d, which means that larger Wi-Fi packets will adversely impact the detection performance of the proposed scheme. In contrast, when T is increased to 320 ms, the overall detection performance is better, i.e., smaller P_{fa} and larger P_d.

6.4 Evaluation

In this section, we evaluate the proposed duty cycle estimation and misbehavior detection schemes.

6.4.1 Simulation Setup

We implement and evaluate the proposed schemes in `ns3` [136], a widely used network simulator. We consider the coc-channel coexistence of a LTE-U cell and a Wi-Fi network that consists of an AP and 20 clients, all of which are located close to each other. Simulation parameters are provided in Table 6.1.

Each Wi-Fi node has a full outgoing buffer of 1000-byte UDP packets. By adjusting the A-MSDU threshold (for all Wi-Fi nodes), variable maximum transmission duration of Wi-Fi (data) packets is obtained. An adaptive but idealized, feed-back Wi-Fi rate control is used, where adjustments are made immediately upon feedback from the peer. PHY layer state information is obtained by tracing the PHY state machine of the Wi-Fi AP.

Table 6.1: Simulation parameters

Parameter	Value
Wi-Fi standard	802.11n (Mixed Format)
Channel	20 MHz (5170-5190 MHz)
Wi-Fi AP/client Tx power	24/18 dBm
CCA-CS/ED threshold	-82/-62 dBm
Traffic model	Full buffer UDP
RTS/CTS	Disabled
Frame aggregation	A-MSDU enabled
Min./max. continuous ON period	6/20 ms [38]
Idle gaps between ON periods	2 ms
LTE-U cycle period (T)	80-480 ms
Max. Wi-Fi packet duration ($L_{\max}$)	300-1100 μs
Max. duty cycle ($\alpha_{\max}$)	0.5

Since LTE-U performance (e.g., throughput) is not our concern in this work, we implement the LTE-U AP as a non-communicating device that switches on or off. We consider the typical duty cycling pattern in Figure 6.2, in which the LTE-U AP transmits continuously for 20 ms and pauses for 2 ms before transmitting for another 20 ms (or less) [37]. Although the transmission duration a Wi-Fi packet can be up to 3ms, it makes little sense for Wi-Fi data packets to be much larger than 1ms when coexisting with LTE-U, since the idle gap is only 2ms. Consistent with [38], we set $\alpha_{\max}$ to 0.5.

6.4.2 Duty Cycle Estimation

In this experiment, we evaluate the proposed duty cycle estimation scheme. We first set $\alpha = 0.5$, $L_{\max} \approx 1100$ μs, and vary T from 80 ms to 480 ms. Each experiment is repeated 100 times for each setting, and results are shown in Figure 6.7(a). As we can see, the median of $\hat{\alpha}$ is very close to α for different T values. As T increases, the deviation of $\hat{\alpha}$ is smaller, and the estimation is more accurate. In all cases, $\hat{\alpha}$ is within $\pm 1\%$ of α.

Then we fix T to 160 μs and vary $L_{\max}$ from 300 μs to 1100 μs. Results from 100 experiments are shown in Figure 6.7(b). We observe that $\hat{\alpha}$ is less accurate as $L_{\max}$ increases, but $\hat{\alpha}$ is still within $\pm 1\%$ of the true duty cycle. In practice, smaller Wi-Fi packets would help estimate α more accurately, but could potentially decrease Wi-Fi throughput due to PHY and MAC overhead.

6.4.3 Detection Performance

In this experiment, we evaluate the proposed misbehavior detection scheme in terms of P_d and P_{fa} with different choices of γ values. We consider a typical cycle period of 160 ms [37], and set $\alpha_{\max}$ to 0.5, $L_{\max}$ to 1100 ms. The true α is varied from 0.49 and 0.52. For each α value, the experiment is repeated 200 times. Results are shown in Figure 6.8.

As we can see, with $\gamma = 0$, P_{fa} is as high as 45% when $\alpha = 0.5$, which is undesirable in practice. By setting γ to 0.01 or 0.014, the spectrum manager can keep P_{fa} under 5% or 1%, but it also leads to a smaller P_d for each $\alpha > \alpha_{\max}$. If the LTE-U AP transmits with

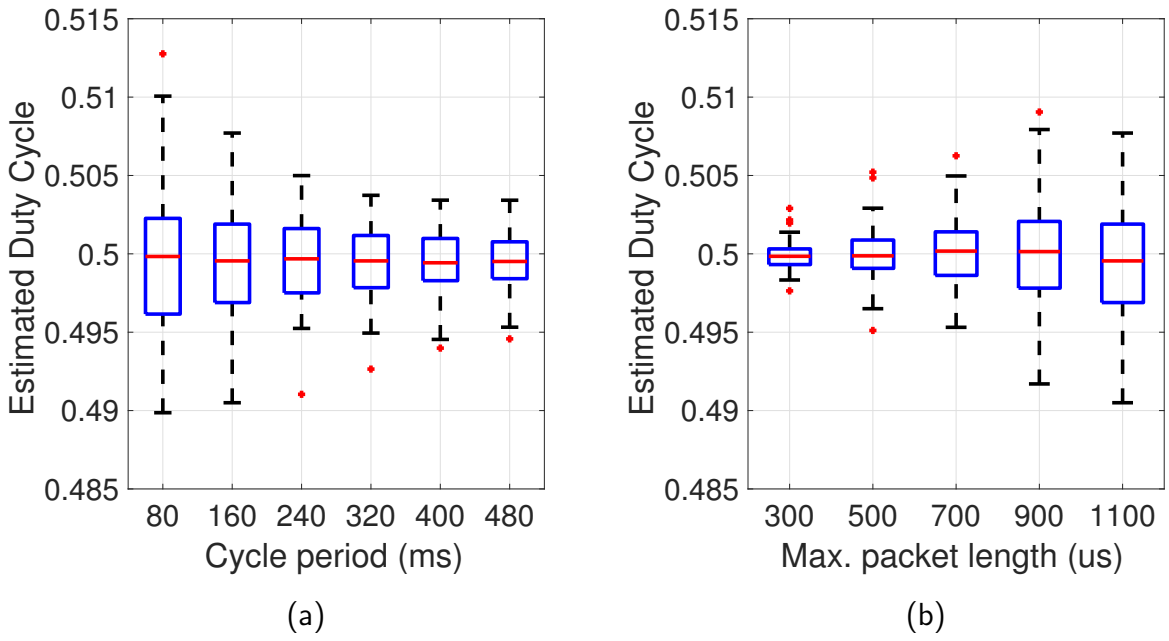

Figure 6.7: Box plot of estimated duty cycle. (a) Impact of T ($L_{\max} = 1100$ μs). (b) Impact of $L_{\max}$ ($T = 160$ μs). We observe that a larger cycle period and a smaller packet length can improve the estimation performance and $\hat{\alpha}$ is within $\pm 1\%$ of α in all cases.

a duty cycle higher than 0.514, that is, 2.8% deviation from $\alpha_{\max}$, the proposed detection scheme with $\gamma = 0.014$ can detect such misbehavior with a probability higher than 95% while keeping P_{fa} less than or equal to 1%.

6.5 Discussion

In this section, we discuss the current status of the LTE-U forum and limitations of this work.

6.5.1 Current Status of LTE-U Forum

LTE-U was proposed in 2013 by Qualcomm and Ericsson and relies on 3GPP Release 10-12 functionality, with specifications defined by the LTE-U Forum, an organization established

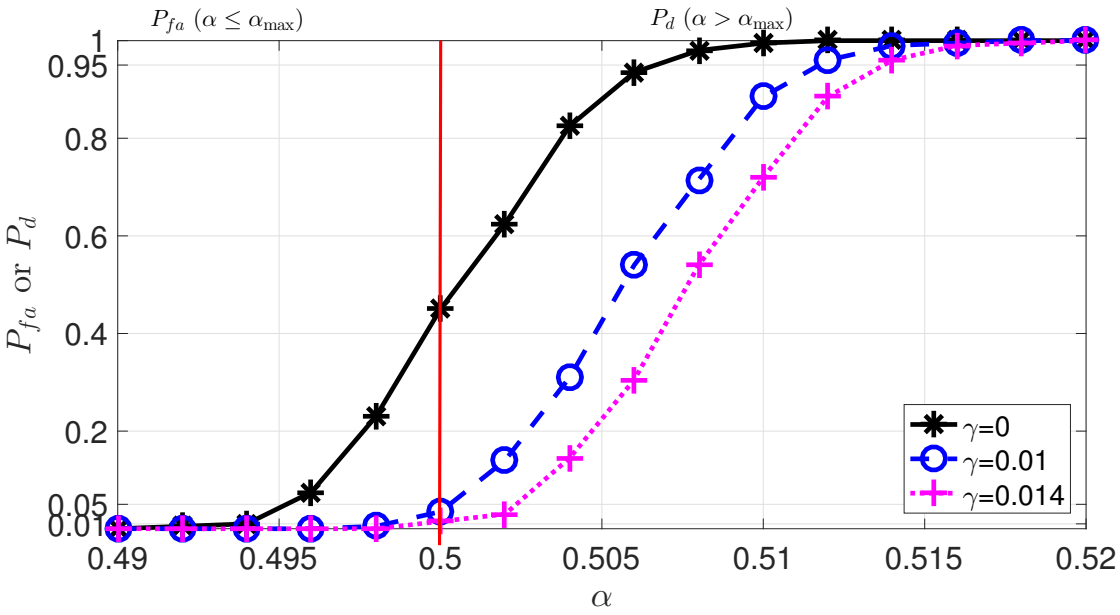

Figure 6.8: Performance of detecting duty cycling misbehavior with different γ values, where $\alpha_{\max} = 0.5$. Note that $\gamma = 0$ is the baseline (in black curve), and the other two γ values are chosen such that P_{fa} is less than 5% (in dashed blue curve) and 1% (in dashed pink curve).

by Verizon in collaboration with Alcatel-Lucent, Ericsson, LG Electronics, Qualcomm Technologies, Inc., and the Sumsung. Since the proposal of LTE-U, it has been considered as a threat by the Wi-Fi and cable industries in unlicensed spectrum. In late February of 2017, Verizon and T-Mobile announced plans to deploy LTE-U after the FCC certified the first LTE-U devices in the 5 GHz band [139], and T-Mobile launched LTE-U service in six cities in June [140]. But later in November 2017, Verizon confirmed shift to LTE-LAA over LTE-U [141]. As of now, the LTE-U Forum seems to have been disbanded, and interest in LTE-U mainly comes from the academia.

6.5.2 Limitations

There are several limitations of this work. First, we assumed that the PHY layer observations are available at a Wi-Fi node, but such PHY layer information from hardware chip may not be exposed in practice. As an alternative, passive spectrum sensors can be deployed that measure the medium occupancy based on energy detection.

Second, we made an asymmetric assumption that all Wi-Fi nodes are honest in reporting the requested information, which may not hold in practice. If the spectrum manager deploys sensors to monitor LTE-U activities, then the proposed scheme would still work. On the other hand, if the spectrum manager collects data from Wi-Fi nodes via crowdsensing, it is more reasonable to assume that the majority of Wi-Fi nodes are honest, if not all, and the current scheme needs to extended to allow the spectrum manager to cross-validate the duty cycles estimated from measurements provided by different nodes.

Third, if multiple LTE-U networks are present and coordinated to transmit at different time portions, the proposed scheme would work by associating observed LTE-U ON periods with different LTE-U networks. If multiple LTE-U networks do transmit asynchronously, they are likely to be located with a distance from each other (or otherwise there will be significant interference and throughput degradation). In this case, the spectrum manager may collect measurements from multiple spatially distributed Wi-Fi nodes and identify any Wi-Fi AP that experiences interference from a single LTE-U AP.

6.6 Conclusion

In this paper, we proposed a scheme that allows the spectrum manager to estimate LTE-U duty cycle via a local Wi-Fi AP. We further proposed a scheme to detect possible misbehavior, and analyzed its performance in terms of detection and false alarm probabilities. We implemented and evaluated the proposed schemes in `ns3`. Our results have shown that the proposed schemes are able to estimate LTE-U duty cycle accurately and detect misbehavior with a high detection probability and a low false alarm probability.

BIBLIOGRAPHY

[1] "Universal software radio peripheral b210," https://www.ettus.com/product/details/UB210-KIT.

[2] Ericsson, "Ericsson mobility report," November 2017.

[3] Cisco, "Cisco visual networking index: Global mobile data traffic forecast update, 2016 – 2021 white paper," February 2017.

[4] QUALCOMM, "Rising to meet the 1000x mobile data challenge," 2012.

[5] UMTS Forum, "Mobile traffic forecasts 2010–2020: A report by the umts forum," January 2011.

[6] P. Xia, "Interference management in heterogeneous cellular networks," Ph.D. Dissertation, University of Texas at Austin, December 2012.

[7] Agilent Technologies Moray Rumney, "Taking 5G from vision to reality," in *The 6th Future of Wireless International Conference*, 2014.

[8] D. Tse and P. Viswanath, *Fundamentals of wireless communication*. Cambridge university press, 2005.

[9] N. Bhushan, J. Li, D. Malladi, R. Gilmore, D. Brenner, A. Damnjanovic, R. Sukhavasi, C. Patel, and S. Geirhofer, "Network densification: the dominant theme for wireless evolution into 5G," *IEEE Communications Magazine*, vol. 52, no. 2, pp. 82–89, 2014.

[10] President's Council of Advisors on Science and Technology, "Realizing the full potential of govt-held spectrum to spur economic growth," July 2012.

[11] M. A. McHenry, P. A. Tenhula, D. McCloskey, D. A. Roberson, and C. S. Hood, "Chicago spectrum occupancy measurements & analysis and a long-term studies proposal," in *Proceedings of the First International Workshop on Technology and Policy for Accessing Spectrum*, ser. TAPAS '06. New York, NY, USA: ACM, 2006.

[12] M. H. Islam, C. L. Koh, S. W. Oh, X. Qing, Y. Y. Lai, C. Wang, Y.-C. Liang, B. E. Toh, F. Chin, G. L. Tan *et al.*, "Spectrum survey in singapore: Occupancy measurements and analyses," in *Cognitive Radio Oriented Wireless Networks and Communications, 2008. CrownCom 2008. 3rd International Conference on.* IEEE, 2008, pp. 1–7.

[13] M. Wellens, J. Wu, and P. Mahonen, "Evaluation of spectrum occupancy in indoor and outdoor scenario in the context of cognitive radio," in *Cognitive Radio Oriented Wireless Networks and Communications, 2007. CrownCom 2007. 2nd International Conference on.* IEEE, 2007, pp. 420–427.

[14] M. López-Benítez, A. Umbert, and F. Casadevall, "Evaluation of spectrum occupancy in spain for cognitive radio applications," in *Vehicular technology conference, 2009. VTC Spring 2009. IEEE 69th.* IEEE, 2009, pp. 1–5.

[15] X. Ying, J. Zhang, L. Yan, G. Zhang, M. Chen, and R. Chandra, "Exploring indoor white spaces in metropolises," in *Proceedings of the 19th Annual International Conference on Mobile Computing & Networking*, ser. MobiCom '13. ACM, 2013, pp. 255–266.

[16] X. Ying, J. Zhang, L. Yan, Y. Chen, G. Zhang, M. Chen, and R. Chandra, "Exploring indoor white spaces in metropolises," *ACM Trans. Intell. Syst. Technol.*, vol. 9, no. 1, pp. 9:1–9:25, August 2017.

[17] F. Hessar and S. Roy, "Capacity considerations for secondary networks in TV white space," *IEEE Transactions on Mobile Computing*, vol. 14, no. 9, pp. 1780–1793, 2015.

[18] X. Ying, F. Hessar, and S. Roy, "Indoor–outdoor TV white and gray space availability: A U.S. case study," in *TV White Space Communications and Networks.* Elsevier, 2018, pp. 47–71.

[19] Federal Communications Commission, "In the matter of unlicensed operation in the TV broadcast bands: Second report and order and memorandum opinion and order," no. ET Docket No. 04-186, No. 02-380, Nov 4, 2008.

[20] J. R. Agre and K. D. Gordon, "A summary of recent federal government activities to promote spectrum sharing," no. IDA Paper P-5186, September 2015.

[21] U.S. Department of Commerce, "Sixth interim progress report on the ten-year plan and timetable," June 2016.

[22] Federal Communications Commission, "In the matter of amendment of the commission's rules with regard to commercial operations in the 1695- 1710 MHz, 1755-1780

MHz, and 2155-2180 MHz bands: Report and order," no. GN Docket No. 13-185, March 31, 2014.

[23] ——, "In the matter of amendment of the commission's rules to provide spectrum for the operation of medical body area networks: Order on reconsideration and second report and order," no. ET Docket No. 08-59, August 21, 2014.

[24] ——, "In the matter of revision of part 15 of the commission's rules to permit unlicensed national information infrastructure (u-nii) devices in the 5 GHz band: First report and order," no. ET Docket No. 13-49, April 1, 2014.

[25] ——, "In the matter of amendment of the commission's rules with regard to commercial operations in the 3550-3650 MHz band: Report and order and second further notice of proposed rulemaking," no. GN Docket No. 12-354, April 21, 2015.

[26] ——, "OET bulletin No. 69, Longley-Rice methodology for evaluating TV coverage and interference," 2004.

[27] C. Phillips, D. Sicker, and D. Grunwald, "A survey of wireless path loss prediction and coverage mapping methods," *IEEE Communications Surveys & Tutorials*, vol. 15, no. 1, pp. 255–270, 2013.

[28] ——, "Bounding the error of path loss models," in *New Frontiers in Dynamic Spectrum Access Networks (DySPAN), 2011 IEEE Symposium on.* IEEE, 2011, pp. 71–82.

[29] J. Howe, "The rise of crowdsourcing," *Wired magazine*, vol. 14, no. 6, pp. 1–4, 2006.

[30] R. K. Ganti, F. Ye, and H. Lei, "Mobile crowdsensing: current state and future challenges," *IEEE Communications Magazine*, vol. 49, no. 11, 2011.

[31] "Part 11 : Wireless LAN Medium Access Control (MAC) and Physical Layer (PHY) Specifications," IEEE Std 802.11-2012, Tech. Rep.

[32] 3GPP, "LTE; Evolved Universal Terrestrial Radio Access (E-UTRA); Physical layer procedures (3GPP TS 36.213 version 13.1.1 Release 13)," *ETSI TS 136 213 V13.1.1*, 2016.

[33] S. Sagari, S. Baysting, D. Saha, I. Seskar, W. Trappe, and D. Raychaudhuri, "Coordinated dynamic spectrum management of LTE-U and Wi-Fi networks," in *Dynamic Spectrum Access Networks (DySPAN), 2015 IEEE International Symposium on.* IEEE, 2015, pp. 209–220.

[34] A. M. Voicu, L. Simić, and M. Petrova, "Inter-technology coexistence in a spectrum commons: A case study of Wi-Fi and LTE in the 5-ghz unlicensed band," *IEEE Journal on Selected Areas in Communications*, vol. 34, no. 11, pp. 3062–3077, 2016.

[35] A. M. Cavalcante, E. Almeida, R. D. Vieira, F. Chaves, R. C. Paiva, F. Abinader, S. Choudhury, E. Tuomaala, and K. Doppler, "Performance evaluation of LTE and Wi-Fi coexistence in unlicensed bands," in *Vehicular Technology Conference (VTC Spring), 2013 IEEE 77th.* IEEE, 2013, pp. 1–6.

[36] F. M. Abinader, E. P. Almeida, F. S. Chaves, A. M. Cavalcante, R. D. Vieira, R. C. Paiva, A. M. Sobrinho, S. Choudhury, E. Tuomaala, K. Doppler *et al.*, "Enabling the coexistence of LTE and Wi-Fi in unlicensed bands," *IEEE Communications Magazine*, vol. 52, no. 11, pp. 54–61, 2014.

[37] "LTE-U technology and coexistence," Qualcomm Technologies, Inc., Tech. Rep., May 2015.

[38] "LTE-U SDL coexistence specifications v1.3," LTE-U Forum, Tech. Rep., Oct 2015.

[39] A. K. Sadek *et al.*, "Extending LTE to unlicensed band-merit and coexistence," in *Communication Workshop (ICCW), 2015 IEEE International Conference on.* IEEE, 2015, pp. 2344–2349.

[40] E. Almeida *et al.*, "Enabling LTE/WiFi coexistence by LTE blank subframe allocation," in *Communications (ICC), 2013 IEEE International Conference on.* IEEE, 2013, pp. 5083–5088.

[41] N. Rupasinghe and İ. Güvenç, "Reinforcement learning for licensed-assisted access of LTE in the unlicensed spectrum," in *Wireless Communications and Networking Conference (WCNC), 2015 IEEE.* IEEE, 2015, pp. 1279–1284.

[42] I. Parvez, M. Sriyananda, I. Güvenç, M. Bennis, and A. Sarwat, "CBRS spectrum sharing between LTE-U and WiFi: A multiarmed bandit approach," *Mobile Information Systems*, vol. 2016, 2016.

[43] Federal Communications Commission, "In the matter of unlicensed operation in the tv broadcast bands: Second memorandum opinion and order," no. ET Docket No. 04-186, No. 02-380, Sep 23, 2010.

[44] ——, "In the matter of unlicensed operation in the tv broadcast bands: Third memorandum opinion and order," no. ET Docket No. 04-186, No. 02-380, April 4, 2012.

[45] A. Achtzehn, J. Riihijarvi, and P. Mahonen, "Improving accuracy for TVWS geolocation databases: Results from measurement-driven estimation approaches," in *Dynamic Spectrum Access Networks (DYSPAN), 2014 IEEE International Symposium on*. IEEE, 2014, pp. 392–403.

[46] A. Achtzehn, J. Riihijärvi, G. M. Vargas, M. Petrova, and P. Mähönen, "Improving coverage prediction for primary multi-transmitter networks operating in the TV whitespaces," in *Sensor, Mesh and Ad Hoc Communications and Networks (SECON), 2012 9th Annual IEEE Communications Society Conference on*. IEEE, 2012, pp. 623–631.

[47] V. Erceg, L. J. Greenstein, S. Y. Tjandra, S. R. Parkoff, A. Gupta, B. Kulic, A. A. Julius, and R. Bianchi, "An empirically based path loss model for wireless channels in suburban environments," *IEEE Journal on selected areas in communications*, vol. 17, no. 7, pp. 1205–1211, 1999.

[48] V. Abhayawardhana, I. Wassell, D. Crosby, M. Sellars, and M. Brown, "Comparison of empirical propagation path loss models for fixed wireless access systems," in *Vehicular Technology Conference, 2005. VTC 2005-Spring. 2005 IEEE 61st*, vol. 1. IEEE, 2005, pp. 73–77.

[49] A. Konak, "A Kriging approach to predicting coverage in wireless networks," *International Journal of Mobile Network Design and Innovation*, vol. 3, no. 2, pp. 65–71, 2009.

[50] C. Phillips, M. Ton, D. Sicker, and D. Grunwald, "Practical radio environment mapping with geostatistics," in *Dynamic Spectrum Access Networks (DYSPAN), 2012 IEEE International Symposium on*. IEEE, 2012, pp. 422–433.

[51] J. Ojaniemi, J. Kalliovaara, J. Poikonen, and R. Wichman, "A practical method for combining multivariate data in radio environment mapping," in *Personal Indoor and Mobile Radio Communications (PIMRC), 2013 IEEE 24th International Symposium on*. IEEE, 2013, pp. 729–733.

[52] S.-J. Kim, E. Dall'Anese, and G. B. Giannakis, "Cooperative spectrum sensing for cognitive radios using kriged kalman filtering," *IEEE Journal of Selected Topics in Signal Processing*, vol. 5, no. 1, pp. 24–36, 2011.

[53] H. B. Yilmaz and T. Tugcu, "Location estimation-based radio environment map construction in fading channels," *Wireless communications and mobile computing*, vol. 15, no. 3, pp. 561–570, 2015.

[54] N. Cressie and D. M. Hawkins, "Robust estimation of the variogram: I," *Journal of the International Association for Mathematical Geology*, vol. 12, no. 2, pp. 115–125, 1980.

[55] P. J. Ribeiro Jr, P. J. Diggle *et al.*, "geor: a package for geostatistical analysis," *R news*, vol. 1, no. 2, pp. 14–18, 2001.

[56] N. A. Cressie and N. A. Cassie, *Statistics for spatial data*. Wiley New York, 1993, vol. 900.

[57] R. Sunila, E. Laine, and O. Kremenova, "Fuzzy model and kriging for imprecise soil polygon boundaries," in *1st International Conference on Advances in Mineral Resources Management and Environmental Geotechnology*. HELIOTOPOS CONFERENCES, 2004, p. 151.

[58] O. Fatemieh, R. Chandra, and C. A. Gunter, "Secure collaborative sensing for crowd sourcing spectrum data in white space networks," in *New Frontiers in Dynamic Spectrum, 2010 IEEE Symposium on*. IEEE, 2010, pp. 1–12.

[59] D.-H. Shin, S. He, and J. Zhang, "Joint sensing task and subband allocation for large-scale spectrum profiling," in *Computer Communications (INFOCOM), 2015 IEEE Conference on*. IEEE, 2015, pp. 433–441.

[60] A. Nika, Z. Zhang, X. Zhou, B. Y. Zhao, and H. Zheng, "Towards commoditized real-time spectrum monitoring," in *Proceedings of the 1st ACM workshop on Hot topics in wireless*. ACM, 2014, pp. 25–30.

[61] V. Krishna, *Auction theory*. Academic press, 2009.

[62] D. Yang, G. Xue, X. Fang, and J. Tang, "Crowdsourcing to smartphones: incentive mechanism design for mobile phone sensing," in *Proceedings of the 18th annual international conference on Mobile computing and networking*. ACM, 2012, pp. 173–184.

[63] Y. Singer, "Budget feasible mechanisms," in *Foundations of Computer Science (FOCS), 2010 51st Annual IEEE Symposium on*. IEEE, 2010, pp. 765–774.

[64] N. Chen, N. Gravin, and P. Lu, "On the approximability of budget feasible mechanisms," in *Proceedings of the twenty-second annual ACM-SIAM symposium on Discrete Algorithms*. SIAM, 2011, pp. 685–699.

[65] Z. Feng, Y. Zhu, Q. Zhang, L. M. Ni, and A. V. Vasilakos, "TRAC: Truthful auction for location-aware collaborative sensing in mobile crowdsourcing," in *INFOCOM, 2014 Proceedings IEEE*. IEEE, 2014, pp. 1231–1239.

[66] L. G. Jaimes, I. Vergara-Laurens, and M. A. Labrador, "A location-based incentive mechanism for participatory sensing systems with budget constraints," in *Pervasive Computing and Communications (PerCom), 2012 IEEE International Conference on*. IEEE, 2012, pp. 103–108.

[67] J. W. Van Groenigen, W. Siderius, and A. Stein, "Constrained optimisation of soil sampling for minimisation of the Kriging variance," *Geoderma*, vol. 87, no. 3, pp. 239–259, 1999.

[68] A. Krause, A. Singh, and C. Guestrin, "Near-optimal sensor placements in gaussian processes: Theory, efficient algorithms and empirical studies," *Journal of Machine Learning Research*, vol. 9, no. Feb, pp. 235–284, 2008.

[69] A. Das and D. Kempe, "Algorithms for subset selection in linear regression," in *Proceedings of the fortieth annual ACM symposium on Theory of computing*. ACM, 2008, pp. 45–54.

[70] A. Krause, H. B. McMahan, C. Guestrin, and A. Gupta, "Robust submodular observation selection," *Journal of Machine Learning Research*, vol. 9, no. Dec, pp. 2761–2801, 2008.

[71] G. L. Nemhauser, L. A. Wolsey, and M. L. Fisher, "An analysis of approximations for maximizing submodular set functions - i," *Mathematical Programming*, vol. 14, no. 1, pp. 265–294, 1978.

[72] R. B. Myerson, "Optimal auction design," *Mathematics of operations research*, vol. 6, no. 1, pp. 58–73, 1981.

[73] X. Ying, C. W. Kim, and S. Roy, "Revisiting tv coverage estimation with measurement-based statistical interpolation," in *Communication Systems and Networks (COMSNETS), 2015 7th International Conference on*. IEEE, 2015, pp. 1–8.

[74] A. Deshpande *et al.*, "Model-driven data acquisition in sensor networks," in *Proceedings of the Thirtieth international conference on Very large data bases-Volume 30*. VLDB Endowment, 2004, pp. 588–599.

[75] A. Singla and A. Krause, "Truthful incentives in crowdsourcing tasks using regret minimization mechanisms," in *Proceedings of the 22Nd International Conference on World Wide Web*, ser. WWW '13. New York, NY, USA: ACM, 2013, pp. 1167–1178. [Online]. Available: http://doi.acm.org/10.1145/2488388.2488490

[76] S. He, D.-H. Shin, J. Zhang, and J. Chen, "Toward optimal allocation of location dependent tasks in crowdsensing," in *INFOCOM, 2014 Proceedings IEEE*. IEEE, 2014, pp. 745–753.

[77] K. Han, H. Huang, and J. Luo, "Posted pricing for robust crowdsensing," in *Proceedings of the 17th ACM International Symposium on Mobile Ad Hoc Networking and Computing*. ACM, 2016, pp. 261–270.

[78] N. Buchbinder, M. Feldman, J. Seffi, and R. Schwartz, "A tight linear time (1/2)-approximation for unconstrained submodular maximization," *SIAM Journal on Computing*, vol. 44, no. 5, pp. 1384–1402, 2015.

[79] H. B. Yilmaz, T. Tugcu, F. Alagöz, and S. Bayhan, "Radio environment map as enabler for practical cognitive radio networks," *IEEE Communications Magazine*, vol. 51, no. 12, pp. 162–169, 2013.

[80] X. Ying, S. Roy, and R. Poovendran, "Incentivizing crowdsourcing for radio environment mapping with statistical interpolation," in *Dynamic Spectrum Access Networks (DySPAN), 2015 IEEE International Symposium on*. IEEE, 2015, pp. 365–374.

[81] I. Koutsopoulos, "Optimal incentive-driven design of participatory sensing systems," in *2013 Proceedings IEEE INFOCOM*. IEEE, 2013, pp. 1402–1410.

[82] T. Luo, S. K. Das, H. P. Tan, and L. Xia, "Incentive mechanism design for crowdsourcing: An all-pay auction approach," *ACM Transactions on Intelligent Systems and Technology (TIST)*, vol. 7, no. 3, p. 35, 2016.

[83] T. Luo, S. S. Kanhere, H.-P. Tan, F. Wu, and H. Wu, "Crowdsourcing with tullock contests: A new perspective," in *Computer Communications (INFOCOM), 2015 IEEE Conference on*. IEEE, 2015, pp. 2515–2523.

[84] Y. Singer and M. Mittal, "Pricing mechanisms for crowdsourcing markets," in *Proceedings of the 22nd international conference on World Wide Web*. ACM, 2013, pp. 1157–1166.

[85] D. Zhao, X.-Y. Li, and H. Ma, "How to crowdsource tasks truthfully without sacrificing utility: Online incentive mechanisms with budget constraint," in *INFOCOM, 2014 Proceedings IEEE*. IEEE, 2014, pp. 1213–1221.

[86] K. Han, C. Zhang, and J. Luo, "Taming the uncertainty: Budget limited robust crowdsensing through online learning," *IEEE/ACM Transactions on Networking (TON)*, vol. 24, no. 3, pp. 1462–1475, 2016.

[87] D. Peng, F. Wu, and G. Chen, "Pay as how well you do: A quality based incentive mechanism for crowdsensing," in *Proceedings of the 16th ACM International Symposium on Mobile Ad Hoc Networking and Computing*. ACM, 2015, pp. 177–186.

[88] K. Han, C. Zhang, J. Luo, M. Hu, and B. Veeravalli, "Truthful scheduling mechanisms for powering mobile crowdsensing," *IEEE Transactions on Computers*, vol. 65, no. 1, pp. 294–307, 2016.

[89] J. Scott, "Rational choice theory," *Understanding contemporary society: Theories of the present*, vol. 129, 2000.

[90] G. J. Pottie and W. J. Kaiser, "Wireless integrated network sensors," *Communications of the ACM*, vol. 43, no. 5, pp. 51–58, 2000.

[91] S. Fujishige, *Submodular functions and optimization*. Elsevier, 2005, vol. 58.

[92] U. Feige, V. S. Mirrokni, and J. Vondrak, "Maximizing non-monotone submodular functions," *SIAM Journal on Computing*, vol. 40, no. 4, pp. 1133–1153, 2011.

[93] E. R. Hansen, "Global optimization using interval analysis: the one-dimensional case," *Journal of Optimization Theory and Applications*, vol. 29, no. 3, pp. 331–344, 1979.

[94] R. Y. Rubinstein and D. P. Kroese, *Simulation and the Monte Carlo method*. John Wiley & Sons, 2016.

[95] Federal Communications Commission, "In the matter of amendment of the commission's rules with regard to commercial operations in the 3550-3650 MHz band: Notice of proposed rulemaking and order adopted:," no. GN Docket No. 12-354, Dec 2012.

[96] ——, "In the matter of amendment of the commission's rules with regard to commercial operations in the 3550-3650 MHz band: Further notice of proposed rulemaking," no. GN Docket No. 12-354, Apr 2014.

[97] Wireless Innovation Forum (WInnForum), "Requirements for commercial operation in the U.S. 3550-3700 MHz citizens broadband radio service band (v1.4.1)," no. Working Document WINNF-TS-0112, January 16, 2018.

[98] "Part 11: Wireless LAN medium access control (MAC) and physical layer (PHY) specifications - amendment 4: Enhancements for very high throughput for operation in bands below 6 GHz," IEEE Std 802.11ac, Tech. Rep., 2013.

[99] A. Mishra, S. Banerjee, and W. Arbaugh, "Weighted coloring based channel assignment for wlans," *ACM SIGMOBILE Mobile Computing and Communications Review*, vol. 9, no. 3, pp. 19–31, 2005.

[100] A. P. Subramanian and H. Gupta, "Fast spectrum allocation in coordinated dynamic spectrum access based cellular networks," in *New Frontiers in Dynamic Spectrum Access Networks, 2007. DySPAN 2007. 2nd IEEE International Symposium on.* IEEE, 2007, pp. 320–330.

[101] A. P. Subramanian, M. Al-Ayyoub, H. Gupta, S. R. Das, and M. M. Buddhikot, "Near-optimal dynamic spectrum allocation in cellular networks," in *New Frontiers in Dynamic Spectrum Access Networks, 2008. DySPAN 2008. 3rd IEEE Symposium on.* IEEE, 2008, pp. 1–11.

[102] F. Hessar and S. Roy, "Resource allocation techniques for cellular networks in tv white space spectrum," in *Dynamic Spectrum Access Networks (DYSPAN), 2014 IEEE International Symposium on.* IEEE, 2014, pp. 72–81.

[103] N. Nie and C. Comaniciu, "Adaptive channel allocation spectrum etiquette for cognitive radio networks," *Mobile networks and applications*, vol. 11, no. 6, pp. 779–797, 2006.

[104] M. Liu and Y. Wu, "Spectrum sharing as congestion games," in *Communication, Control, and Computing, 2008 46th Annual Allerton Conference on.* IEEE, 2008, pp. 1146–1153.

[105] D. Li and J. Gross, "Distributed tv spectrum allocation for cognitive cellular network under game theoretical framework," in *Dynamic Spectrum Access Networks (DYSPAN), 2012 IEEE International Symposium on.* IEEE, 2012, pp. 327–338.

[106] "NYC Wi-Fi hotspot locations," https://nycopendata.socrata.com/Social-Services/NYC-Wi-Fi-Hotspot-Locations/a9we-mtpn/data, accessed: 2016-09-22.

[107] I. Katzela and M. Naghshineh, "Channel assignment schemes for cellular mobile telecommunication systems: A comprehensive survey," *IEEE personal communications*, vol. 3, no. 3, pp. 10–31, 1996.

[108] W. Si, S. Selvakennedy, and A. Y. Zomaya, "An overview of channel assignment methods for multi-radio multi-channel wireless mesh networks," *Journal of Parallel and Distributed Computing*, vol. 70, no. 5, pp. 505–524, 2010.

[109] I. F. Akyildiz, W.-Y. Lee, M. C. Vuran, and S. Mohanty, "Next generation/dynamic spectrum access/cognitive radio wireless networks: A survey," *Computer networks*, vol. 50, no. 13, pp. 2127–2159, 2006.

[110] L. Cao and H. Zheng, "Distributed spectrum allocation via local bargaining." in *SECON*, 2005, pp. 475–486.

[111] W. Wang and X. Liu, "List-coloring based channel allocation for open-spectrum wireless networks," in *Vehicular Technology Conference, 2005. VTC-2005-Fall. 2005 IEEE 62nd*, vol. 1. IEEE, 2005, pp. 690–694.

[112] C. Peng, H. Zheng, and B. Y. Zhao, "Utilization and fairness in spectrum assignment for opportunistic spectrum access," *Mobile Networks and Applications*, vol. 11, no. 4, pp. 555–576, 2006.

[113] X. Yue, C.-F. Wong, and S.-H. G. Chan, "Cacao: Distributed client-assisted channel assignment optimization for uncoordinated wlans," *IEEE Transactions on Parallel and Distributed Systems*, vol. 22, no. 9, pp. 1433–1440, 2011.

[114] M. Hoefer, T. Kesselheim, and B. Vöcking, "Approximation algorithms for secondary spectrum auctions," *ACM Transactions on Internet Technology (TOIT)*, vol. 14, no. 2-3, p. 16, 2014.

[115] M. M. Halldórsson, "Approximations of weighted independent set and hereditary subset problems," *Journal of Graph Algorithms and Applications*, 2000.

[116] S. Sakai, M. Togasaki, and K. Yamazaki, "A note on greedy algorithms for the maximum weighted independent set problem," *Discrete Applied Mathematics*, vol. 126, no. 2-3, pp. 313–322, 2003.

[117] A. Kako, T. Ono, T. Hirata, and M. M. Halldórsson, "Approximation algorithms for the weighted independent set problem," in *International Workshop on Graph-Theoretic Concepts in Computer Science*. Springer, 2005, pp. 341–350.

[118] Federal Communications Commission, "In the matter of amendment of the commission's rules with regard to commercial operations in the 3550-3650 MHz band: Order on reconsideration and second report and order," no. GN Docket No. 12-354, May 2, 2016.

[119] Wireless Innovation Forum (WInnForum), "Signaling protocols and procedures for citizens broadband radio service (CBRS): Spectrum access system (SAS) - citizens broadband radio service device (CBSD) interface technical specification (v1.2.1)," no. Working Document WINNF-TS-0116, January 3, 2018.

[120] T. H. Cormen *et al.*, *Introduction to Algorithms, Third Edition*, 3rd ed. The MIT Press, 2009.

[121] P. Gupta and P. R. Kumar, "The capacity of wireless networks," *IEEE Transactions on information theory*, vol. 46, no. 2, pp. 388–404, 2000.

[122] A. Mishra, V. Brik, S. Banerjee, A. Srinivasan, and W. A. Arbaugh, "A client-driven approach for channel management in wireless lans." in *Infocom*, 2006.

[123] D. Niculescu, "Interference map for 802.11 networks," in *Proceedings of the 7th ACM SIGCOMM conference on Internet measurement*. ACM, 2007, pp. 339–350.

[124] C. Bron and J. Kerbosch, "Algorithm 457: finding all cliques of an undirected graph," *Communications of the ACM*, 1973.

[125] S. Eilon and N. Christofides, "The loading problem," *Management Science*, vol. 17, no. 5, pp. 259–268, 1971.

[126] G. Dósa, "The tight bound of first fit decreasing bin-packing algorithm is FFD(I) $\leq$ 11/9 OPT(I)+ 6/9," in *Combinatorics, Algorithms, Probabilistic and Experimental Methodologies*. Springer, 2007, pp. 1–11.

[127] S. Bandyapadhyay, "A variant of the maximum weight independent set problem," *arXiv preprint arXiv:1409.0173*, 2014.

[128] A. Hertz and D. de Werra, "Using tabu search techniques for graph coloring," *Computing*, vol. 39, no. 4, pp. 345–351, 1987.

[129] A. Bar-Noy, M. M. Halldórsson, G. Kortsarz, R. Salman, and H. Shachnai, "Sum multicoloring of graphs," *Journal of Algorithms*, vol. 37, no. 2, pp. 422–450, 2000.

[130] E. Damosso, *Digital mobile radio towards future generation systems: COST action 231*. European Commission, 1999.

[131] J. Padhye, S. Agarwal, V. N. Padmanabhan, L. Qiu, A. Rao, and B. Zill, "Estimation of link interference in static multi-hop wireless networks," in *Proceedings of the 5th ACM SIGCOMM conference on Internet Measurement*. USENIX Association, 2005, pp. 28–28.

[132] C. Reis, R. Mahajan, M. Rodrig, D. Wetherall, and J. Zahorjan, "Measurement-based models of delivery and interference in static wireless networks," in *ACM SIGCOMM Computer Communication Review*, vol. 36, no. 4. ACM, 2006, pp. 51–62.

[133] C. W. Kim, J. Ryoo, and M. M. Buddhikot, "Design and implementation of an end-to-end architecture for 3.5 ghz shared spectrum," in *Dynamic Spectrum Access Networks (DySPAN), 2015 IEEE International Symposium on.* IEEE, 2015, pp. 23–34.

[134] J. Lee, V. S. Mirrokni, V. Nagarajan, and M. Sviridenko, "Maximizing nonmonotone submodular functions under matroid or knapsack constraints," *SIAM Journal on Discrete Mathematics*, vol. 23, no. 4, pp. 2053–2078, 2010.

[135] S. Bhattarai *et al.*, "An overview of dynamic spectrum sharing: Ongoing initiatives, challenges, and a roadmap for future research," *IEEE Transactions on Cognitive Communications and Networking*, vol. 2, no. 2, pp. 110–128, 2016.

[136] "ns-3," http://www.nsnam.org.

[137] T. Nihtilä, V. Tykhomyrov, O. Alanen, M. A. Uusitalo, A. Sorri, M. Moisio, S. Iraji, R. Ratasuk, and N. Mangalvedhe, "System performance of LTE and IEEE 802.11 coexisting on a shared frequency band," in *Wireless Communications and Networking Conference (WCNC), 2013 IEEE.* IEEE, 2013, pp. 1038–1043.

[138] C. Cano and D. J. Leith, "Coexistence of WiFi and LTE in unlicensed bands: A proportional fair allocation scheme," in *Communication Workshop (ICCW), 2015 IEEE International Conference on.* IEEE, 2015, pp. 2288–2293.

[139] FierceWireless, "Verizon, T-Mobile gear up to launch LTE-U after FCC authorizes devices in 5 GHz band," https://www.fiercewireless.com/tech/verizon-t-mobile-gear-up-to-launch-lte-u-after-fcc-authorizes-devices-5-ghz-band.

[140] Engadget, "T-Mobile launches speedy LTE-U service in six cities," https://www.engadget.com/2017/06/26/t-mobile-launches-unlicensed-lte/.

[141] Mobile World Live, "Verizon confirms shift to LAA over LTE-U," https://www.mobileworldlive.com/featured-content/top-three/verizon-confirms-shift-to-laa-over-lte-u/.

[142] X. Ying, R. Poovendran, and S. Roy, "Fairness monitoring between Wi-Fi and duty cycled LTE-U in shared bands," *IEEE Transactions on Vehicular Technology (In preparation).*

[143] X. Ying, M. Buddhikot, and S. Roy, "SAS-assisted coexistence-aware dynamic channel allocation for 3.5 GHz shared spectrum," *IEEE Transactions on Wireless Communications (Under review).*

[144] X. Ying, S. Roy, and R. Poovendran, "Pricing mechanisms for crowd-sensed spatial-statistics-based radio mapping," *IEEE Transactions on Cognitive Communications and Networking*, vol. 3, no. 2, pp. 242–254, June 2017.

[145] S. U. Sagong, X. Ying, A. Clark, L. Bushnell, and R. Poovendran, "Cloaking the clock: Emulating clock skew in controller area networks," in *Proceedings of the 9th ACM/IEEE International Conference on Cyber-Physical Systems*, ser. ICCPS '18. IEEE Press, 2018, pp. 32–42.

[146] X. Ying, R. Poovendran, and S. Roy, "Detecting LTE-U duty cycling misbehavior for fair sharing with Wi-Fi in shared bands," in *2017 IEEE 28th Annual International Symposium on Personal, Indoor, and Mobile Radio Communications (PIMRC)*, Oct 2017, pp. 1–7.

[147] X. Ying, M. M. Buddhikot, and S. Roy, "Coexistence-aware dynamic channel allocation for 3.5 ghz shared spectrum systems," in *2017 IEEE International Symposium on Dynamic Spectrum Access Networks (DySPAN)*, March 2017, pp. 1–2.

[148] X. Ying, S. Roy, and R. Poovendran, "Pricing mechanism for quality-based radio mapping via crowdsourcing," in *2016 IEEE Global Communications Conference (GLOBECOM)*, Dec 2016, pp. 1–6.

Appendix A

LIST OF PUBLICATIONS

Journal Publications & Book Chapter

1. X. Ying, R. Poovendran, and S. Roy, "Fairness monitoring between Wi-Fi and duty cycled LTE-U in shared bands," *IEEE Transactions on Vehicular Technology (In preparation).*

2. X. Ying, M. Buddhikot, and S. Roy, "SAS-assisted coexistence-aware dynamic channel allocation for 3.5 GHz shared spectrum," *IEEE Transactions on Wireless Communications (Under review).*

3. X. Ying, F. Hessar, and S. Roy, "Indoor–outdoor TV white and gray space availability: A U.S. case study," in *TV White Space Communications and Networks.* Elsevier, 2018, pp. 47–71.

4. X. Ying, J. Zhang, L. Yan, Y. Chen, G. Zhang, M. Chen, and R. Chandra, "Exploring indoor white spaces in metropolises," *ACM Trans. Intell. Syst. Technol.,* vol. 9, no. 1, pp. 9:1–9:25, August 2017.

5. X. Ying, S. Roy, and R. Poovendran, "Pricing mechanisms for crowd-sensed spatial-statistics-based radio mapping," *IEEE Transactions on Cognitive Communications and Networking,* vol. 3, no. 2, pp. 242–254, June 2017.

Conference Publications

1. S. U. Sagong, X. Ying, A. Clark, L. Bushnell, and R. Poovendran, "Cloaking the clock: Emulating clock skew in controller area networks," in *Proceedings of the 9th*

ACM/IEEE International Conference on Cyber-Physical Systems, ser. ICCPS'18. IEEE, 2018, pp. 32–42.

2. X. Ying, R. Poovendran, and S. Roy, "Detecting LTE-U duty cycling misbehavior for fair sharing with Wi-Fi in shared bands," in *2017 IEEE 28th Annual International Symposium on Personal, Indoor, and Mobile Radio Communications (PIMRC),* Oct 2017, pp. 1–7.

3. X. Ying, M. M. Buddhikot, and S. Roy, "Coexistence-aware dynamic channel allocation for 3.5 GHz shared spectrum systems," in *2017 IEEE International Symposium on Dynamic Spectrum Access Networks (DySPAN),* March 2017, pp. 1–2.

4. X. Ying, S. Roy, and R. Poovendran, "Pricing mechanism for quality-based radio mapping via crowdsourcing," in *2016 IEEE Global Communications Conference (GLOBECOM),* Dec 2016, pp. 1–6.

5. X. Ying, S. Roy, and R. Poovendran, "Incentivizing crowdsourcing for radio environment mapping with statistical interpolation," in *Dynamic Spectrum Access Networks (DySPAN),* 2015 IEEE International Symposium on. IEEE, 2015, pp. 365–374.

6. X. Ying, C. W. Kim, and S. Roy, "Revisiting tv coverage estimation with measurement-based statistical interpolation," in *Communication Systems and Networks (COMSNETS), 2015 7th International Conference on. IEEE,* 2015, pp. 1–8.

7. X. Ying, J. Zhang, L. Yan, G. Zhang, M. Chen, and R. Chandra, "Exploring indoor white spaces in metropolises," in *Proceedings of the 19th Annual International Conference on Mobile Computing & Networking, ser. MobiCom'13. ACM,* 2013, pp. 255–266.

VITA

Xuhang Ying was born in Ninghai, Zhejiang Province, People's Republic of China, 1991. He received his Bachelor of Engineering in Information Engineering from the Chinese University of Hong Kong, Hong Kong in 2013 with the highest honor. He received his Master of Science in Electrical Engineering from University of Washington in 2016. His research interests include spectrum sharing, incentive mechanism, and platform security for in-vehicle controller area networks and GPS systems. He was a co-author of the ACM/IEEE ICCPS Best Paper finalist (2018).